Condensation of DNA by spermine in the bulk and in the bacteriophage capsid : a cryo-electron microscopy study

Baeckkyoung Sung

UNIVERSITÉ PARIS-SUD 11

ECOLE DOCTORALE :

INNOVATION THÉRAPEUTIQUE : DU FONDAMENTAL A L'APPLIQUÉ

PÔLE : INGENIERIE DES PROTEINES ET CIBLES THERAPEUTIQUES

DISCIPLINE : Biophysique
Pharmacotechnie et Biopharmacie

ANNÉE 2010 - 2011 SÉRIE DOCTORAT N° 1116

THÈSE DE DOCTORAT
soutenue le 25/08/2011

par

Baeckkyoung SUNG

Condensation of DNA by spermine in the bulk and in the bacteriophage capsid: A cryo-electron microscopy study

Directeur de thèse :	Françoise LIVOLANT	DR CNRS, Université Paris-Sud XI
Composition du jury :		
Président du jury :	Kwang-Sup SOH	Director, Adv. Instit. Converg. Tech., Seoul Natl. Univ.
Rapporteurs :	Denis CHRETIEN	DR CNRS, Université de Rennes 1
	Yves LANSAC	M. Conférence, Université de Tours
Examinateurs :	Yun Hee JANG	Associate Prof, Gwangju Instit. Sci. Tech.
	Soong Ho UM	Assistant Prof, Gwangju Instit. Sci. Tech.

REMERCIEMENT

J’adresse mes remerciements les plus sincères aux personnes qui m'ont apporté leur aide et qui ont contribué à l'élaboration de cette thèse.

En premier lieu, je remercie sincèrement Françoise LIVOLANT de m’avoir accordé cette chance de travailler sur biophysique d’ADN dans son équipe. En tant que directrice de thèse, elle s'est toujours montrée à l'écoute et très disponible tout au long de la réalisation de ce travail, ainsi pour l'inspiration, l'aide et le temps qu'elle a bien voulu me consacrer et sans qui cette thèse n'aurait jamais vu le jour.

Mes remerciements s’adressent également à Amélie LEFORESTIER pour ses chaleureux encouragements et pour les précieux conseils. Grâce à son aide, j’ai pu apprendre les méthodologies essentielles sur la microscopie électronique et la biochimie de bactériophages.

Toute ma reconnaissance va aussi à Jéril DEGROUARD qui m’a initié aux techniques de cryo-microscopie électronique. Merci pour ta gentillesse et ta disponiblité tout au long de ce travail.

J’exprime mes remerciements en particulier à Eric RASPAUD qui m’a appris la physique de polyélectrolytes et la manière d’interpréter les données des expériences. Ses critiques et ses conseils m’ont beaucoup aidé à la réalisation de cette thèse.

Je tiens à exprimer ma reconnaissance envers Yves LANSAC qui a accepté la lourde tâche de rapporteur. Merci pour tes conseils précieux sur la recherche et aussi sur le reste des choses. Ca était un grand plaisir pour moi de discuter avec toi.

J'exprime ma gratitude à Denis CHRETIEN pour sa générosité d’avoir accepté de rédiger le rapport sur ma thèse et pour ses critiques importantes qui m’ont permis de finir le travail.

Je n’oublie pas Guillaume TRESSET, Nicolas LEMERCIER et Miguel TREJOT pour toutes les discussions intéressantes que nous avons pu avoir ainsi que pour ses soutiens. Un grand merci à vous.

Que les membres du jury, Kwang-Sup SOH, Yun Hee JANG et Soong Ho UM soient ici remerciés d’avoir accepté de juger ce travail.

Enfin, j'adresse mes plus sincères remerciements à toute ma famille, qui m'ont toujours soutenue et encouragée durant toutes ces années de travail, plus particulièrement à ma femme Jiyoung qui restait toujours à mes côtés, à ma mère et mon frère qui m’ont fait confiance dans la poursuite de mes études.

Condensation of DNA by spermine in the bulk and in the bacteriophage capsid:
A cryo-electron microscopy study

Abstract

By using cryo-electron microscopy, we analyzed the morphology and structure of long double-stranded DNA chains condensed upon addition of varying amounts of the tetravalent polycation spermine (polyamine). Experiments have been performed i) with chains diluted in the bulk and ii) with individual chains confined in a virus capsid.

Bulk experiments have been done with lambda DNA (48.5 kbp) at low concentration (0.03 mM Ph) and in low salt conditions (10 mM Tris HCl, 1 mM EDTA, pH 7.6). We explored a wide range of spermine concentration, from the onset of precipitation (0.05 mM sp) up to above the resolubilization limit (400 mM sp). Sixteen min after mixing spermine and DNA, samples have been trapped in thin films and vitrified in liquid ethane to keep ionic conditions unchanged, and imaged at low temperature with low doses of electrons (cryoTEM). DNA chains mostly form large aggregates of toroids in which DNA chains are hexagonally packed with interhelical spacings of 2.93, 2.88, and 2.95 nm at 0.05, 1 and 100 mM spermine, respectively, in agreement with previous X-ray data. At higher spermine concentration (200 mM), hexagonal toroids are replaced by cholesteric bundles with a larger interhelical spacing (3.32 nm). We conclude that the shape and the structure of the liquid crystalline sp-DNA condensates are linked to the DNA interhelix spacing and determined by the ionic conditions *i.e.* by the cohesive energy between DNA strands. Outside of the precipitation domain (400 mM spermine), DNA chains form a soluble network of thin fibers (4-6 nm in diameter) that let us reconsider the state of these DNA chains in excess of spermine. We also designed experiments to visualize condensates formed 6-60 sec after mixing Lambda DNA with 0.05 mM spermine, under identical buffer conditions. Among multiple original shapes (not found after 16 min), the presence of stretched and helical elongated fibers seen only 9 sec after addition of spermine let us propose that DNA chains are immediately stretched upon addition of spermine, relax into helical structures and finally form small toroids (containing in some cases less than one Lambda chain) that further grow and aggregate. We also analyzed the dimensions and structural details of the complete collection of toroids, and reveal the existence of geometric constraints that remain to be clarified.

Since it was only exceptionally possible to prevent the aggregation of DNA in dilute solution, we used another approach to observe the collapse of single DNA chains. We handled a population of T5 viruses containing a fraction of their initial genome (12-54 kbp long). The Na-DNA chain, initially confined in the small volume of the capsid (80 nm in diameter) is collapsed by the addition of spermine. Compared to the first set of experiments, we explored a higher DNA concentration range (0.45 mM Phosphates in the whole sample) and the spermine concentration was varied from 0.05 to 0.5 mM (which corresponds to much lower +/- charge ratios). Experiments are thus performed close to the precipitation line, in the coexistence region, between the region where all chains are in a coil conformation, and the region where all chains are collapsed into toroids. We describe the existence of intermediate states between the coil and the toroidal globule that were not reported yet. In these “hairy toroids”, part of the DNA chain is condensed in the toroid and the other part stays uncondensed outside of it. The interhelical spacing was also measured; it is larger in these partly-condensed toroids than in the fully organized toroids formed at higher spermine concentration.

These two series of experiments show the interest of cryoEM to analyze the structural polymorphism and local structure of spermine-DNA aggregates. We also demonstrated how the confinement interferes with DNA condensation and the interest to investigate such effects that are important in the biological context.

Key Words: Cryo-electron microscopy, DNA condensation, spermine, bacteriophage, toroid, liquid crystal

Condensation de l'ADN par la spermine en solution et dans la capside de bactériophage: Une étude par cryo-microscopie électronique

Résumé

Nous avons analysé par cryomicroscopie électronique la morphologie et la structure de longues chaines d'ADN condensées par un polycation tétravalent, la spermine (polyamine). Les expériences ont été réalisées i) avec des solutions de chaînes diluées et ii) avec des chaines isolées confinées dans la capside d'un virus.

Les expériences ont été réalisées avec de l'ADN Lambda (48 kbp) en solution diluée (0.03 mM Ph) et à faible concentration ionique (10 mM Tris HCl, 1 mM EDTA, pH 7.6). Nous avons exploré une large gamme de concentrations en spermine, allant du seuil de précipitation (0.05 mM sp) jusqu'à la limite de re-solubilization et au-delà (400 mM sp). Seize minutes après mélange de l'ADN et de la spermine, les échantillons sont piégés en film mince et vitrifiés à basse température pour garder intactes les conditions ioniques, puis imagés à basse température sous faibles doses d'électrons (cryoMET). La plupart des chaînes d'ADN forment des agrégats de tores de structure hexagonale avec des interdistances entre hélices de 2.93, 2.88, et 2.95 nm pour des concentrations en spermine respectivement égales à 0.05, 1 et 100 mM spermine, ce qui est en bon accord avec les données collectées précédemment par diffraction des rayons X. A concentration plus élevée en spermine (200 mM), les tores hexagonaux sont remplacés par des faisceaux cholestériques de structure plus lâche (3.32 nm entre hélices). Nous en déduisons que la forme comme la structure des condensats cristallins liquides ADN-sp sont liées aux interdistances entre hélices et déterminés par les conditions ioniques *i.e.* par l'énergie cohésive entre chaînes d'ADN. En dehors du domaine de précipitation (400 mM sp), les molécules d'ADN forment un réseau soluble de fines fibres (4-6 nm de diamètre) qui nous amènent à reconsidérer l'état de ces chaiînes en présence de spermine. Nous avons également conçu des expériences pour visualiser les agrégats formés 6 à 60 sec après addition de la spermine dans les mêmes conditions de tampon. Parmi les nombreuses formes originales que nous avons observées (absentes après 16 min), la présence de fibres étirées ou en hélice, visibles seulement après 9 sec, nous conduit à proposer que les chaines d'ADN soient immédiatement étirées après addition de spermine puis relaxent sous forme de fibres hélicoïdales qui donnent naissance à de petits toroids (comprenant quelquefois moins d'une chaine) qui grandissent et fusionnent. Nous avons également analysé les dimensions de l'ensemble des tores observés et montré l'existence de contraintes géométriques qui restent à élucider.

Puisqu'il était généralement impossible de prévenir l'agrégation des chaines d'ADN, nous avons choisi une autre approche pour analyser le collapse de chaines d'ADN individuelles. Nous avons utilisé une population de virus T5 contenant une fraction de leur génome initial (12-54 kbp). La molécule d'ADN, initialement confinée dans le petit volume de la capside (de 80 nm diamètre) est collapsée par addition de spermine. Par comparaison avec le premier jeu de données, nous avons travaillé à concentration plus élevée en ADN (0.45 mM Phosphates dans l'ensemble de l'échantillon) et la concentration en spermine a été ajustée entre 0.05 et 0.5 mM (ce qui correspond à des rapports de charges +/- bien inférieurs). Ces expériences ont donc été réalisées au voisinage de la ligne de précipitation, dans la « région de coexistence », entre le domaine où les chaines sont en condition de pelote et le domaine ou les chaines sont toutes collapsées sous forme de tores. Nous avons montré l'existence de formes intermédiaires entre ces deux états que nous appelons « tores chevelus » dans lesquels une partie de la molécule est condensées dans le tore alors que l'autre partie reste non condensée. Les distances entre hélices ont également été mesurées. Elles sont plus grandes dans ces structures intermédiaires que dans les tores formés à plus forte concentration en spermine.

Ces deux séries d'expériences montrent l'intérêt des méthodes de cryo-microscopie pour étudier la structure locale des phases condensées de l'ADN. Nous avons montré comment le confinement modifie le comportement de l'ADN en solution et l'intérêt d'étudier ces effets compte tenu de son importance dans le contexte biologique.

Key Words: Cryo-microscopie électronique, condensation de l'ADN, spermine, bactériophage, tore, cristal liquide.

Content of the thesis

1. INTRODUCTION

1.1 DNA as a polyelectrolyte and its interaction with counterions

1.1.1 Structure of the DNA molecule

The DNA molecule consists of two polynucleotide strands that form a right-handed double-helix, 2 nm in diameter (Fig. 1.1a) (Watson and Crick, 1953; Franklin and Gosling, 1953). The two strands have opposite directions and are linked by the hydrogen bonding of complementary base pairs [adenine-thymine (A-T) and cytosine-guanine (C-G)] (Fig. 1.1b). The bases are located inside the double-helix, and the phosphates are aligned along the outside of the helix. Under physiological condition (neutral pH, room temperature, about 200 mM NaCl), the B-form of DNA is dominant (Frank-Kamenetskii, 1997). In its B form, the periodicity of the helix is 3.4 nm, with 10 base pairs per helical turn; the base pairs are perpendicular to the helical axis.

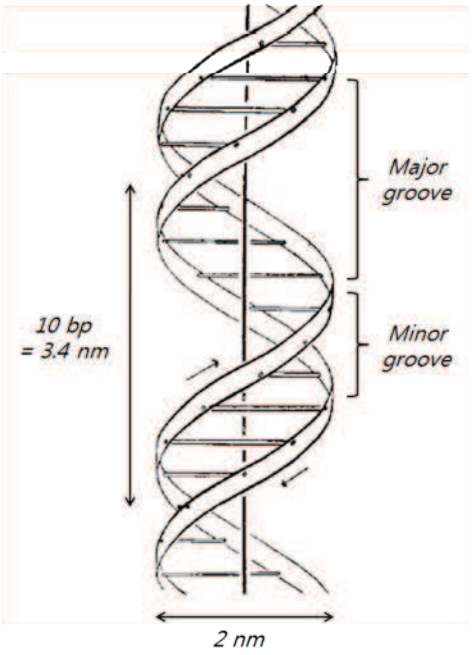

Fig. 1.1a: A schematic drawing of the B-DNA structure [Watson and Crick (1953)]. The two strands of the phosphate backbones have opposite directions.

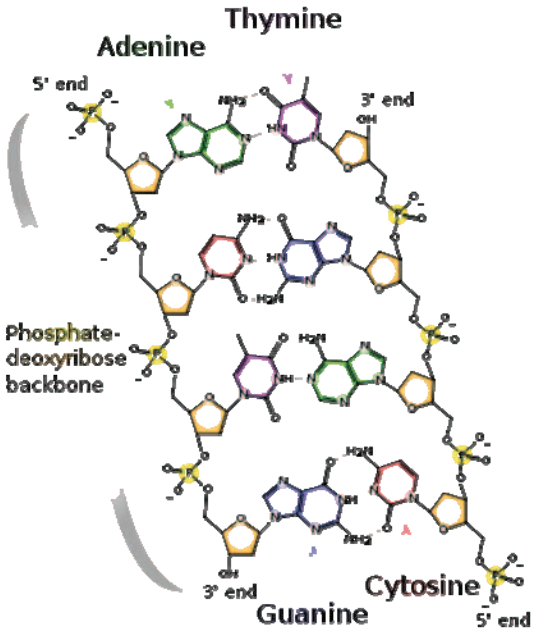

Fig. 1.1b: Formation of the phosphate-deoxyribose backbones and the complementary hydrogen bonding of adenine-thymine (A-T) and guanine-cytosine (G-C).

1.1.2 DNA as a polyelectrolyte

DNA molecule has an extremely high linear charge density (-2e / 0.34 nm = -5.9e / nm), when compared to other biological materials, such as proteins (approximately -0.6e / nm) or cell membranes (-0.1-1e / nm^2). This is due to the fact that each base pair carries two elementary negative charges, the phosphate groups, and the interval between the two base pairs is 0.34 nm. Since these charges are regularly located along the whole polymer surface, a DNA can be treated as a uniformly negatively-charged cylinder of radius R_c = 1 nm (Frank-Kamenetskii, 1997). In aqueous environments, monovalent cations (let say Na^+) would be attracted by the negatively-charged DNA polymer, in a Coulomb potential, when they are close enough the DNA to overcome the thermal fluctuation energy (~kT). The distance r between two charges at which the Coulomb and the fluctuation forces reach in an equilibrium is defined as a characteristic length, the Bjerrum length ($l_B \equiv e^2/4\pi\varepsilon_0\varepsilon_r kT$, where e is the elementary charge, ε_0 is the vacuum permeability, ε_r is the relative dielectric constant, k is the Boltzmann constant, and T is the temperature). That is, the Bjerrum length is the limit where ions association/disassociation occurs, and if $r < l_B$, the monovalent cations are attracted by these negatively charges. Depending on how ions are hydrated, they can form an associated complex or remain close to each other but still mobile. Since l_B = 7.14 Å in water, the high negative charge density of DNA (= -5.9e/nm) induces a concentrated cloud of mobile and hydrated monovalent counterions on the DNA surface. The concentration of the monovalent counterions in the cloud is approximately 1 M, and this value is nearly independent of the bulk cation concentration. This layer of monovalent counterions neutralizes ~76% of the DNA phosphate charges to reduce each phosphate charge to -0.24e (Manning, 1972). [For divalent (+2) and trivalent (+3) counterions, this reduction of residual phosphate charge becomes -0.12e and -0.08e, respectively.] For strong electrolytes in which the electrostatic interaction energy is much larger than the thermal fluctuation energy, this charge compensation makes the DNA electrically “shielded” or “screened” when observed from outside of the counterion cloud [Debye-Hückel screening], where the shielded Coulomb potential is proportional to $e^{-\kappa r}/r$. It means that the electrostatically attracting force decreases rapidly as the distance increases. The Debye screening length (κ^{-1}) becomes ~10 Å when the monovalent salt concentration is 100 mM. Here, the Debye screening length can be thought of as the distance over which mobile charge carriers screen out an oppositely-charged object. We can define an “effective diameter” of a charged polymer in solution as the distance including the geometrical diameter of the polymer and the Debye screening length that is determined by the ionic environment of the solution. In the models of pure electrolyte solution, counterions around DNA are mobile and distributed with radial dependence (Record et al., 1978).

The ionic environment can affect the effective diameter, the elastic stretch modulus, and the persistence length of the DNA molecule. The persistence P of a polymer is defined as the contour length over which correlations in the direction of the tangent are lost (Grosberg and Khokhlov, 1994). DNA being highly negatively charged, its effective diameter is much larger than the geometrical diameter (2 nm) in low salt concentrations (Frank-Kamenetskii, 1997). With high concentration of cations, this effective diameter can decrease significantly because of the screening of Coulomb interactions. Numerous experiments (including single-molecule experiments) measured the decrease of the persistence length as monovalent cations are added (Fig. 1.2; Baumann et al., 1997). This result showed good agreement with the theoretical expectations in which charge contributions to the bending flexibility of the polyelectrolyte chain have been considered (Odijk, 1977; Skolnick and Fixman, 1977; Fixman, 1982; Le Bret, 1982). When increasing the monovalent salt concentration above 0.1 M, the persistence length of DNA decreases and stays constant (around 50 nm). On the other hand, it is known that the torsional rigidity of the chain is nearly independent of the ionic environments (Williams and Maher III, 2000).

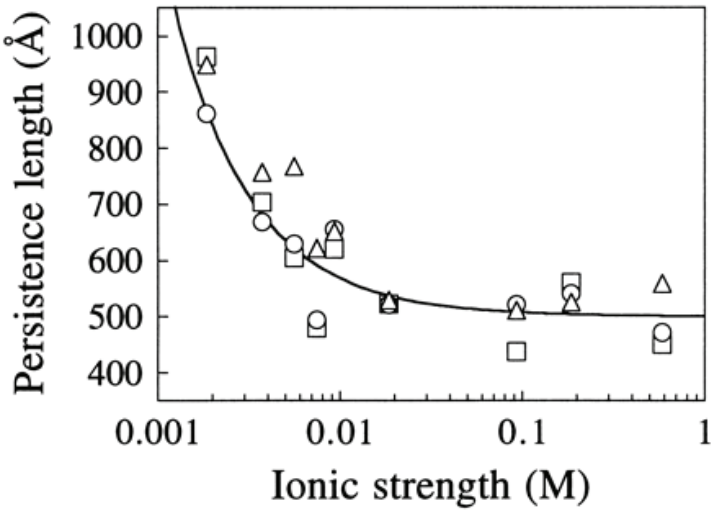

Fig. 1.2: Dependence of DNA persistence length on monovalent (Na+) ionic strength (Baumann et al., 1997).

1.1.3 Polyelectrolyte theories

In order to qualitatively understand the electrostatic behavior of the DNA-polycation system, it is needed to introduce basic theories of polyelectrolytes. The DNA solution with mono- or multivalent cations is a typical example of the many-body system with interactions, which is very difficult to exactly solve mathematically. In this situation, the n-body system can be replaced by a 1-body problem with a well-chosen external field to be easily treated. This approach is called the mean-field theory. In this context, we start from the mean-field Poisson-Boltzmann theory.

1.1.3.1 Poisson-Boltzmann theory

Let us consider a system comprised of a macro-ion and *i*-sort of mobile ions. Then we can approximate the free energy of a solution of macro-ions (polyelectrolyte), counterions, and added salt by the following function of the ion concentrations (Gelbart et al., 2000):

$$F_{PB}\left(\{n_i\}\right) = \int d\vec{r}\left\{\frac{1}{2}\rho\Psi + kT\sum_i n_i \ln\left(\frac{n_i}{n_0}\right)\right\}$$

The second term is the mean-field entropic free energy of the ions with n_i being the concentration of the *i*-th ion species carrying charge $z_i e$. The n_0 is the bulk concentration far away from the considered ions. The first term is the electrostatic energy, with the charge density ρ(**r**) being the sum of charge densities of the macro-ions and the mobile ions:

$$\rho(\vec{r}) = \rho_{macro}(\vec{r}) + \sum_i z_i e n_i(\vec{r})$$

The local electrostatic potential is Ψ(r). The charge density and the potential are related by Poisson's equation,

$$-\nabla^2\Psi = \frac{4\pi}{\varepsilon}\rho(\vec{r})$$

where ε is the dielectric constant of the medium. Minimization of the free-energy equation with respect to the ion concentrations leads to the condition that obeys the Boltzmann distribution:

$$n_i(r) = n_0 \exp\left\{-\frac{z_i e\Psi(r)}{kT}\right\}$$

Using Poisson's equation, we obtain the relation

$$\nabla^2\Psi = -\frac{4\pi e n_0}{\varepsilon}\sum_i z_i \exp\left(\frac{-z_i e\Psi}{kT}\right)$$

for the potential outside the surface of the macro-ions. This nonlinear differential equation is called the Poisson-Boltzmann (PB) equation.

1.1.3.2 Debye-Hückel theory

Now let us consider a specific case in which only one kind of *z*-valent mobile ions exist with the macro-ions. In this case, the Poisson-Boltzmann equation is written as follows (Gelbart et al., 2000):

$$\nabla^2\Psi = -\frac{4\pi e n_0 z}{\varepsilon}\left[\exp\left\{-\frac{ze\Psi(r)}{kT}\right\} - \exp\left\{\frac{ze\Psi(r)}{kT}\right\}\right] = -\frac{4\pi e n_0 z}{\varepsilon}\left[-2\sinh\left\{\frac{ze\Psi(r)}{kT}\right\}\right]$$

To simply solve this equation, we can linearize the hyperbolic sine function by the approximation

$$\frac{e\Psi(r)}{kT} << 1$$

which means that, for large distances *r*, the electrostatic potential eΨ(r) of the macro-ion is small compared to the thermal fluctuation energy kT. With this linearization, the above Poisson-Boltzmann equation reduces to the Debye-Hückel (DH) equation:

$$\nabla^2\Psi = z^2\kappa^2\Psi$$

where $\kappa^2 \equiv 8\pi l_B z^2 n_0 \equiv 8\pi\left(\frac{e^2}{4\pi\varepsilon kT}\right)n_0$

The κ^{-1} is called the Debye screening length and the l_B is the Bjerrum length, where *e* is the elementary charge, *ε* is the water dielectric constant. In water, $l_B \approx 7$ Å at room temperature. Note that, increasing the ionic strength z, the Debye screening length becomes smaller.

Considering the polyelectrolyte (macro-ion) as a long cylinder of radius *a*, with a negatively charged surface in which the charges are uniformly distributed along the axis of the cylinder with distance b, we can obtain an analytical solution as follows (Toma, 2008):

$$-\frac{ze\Psi(r)}{kT} = \frac{2l_B}{b}\frac{K_0(\kappa r)}{\kappa a K_1(\kappa a)}$$

where $K_0(\kappa a)$ and $K_1(\kappa a)$ are the modified Bessel functions. This potential profile is shown in Fig. 1.3 (in solid line).

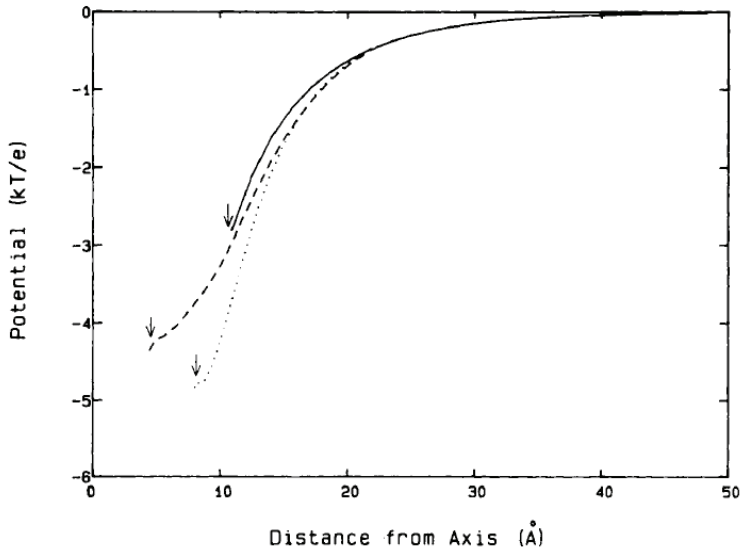

Fig. 1.3: Radial profiles along a line perpendicular to the DNA polymer axis passing through the center of the minor groove (dashed line) and through a phosphate group (dotted line) based on a simulation model (Jayaram et al., 1989). The solid line represents the potential profile for the analytical cylinder model.

For a more realistic case of polyelectrolyes (because DNA is a highly-charged polymer), where the Coulomb interaction energy is no more negligible compared to the thermal fluctuation energy, the (positive) charges condensation near the DNA chain even more proceeds so that numerical calculations are needed to solve the resulting nonlinear Poisson-Boltzmann equation (Le Bret and Zimm, 1984; Fig. 1.4).

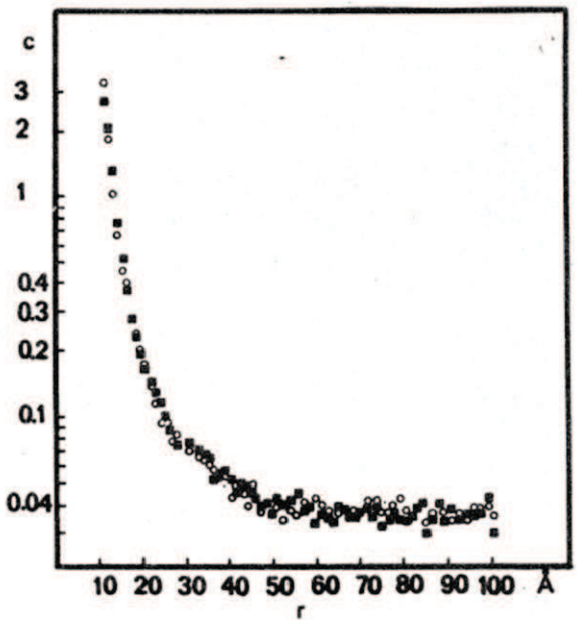

Fig. 1.4: A result of a Monte Carlo simulation on the counterion distribution around a cylindrical polyelectrolyte. The vertical and the horizontal axes represent the local concentration of counterions and the radial distance from the cylindrical polyelectrolyte, respectively (Le Bret and Zimm, 1984).

1.2 DNA condensation

1.2.1 What is DNA condensation?

Let us consider the dimensions of the DNA chain in dilute solution in a classical buffer with monovalent cations (for example, NaCl). Its radius can be estimated by using the relation $R = a \times N^{0.6.}$

with (a) the persistence length of DNA (50 nm). In such good solvent conditions, the chain is swollen (bigger than the Gaussian chain, where the exponent is 0.5). As an example, let us consider the DNA from the bacteriophages Lambda and T5 that we will use in our experiments. The T5 DNA chain, with its 121000 bp has a contour length of 41.14 µm. In solution, this chain would occupy a volume with a radius of 2806 nm (about 70 times the 40Å radius of the capsid) in which it is contained. For lambda phage DNA (48 kbp; 16.5 µm), its occupying volume in hydrated condition would have the radius of 1.6 µm. For human genome (~3×10^9 bp), it would not be 1 m (its contour length) but a volume with 1.2 mm in radius that is much larger than the size of cell nucleus (less than 10 µm in diameter). These comparisons demonstrate that DNA needs to be ***condensed*** to fit into the capsid or the cell nucleus.

Multivalent cations can cause DNA to collapse from the randomly coiled state in aqueous solution into the condensed nanometer scale particles. Various kinds of condensing agents exist, such as cobalt hexamine, polyamines (e.g., spermine and spermidine), polypeptides, proteins, lipids with positively-charged head groups, and positively-charged detergents. All these compounds are able to condense DNA owing that their charge is ≥3 in aqueous solution (Gosule and Schellman, 1976; Chattoraj et al., 1978; Widom and Baldwin, 1980), although divalent cations (+2) will serve in solutions of lower dielectric constant such as water-alcohol mixtures (Wilson and Bloomfield, 1979).

When condensing agents are added to a very dilute solution of long DNA chains, each DNA molecule, initially in a coil configuration, collapses into a compact globule (Fig. 1.5). These globules are usually toroids but rods and spheres or their intermediates are also found (Bloomfield, 1996). This phenomenon is called “DNA condensation”. In the condensed state, the helical segments are locally aligned, the volume fractions of solvent and DNA are comparable, and DNA helices may be separated by just one or two layers of water (Bloomfield, 1996). The highly ordered condensates may thus occupy approximately 10^{-4} the volume of the random coils. For example, the local concentration of DNA within the toroid may be as large as 400-500 mg/ml.

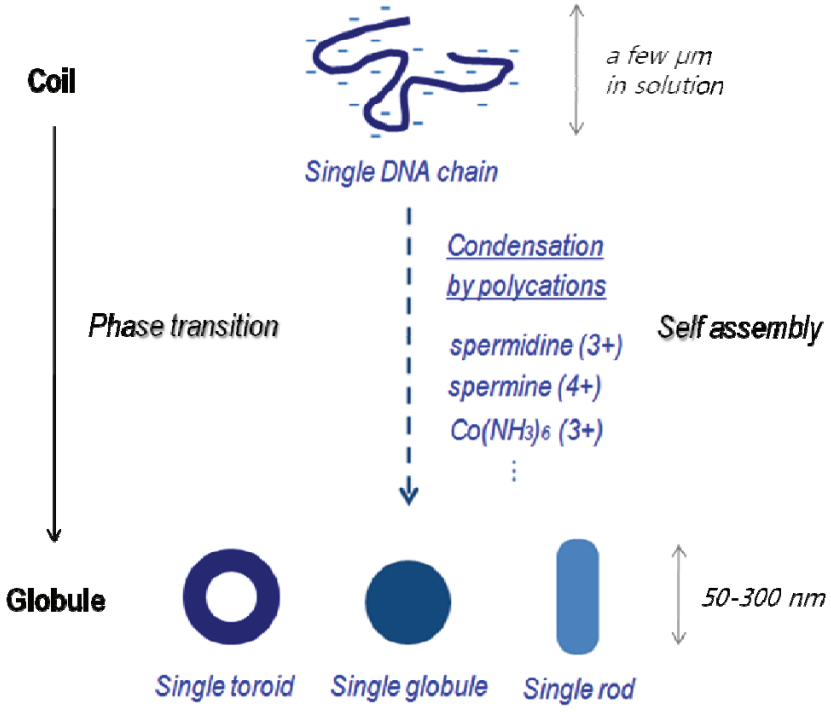

Fig. 1.5: DNA condensation (single-chain collapse or coil-globule transition) into a nanometer-scaled toroid, globule, or rod by multivalent cations.

The DNA chain transition between the extended coil and the collapsed state has been theoretically and experimentally proposed to be discontinuous (or discrete) (Post and Zimm, 1982), or even to be a first order phase transition (Yoshikawa et al., 1996; Baumann et al., 2000). Furthermore, it has been known that the DNA condensation is a reversible process, that is, the condensed DNA can be uncondensed when the physical environment is changed (for example by addition of a large amount of monovalent salt).

The transition of a single DNA chain from the coil configuration to the condensed globule is called "DNA collapse". The DNA collapse means that we are dealing with an intramolecular (or single-molecular) phenomenon, whereas, "DNA aggregation" indicates the multimolecular condensation in which intermolecular phenomena are included.

1.2.2. Collapse versus aggregation

Light scattering experiments have shown that, in the bulk states; (1) There exist fast (millisecond range; at low polycation concentration) and slow (with time constants of ~100 s) processes in DNA condensation, in which the former and the latter have been assigned to the intramolecular and the intermolecular condensations, respectively (Porschke, 1984; Fig. 1.6). It has been reported that the condensation rate depends on the polycation concentration added to the lambda DNA (C_{DNA} = 0.1-0.2 μg/ml) (Widon and Baldwin, 1983): the reaction is very slow (several hours to reach an equilibrium) when the concentration of cobalt hexamine is low ($C_{Co(NH3)6}$ = 8 μM). When the concentration of cobalt hexamine is higher, the reaction completes within 1 min (Fig. 1.6).

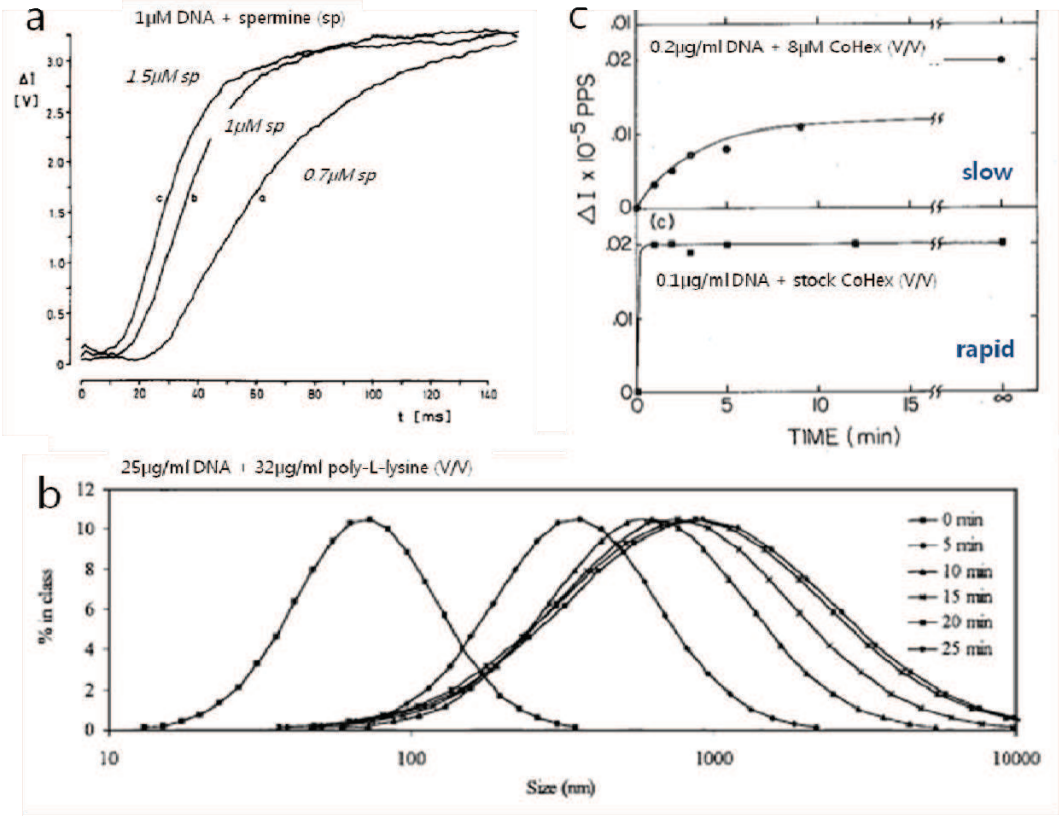

Fig. 1.6: (a) Change of the scattered light intensity (ΔI) as a function of the time (t) after mixing 1 μM T4 DNA with ⓐ 0.7, ⓑ 1.0, and ⓒ 1.5 μM spermine, up to t = 150 ms (Porschke, 1984). (b) Size distribution of polylysine-calf thymus DNA aggregates after various time periods (in the solution of 150 mM NaCl and 20 mM HEPES, pH 7.2), measured by dynamic light scattering up to t = 25 min (Lee et al., 2001). (c)

Lambda DNA condensation rates measured by static light scattering, up to t = 16 h after addition of cobalt hexamine 3+) at two different concentrations. Upper: slow reaction in low CoHex concentration. Lower: rapid reaction in high CoHex concentration (Widom and Baldwin, 1983).

(2) The uncondensed DNA fraction decays approximately exponentially with time, and the condensation rate in its early stage is insensitive to the DNA concentration but proportional to the excessive concentration of the polycation over its critical value at the onset of DNA condensation (He et al., 2000). (3) The size of the DNA aggregates continues to increase over a period of nearly 30 minutes after mixing of DNA and polycation (Lee et al., 2001).

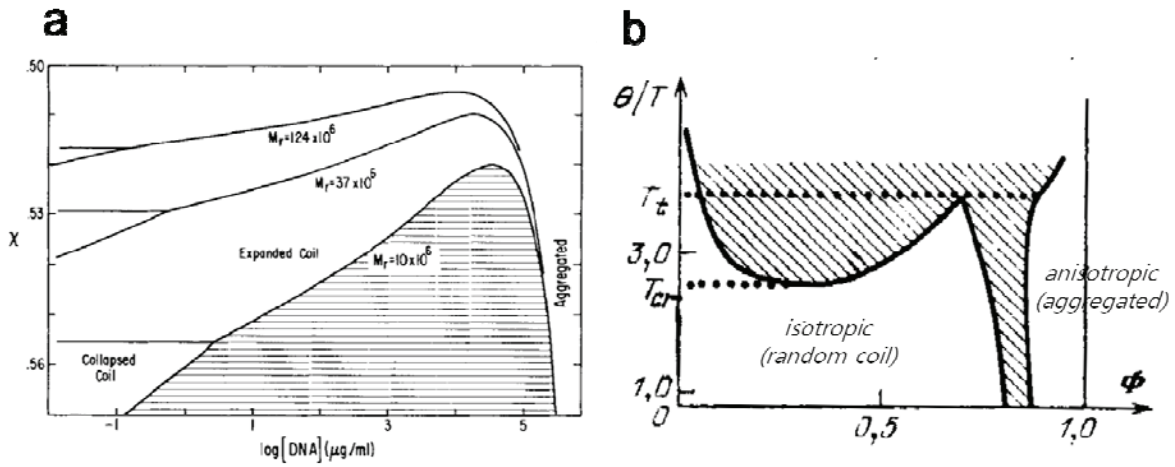

Fig. 1.7: (a) Phase diagram of DNA concentration versus polymer-solvent interaction parameter (χ) for different DNA molecular weight. For each molecular weight, the boundaries separate three regions – expanded coils in solution, collapsed DNA in solution, and concentrated precipitate ("aggregated"). The shaded area marks the two-phase region of the expanded and the collapsed coils (Post and Zimm, 1982). (b) State diagram of liquid crystalline solution of semiflexible rod-like macromolecule (short DNA fragment). The parameter Φ is volume fraction of the rods in the solution [$\Phi = \pi(N/V)Ld^2/4$, where N is the number of rods, V is the volume, L is the length of a rod, and d is the diameter of a rod (L>>d)], and θ is the temperature at which the osmotic second-virial coefficient becomes zero. The shaded area represents the coexistence (two-phase) region of the random coil state and the aggregated liquid crystalline state (Grosberg and Khokhlov, 1994).

This DNA aggregation involves intermolecular (multimolecular) interactions. Through thermodynamical considerations, Post and Zimm (1982) have obtained a state diagram (DNA concentration versus polymer-solvent interaction parameter) of DNA collapse/aggregation, in which three different states exist: (1) the "expanded" random coil, (2) the collapsed coil, and (3) a concentrated phase of aggregated random coils (Fig. 1.7a). In this model, the chain has been considered as a flexible polymer. Collapsed coils can be found only at very low DNA concentration. On the other hand, Grosberg and Khokhlov (1994) have shown essentially the same kind of phase diagram for semiflexible rods (which correspond to the short DNA fragments) (Fig. 1.7b). This diagram (the inverse of temperature versus the volume fraction of the rods in the solution) indicates the phase separation of the isotropic phase (random coil state), the anisotropic phase (aggregated liquid crystalline state), and their coexistence phase in between.

1.2.3 Mechanisms of DNA condensation

From the mean-field PB theory (including the DH theory), as we have already introduced, one can induce two effects of mobile counterions on the macro-ion as follows: (1) The counterions can

reduce the effective charge on the macro-ions. (2) The mobile counterions act to screen the charge of the macro-ion. That is, they give rise to an exponentially decaying electrostatic potential at large distances. As a result, the interaction between the two identical macro-ions always remains repulsive, albeit reduced in magnitude.

Then, why the like-charged (for DNA, negatively charged) chains attract each other by addition of counterions (for DNA, multivalent cations)? How does the attractive interaction come into the polyelectrolyte-counterion system? There are two mechanisms to explain the appearance of attractive interaction between the polyelectrolyte rods (the DNA chains, in our case) induced by the charge compensation of counterions:

The first mechanism involves a Gaussian fluctuation correction to the PB mean-field theory (Oosawa, 1971). By including correlations between the fluctuations of the two rods, Oosawa obtained a nonspecific long-range attractive contribution to the force between rods that varies inversely with the square of the inter-rod distance (a_H, in our case).

Since DNA is a highly charged polyelectrolyte, the condensation of DNA into a nanoparticle requires overcoming an enormous Coulomb energy barrier. Thus the countercharge compensation is essential for the DNA condensation process. By using counterion condensation theory (Manning, 1978), it is calculated that DNA condensation occurs when 89-90% of the DNA phosphate charge is neutralized (Wilson and Bloomfield, 1979). The Manning parameter ξ is defined as $\xi = l_B/b$, where l_B is the Bjerrum length and b is the monomer-monomer distance. Weakly charged DNA chains with below the Manning threshold $\xi_M \approx 1$, the DNA chains swell due to electrostatic repulsions between the segments and their end-to-end distance grows with an increase of the chain length. For $\xi_M \geq 1$, the adsorption of counterions on the DNA chain sets in and transient dipoles are formed between the chain segments (Cherstvy, 2010).]

The second mechanism focuses on the short-range electrostatic correlations between the two counterion clouds on the both polyelectrolyte rods. By using computer simulation methods, a strong short-range interaction is obtained whose strength of attraction increases on lowering the temperature (Grønbech -Jensen et al., 1997; Ha and Liu, 1997).

Other mechanisms explain the condensation phenomenon by (1) the direct “ion-bridging” of neighboring DNA chain segments by polycations based on short-range electrostatic attractions (Raspaud et al., 1998) [Contrarily to trivalent ions where the effect on DNA is very local, limited to a few consecutive monomers, linear flexible polycations interact with DNA bases that are significantly far apart, promoting bridging between different sites of in the DNA chain or between different DNA chains (Dias and Pais, 2010; Korolev et al., 2010).], and/or (2) the attraction force induced by long-range attractive hydration forces caused by the counterion-induced restructuring of water molecules between adjacent DNA chains (Rau and Parsegian, 1992; Rouzina and Bloomfield, 1996).

1.2.4. Toroids, globules and rods

Early conventional TEM studies (Haynes et al., 1970; Chattoraj and Gosule, 1978) showed that various shapes of the polycation-DNA condensates, such as toroids, rods, spheroids, bundles, and their intermediates, formed from bulk solutions (Fig. 1.8). The toroids are usually co-produced with other minor morphologies (rods, spheroids, and bundles) in the same ionic environment, and in most cases they are found to be clustered or aggregated. Haynes et al. (1970) observed that (with sperm DNA and poly-L-lysine) only bundle networks were formed in a low salt concentration, whereas toroids

and rods were found in a high salt concentration (1.1-2.0 M NaCl). Recent AFM studies have also reported similar diverse morphologies (Martin et al., 2000; Wan et al., 2009; Fig. 1.9).

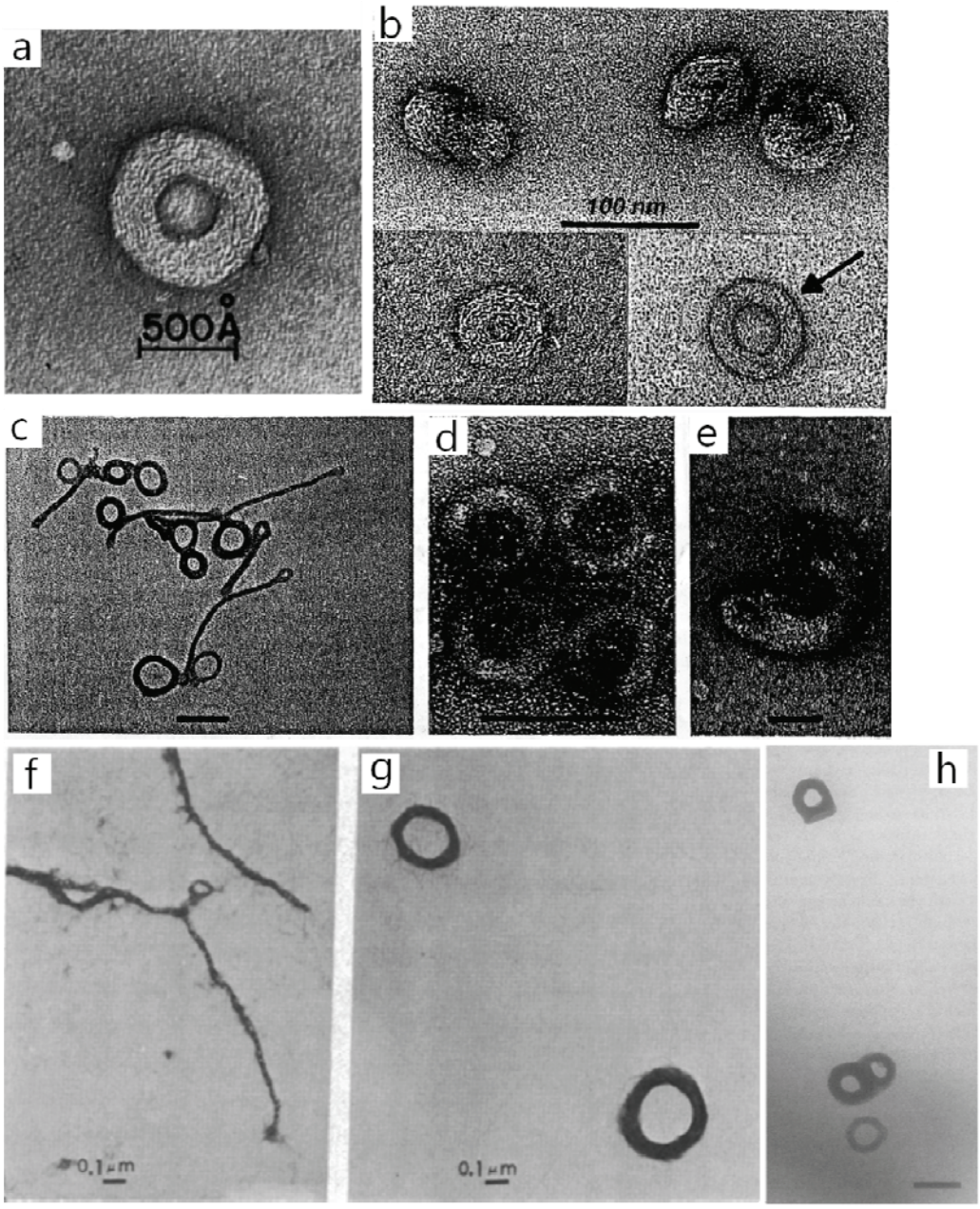

Fig. 1.8: Diverse shapes of the DNA condensates in the early conventional TEM studies. The micrographs present the condensates of (a) Toroid - T7 DNA + spermidine (Gosule and Schellman, 1976), (b) Spheroids and toroids - P4 DNA + spermidine (Chattoraj et al., 1978), (c) Rods, toroids, and their intermediates - T7 DNA + spermidine (Chattoraj et al., 1978), (d) Monomolecular toroids - T7 DNA + spermidine (Chattoraj et al., 1978), (e) Intermediate morphology between toroid and rod - T7 DNA + spermidine (Chattoraj et al., 1978), (f, g) Rods, toroids, and their intermediates - calf thymus DNA + H1 (Hsiang and Cole, 1977), (h) Toroids – lambda DNA + cobalt hexamine (Widom and Baldwin, 1980).

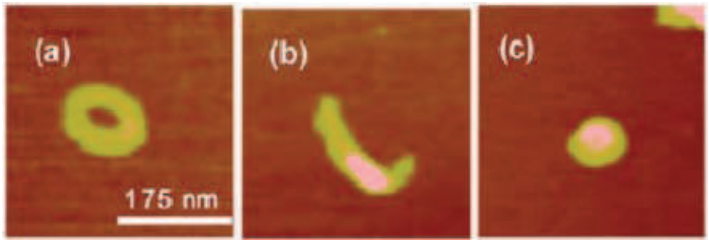

Fig. 1.9: AFM images of a toroid (a), a rod (b), and a spheroid (c), produce with 6.7 kbp plasmid DNA (10 µg/ml) on a chemically modified mica surface (Wan et al., 2009).

The mechanisms for polycation-induced attraction of DNA segments are relatively short-ranged, while the electrostatic repulsion between imperfectly compensated DNA segments is a long-range interaction. The competition between long-ranged electrostatic repulsion and short-range attractions can drive the formation of a rich polymorphism of structures, interplaying with the semi-flexibility of the DNA chain (Wong, 2006).

A simulation study (Stukan et al., 2003) has obtained state diagrams for the collapse transition of a stiff macromolecule as a function of temperature and chain stiffness: it was predicted that the regimes for extended coil, toroid, spheroid, and disc-like globule can exist in the temperature-stiffness domain, dependent on the chain length (Fig. 1.10). For the internal structures of the DNA condensates, it has been experimentally/theoretically accepted that the toroid and the bundle are built up by circumferential winding of DNA chain(s) and multimolecular aggregation in parallel ordering, respectively (Iwataki et al., 2004).

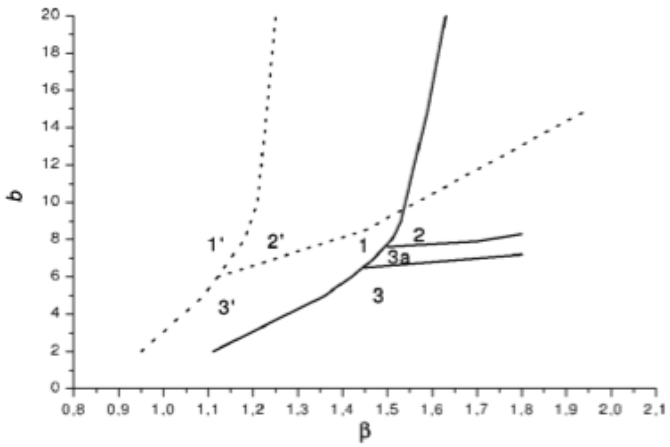

Fig. 1.10: Computer-simulated diagrams of states for semiflexible polymer chains with the number of monomers N = 80 (dotted lines) and N = 40 (solid lines) in variables stiffness (b) versus inverse temperature (β = 1/T). The regions of coil (1, 1'), toroid (2, 2'), spheroid (3, 3'), and disk-like globule (3a) are shown (Stukan et al., 2003).

Many studies have been done to determine the physicochemical parameters that govern the shape, dimension, and structure of the DNA condensates. In cryo-EM, TEM, and AFM observations, linear DNA molecules tend to condense into mostly toroids, plus partly rods (Böttcher et al., 1998; Allen et al., 1997; Haley and Geng, 2010; Hud et al., 1993; Hsiang and Cole, 1977), whereas circular DNA molecules resulted in toroids (Böttcher et al., 1998; He et al., 2000; Haley and Geng, 2010). A TEM study by Sarkar et al. (2007) reported that HU, a non-sepuence-specific DNA binding protein, can completely shift the condensed DNA morphology from toroids to rods. This was thought to be because, in contrast to the toroid where DNA is only smoothly bent, the HU sharply bends DNA chain so that rod-like shape is favored for the condensates. On the other hand, supercoiled and single-stranded (ss) DNA molecules condensed principally into rods and small spheroids, respectively (Hsiang and Cole, 1977; Sarkar et al., 2007; Haley and Geng, 2010). For the case of ssDNA, the

formation of condensed spheroid was contributed to the high flexibility of the ssDNA chain. This is also supported by simulation study by Ou and Muthukumar (2005), which showed that for high strengths of electrostatic interactions, sufficiently stiff polyelectrolytes form toroids in the presence of multivalent counterions, whereas flexible polyelectrolytes form disordered globules. It has also been suggested that the inhomogeneity of the shape of DNA condensates in a single ionic condition may be due to the difference in diffusion coefficients of the DNA and the polycations in their mixing process (Pinto et al., 2009).

Continuous transitions between toroid-spheroid (Takenaka et al., 2005) and toroid-rod (Stevens, 2001) have been modeled as a function of persistence length, surface energy and/or bond angle energy of the DNA chain. There is also a report by using fluorescence microscopy and TEM (Baigl and Yoshikawa, 2005) stating that, at a constant spermine concentration (20-1000 μM), compact T4 DNA (166 kbp) toroids partially unfold with an increase in dielectric constant (ε_r; from 80 to 170) of the medium.

The DNA bundles have been observed in the early work by Klimenko et al. (1967) by using conventional TEM. The bundles, as well as the toroids, were formed in the bulk by the T2 phage DNA chains (200 kbp) from damaged capsids by the contrasting acidic agents (uranyl acetate or phosphotungstic acid). They were 5-30 nm in diameter and showed branching morphologies in some cases. By using fluorescence microscopy and AFM, Iwataki et al. (2004) have observed the DNA bundles formed with T4 DNA (166 kbp; C_{DNA} = 10 μM) and an excess of trivalent polyamine spermidine (Cspd = 150-200 μM). The diameter and the length of the bundles were approximately 250 nm and several μm to several hundreds μm, respectively. The DNA bundles coexisted with globules and coils in Cspd = 150 μM. On the other hand, only bundles were found in higher spermidine concentration (Cspd = 200 μM). In lower DNA concentration (C_{DNA} < 1 μM), no bundle structures formed regardless of the spermidine concentration. Recently, the DNA bundles have been observed by using cryo-EM (Leforestier and Livolant, 2009). The bundles were formed by T5 DNA and spermine (Csp = 50 mM), and alternating domains of parallel striations have been observed with a_H = 2.88 nm.

Among the various morphologies of the condensed DNA self-assemblies, the toroids have attracted the highest interests because of their fundamental geometry and structural uniqueness.

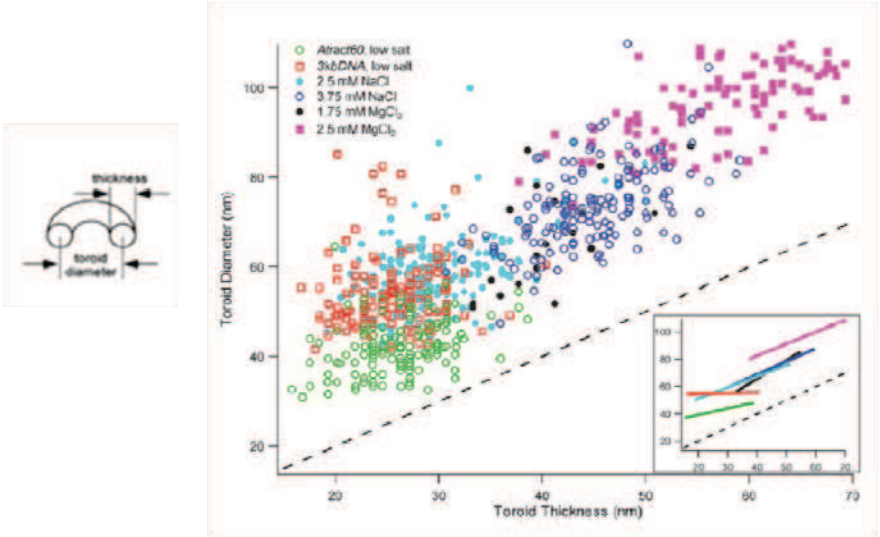

Fig. 1.11: Plot of the diameter versus the thickness of 3 kbp plasmid DNA toroids (condensation induced by cobalt hexamine 3+ under several ionic conditions). The "Atrack60" is the same plasmid DNA with an additional 720 bp insert in which 60 A-tracks are contained. The dashed line represents the position where the diameter and the thickness are equal (Conwell et al., 2003).

The outer diameter and the inner hole size have been measured to be generally ~100 nm and ~30 nm, respectively. Nevertheless, larger spermidine-T5 DNA toroids (outer diameter ~200 nm) have been produced in certain physicochemical conditions (Yoshikawa et al., 1999, Lambert et al., 2000). Ionic salt conditions in the solution have been found to be able to affect the formation for DNA toroids (Plum et al., 1990). In a recent TEM study by Conwell et al. (2003), it has been reported (with linearized plasmid DNA (3 kbp) plus Cobalt hexamine (3+) that (i) the diameter and the thickness of a toroid are correlated, (ii) the increased ionic strength causes a greater increase in toroid diameter than toroid thickness, and (iii) the toroid dimensions vary as a function of salt (Fig. 1.11).

A cryo-EM study on the condensation of an open circular plasmid DNA (~7.7 kbp) with spermine, the number of chains in a toroid was estimated to be 1-19 (Böttcher et al., 1998) For shorter linearized plasmid DNAs with spermidine, a TEM observation reported that the number of chains in a toroid seems to increase for the shorter DNA molecules [~10 chains for 4.4 kbp DNA and ~100 chains for 400 bp DNA]. For even shorter DNA (140 bp), no toroids but numerous clumps of condensates were formed (Widom and Baldwin, 1980). There is also an AFM report in which spermidine-DNA (48 kbp) toroids formed by a single DNA chain were obtained in very low DNA concentrations ($C_{DNA} \leq 1$ ng/μl) with a short reaction time (10 min), whereas multimolecular toroids were observed in higher C_{DNA} (1-10 ng/μl) with a longer reaction time (10-35 min) (Lin et al., 1998).

Since the early investigations by using optical dichroism, X-ray diffraction and EM, it has long been thought that a DNA toroid would be formed by the circumferential wounding of DNA chain(s), with an interchain (interhelical) spacing of 2.0-3.3 nm, and/or forming liquid-crystalline structure (Haynes et al., 1970; Marx and Reynolds, 1982; Marx and Ruben, 1983), remaining in its B-form (Haynes et al., 1970; Widom and Baldwin, 1980). The electrostatic bridging of adjacent helices by multivalent cations has been thought to be the reason for the side-by-side structure (Widom and Baldwin, 1980). A recent cryo-EM study by Hud and Downing (2001) has obtained images that clearly showed a series of concentric fringes and hexagonal arrangements in top- and side-views, respectively, of the lambda DNA-cobalt hexamine toroid, in which the DNA chains are packed with an interhelical spacing of 2.8 nm (Fig. 1.12).

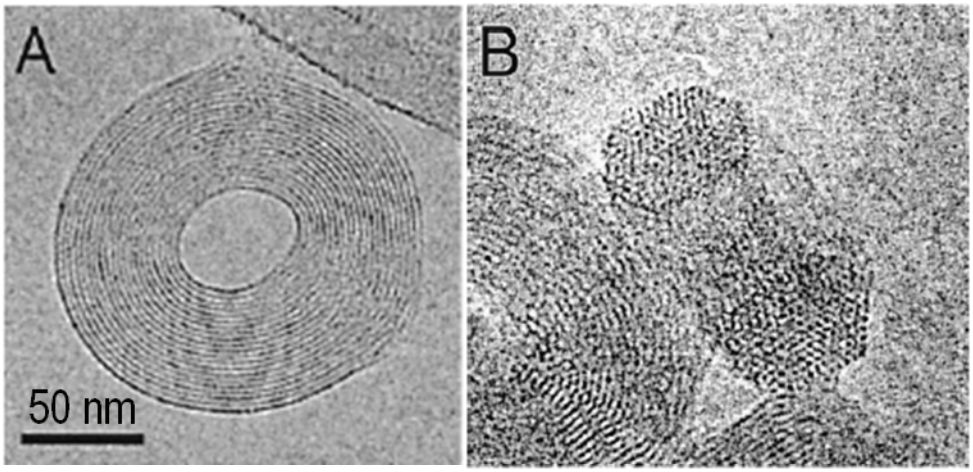

Fig. 1.12: Cryo-electron microscopic images of the DNA toroids formed in the bulk solution (lambda DNA + cobalt hexamine) (Hud and Downing, 2001).

1.2.5. Intermediate states of toroid formation

Real-time AFM studies in aqueous environment provided images showing DNA structures at intermediate states of the condensation process, in the time range 20-200 minutes. Fang and Hoh (1998) showed that, by using 3 kbp DNA (C_{DNA} = 0.5 nM) and 30 μM spermidine (3+), there is a variability in the morphology of the mica-adsorbed DNA condensates (multiloop or flower-shaped structures) during 30 min, with no more structural changes after this period of time. Ono and Spain (1999) have observed that, with supercoiled 4.3 kbp DNA (0.4 ng/μl) and 1% 3-aminopropyltriethoxysilane-treated mica, the interhelical distance in the DNA rods and toroids adsorbed on a mica surface fluctuates during 25 min (Fig. 1.13). Martin et al. (2000) have reported the transition between the mica-adsorbed toroids and rods during 40 min, by using 4.4 kbp DNA (C_{DNA} = 10 μg/ml) and a cationic polymer (PEG-modified polyamidoamine; 70 μg.ml) (Fig. 1.14). These data cannot be directly compared to the DNA condensates formed in the bulk because, in AFM experiments, positively charged surfaces (e.g. mica) interact with the polycation-DNA condensation system and interfere with the condensation mechanisms.

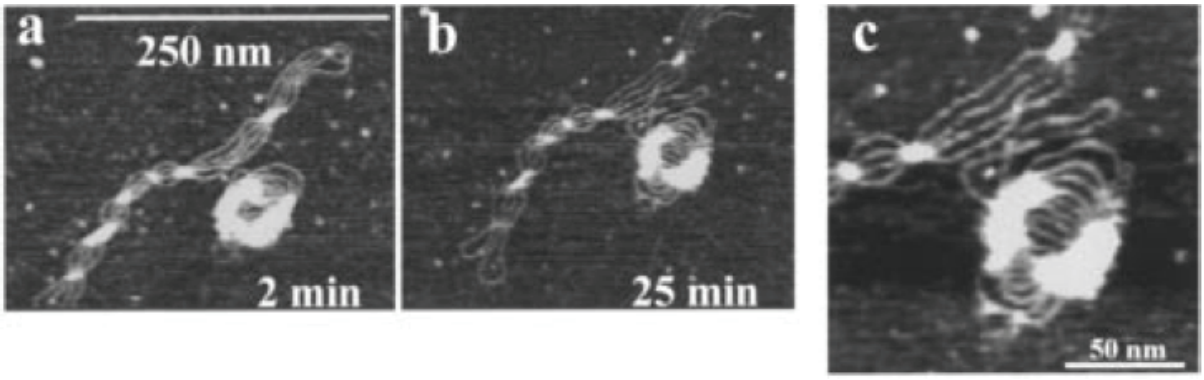

Fig. 1.13: Real-time AFM imaging of the DNA condensation: (a) reaction time = 2 min, (b) reaction time = 25 min, (c) enlarged image of (b). These images show dynamic interhelical distance fluctuations in the toroidal and rod-like DNA condensates with time. The DNA condensates were produced by depositing supercoiled plasmid DNA (4.3 kbp; 0.4 ng/μl) in Tris-EDTA buffer on a chemically modified mica surface (1% 3-aminopropyltriethoxysilane-treated mica) (Ono and Spain, 1999).

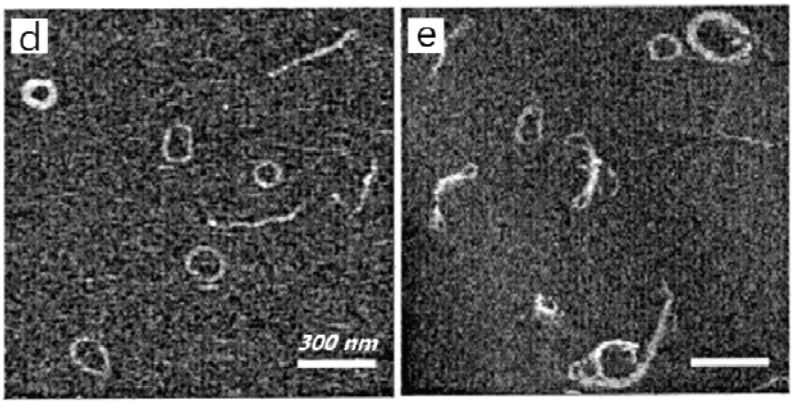

Fig. 1.14: AFM images of toroidal, rod-like, and intermediate condensates formed with 4.4 kbp plasmid DNA, and a cationic poly(amidoamine) (Martin et al., 2000).

A simulation study for the kinetics of DNA collapse (Ou and Muthukumar, 2005) has shown that: (1) during the condensation process, there exist several metastable structures which frustrate the

formation of toroids, and (2) there is a generic pathway involving the nucleation of primary loop followed by a growth process where the rest of the chain is folded continuously on the primary loop (Fig. 1.15).

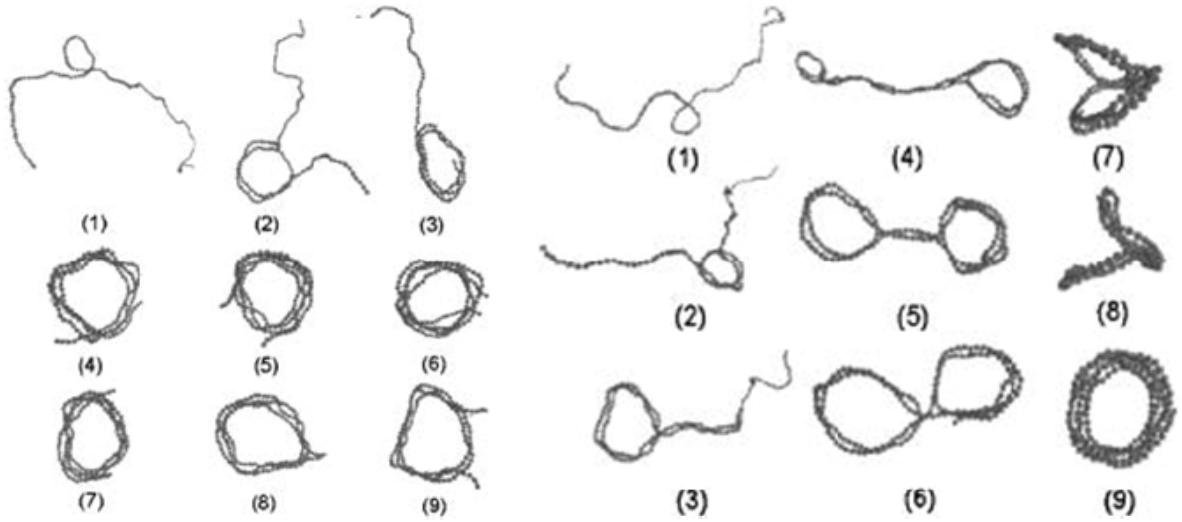

Fig. 1.15: Computer-simulated snapshots of the formation for a DNA toroid with single/multiple nucleation(s) by a trivalent cation. The left part represents the condition of higher εT, when compared to the right, where ε is the dielectric constant and T is the absolute temperature. The index (1)-(9) represents the evolution of time (Ou and Muthukumar, 2005).

1.2.6. Electrophoretic mobility of the DNA condensates

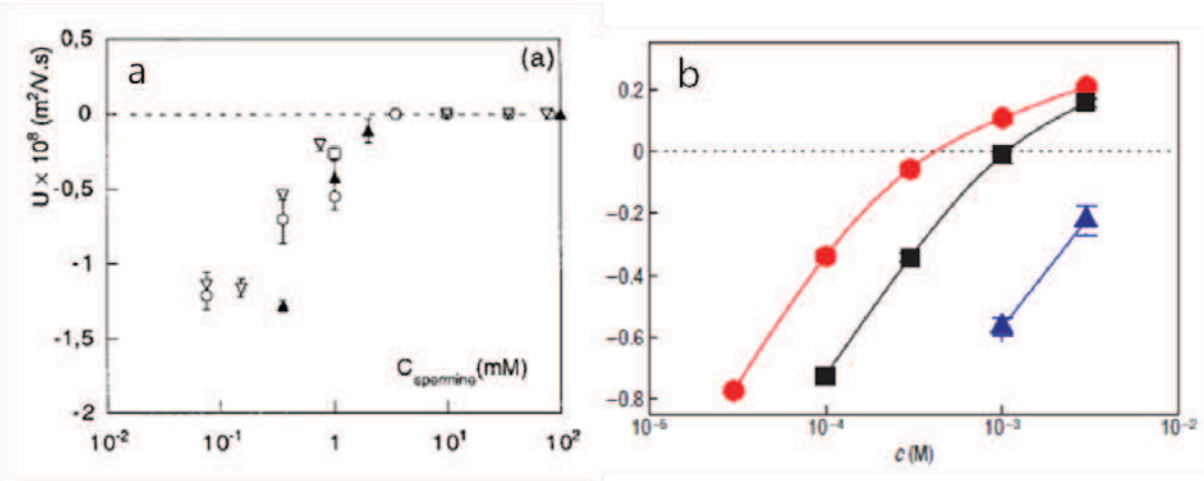

Fig. 1.16: (a) Electrophoretic mobility of dsDNA condensed with protamines (filled circles) or condensed with histones H1 proteins (filled squares) in 10 and 2mM monovalent salt respectively. Aggregates turn from negative to positivce (Raspaud et al., 2006).(b) Electrophoretic mobility (μ) of condensed dsDNA (8 kbp; 50 ng/ μl) as a function of the spermine concentration in a buffer containing 1 mM TRIS (red circles), 10 mM TRIS (black squares) and 10 mM TRIS + 50 mM KCl (blue triangles) (Besteman et al., 2007).

DNA condensates behave as soluble colloidal particles, where the strong electrostatic repulsive interactions between the DNA segments are screened by the counterions (Yamasaki et al., 2001). By measuring the electrophoretic mobility of the polycation-DNA complexes, it has been known that the charge inversion of the DNA may accompany the condensation of DNA (Raspaud et al., 2005; Besteman et al., 2007; Fig. 1.16a).

1.3. Condensation of DNA by polyamines

1.3.1. Polyamines

Polyamines are basic organic compounds and are present in all living cells and tissues - from prokaryotes to eukaryotes. Naturally occurring polyamines [putrescine [$NH_2(CH_2)_4NH_2$], spermidine [$NH_2(CH_2)_4NH(CH_2)_3NH_2$], and spermine [$NH_2(CH_2)_3NH(CH_2)_4NH(CH_2)_3NH_2$]; exist in (or around) bacteria and eukaryotic cells in millimolar concentrations (Ames and Dubin, 1960; Pegg and McCann, 1982). Polyamines are small linear (approximately 6-16 Å in length) polycations (Thomas and Thomas, 2001; Ouameur and Tajmir-Riahi, 2004): putrescine (diamine) is divalent (2+), spermidine (triamine) is trivalent (3+), and spermine (tetra-amine) is tetravalent (4+). Since polyamines are completely protonated under physiological environments, they can interact with negatively charged biomolecules and especially with nucleic acids, proteins, and phospholipids (Tabor and Tabor, 1985). The polyamines participate in many cellular processes through binding to DNA, RNA, nucleotide triphosphates and other acidic substances (Igarashi and Kashiwagi, 2000). Especially, polyamines are related to many metabolic pathways in which nucleic acids are involved, by means of regulating the rate of replication, transcription, and translation, because they play central roles in DNA/RNA conformational transition and compaction (Ames and Dubin, 1960; Baeza et al., 1987; Ouameur and Tajmir-Riahi, 2004). Polyamines are therefore essential for cell growth processes, and they have also been associated with carcinogenesis (Bachrach et al., 2001).

1.3.2 Spermine-DNA phase diagram

A long single DNA molecule, which is in a coil configuration in the presence of monovalent cations, may condense into a compact globule (and precipitates from the solution) upon addition of polyamines spermidine (+3) and spermine (+4) (Bloomfield, 1996). However, at high polyamine concentration, the DNA chain is soluble again. This dissolution-precipitation-redissolution phenomenon can be expanded to a general phase diagram when we change the parameters, for example, the concentrations of DNA and polyamine. Raspaud et al. (1998) investigated the phase change of dsDNA with spermine as a function of the DNA length and the concentrations of DNA, polyamines, and monovalent salt. The domain where the precipitated DNA coexist with the dilute solution (two phases system) is limited by the precipitation line and the resolubilization line, as drawn on Fig 1.17. Considering the precipitation threshold, there are three regimes of DNA concentration. In the low C_{DNA} regime (below 0.1 mM; regime n˚3 in the figure), the spermine $C_{precip.}$ increases smoothly with C_{DNA} and depends on the DNA molecular weight. In the intermediate C_{DNA} regime (between 0.1 and 10 mM; regime n˚2 in the figure), the precipitation threshold ($C_{spermine}$ precip.) increases linearly with the DNA concentration. In the high C_{DNA} regime (above 10 mM; regime n˚1 in the figure), the increasing rate of the spermine $C_{precip.}$ lowers and deviates from the linearity. In contrast, the redissolution threshold ($C_{spermine}$ redissol.) remains nearly constant throughout the whole C_{DNA} regimes. [For lambda DNA, the redissolution threashold is 200 mM.] The presence of the initial monovalent counterions reduces the domain in which DNA precipitation occurs, for both short and long DNA chains.

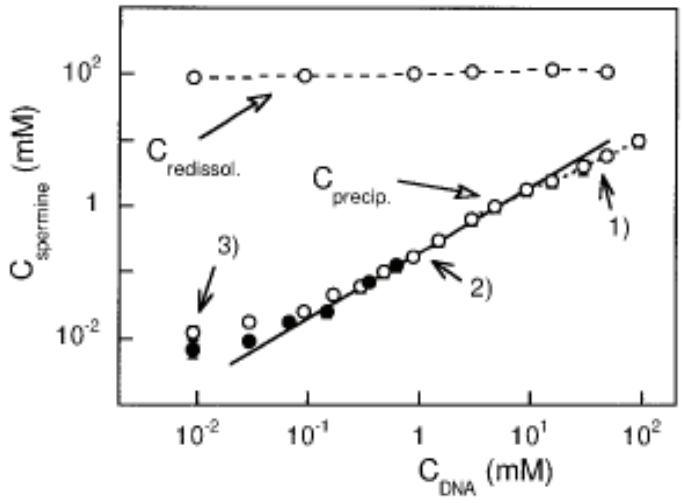

Fig. 1.17: Phase diagram of short DNA fragments (50 nm, 146bp) precipitated by spermine, covering a large range of DNA and spermine concentrations (C_{DNA} and $C_{spermine}$). DNA is soluble below the precipitation line ($C_{precip.}$) and above the redissolution line ($C_{redissol.}$). Between these two lines, DNA is partially or totally precipitated, in equilibrium with the soluble fraction (two-phases region). Conditions of precipitation depend on the DNA concentration and three regimes have been identified (1, 2, 3) (Raspaud et al., 1998).

1.3.3 Structure of polyamine-DNA condensates

Pelta et al (1996) reported that the polyamines-DNA aggregates, formed by short DNA fragments (146 bp), are liquid crystals. The liquid crystalline state corresponds to a particular state of matter where molecules are ordered (as in a crystal) and free to move the ones with respect to the others (as in a fluid). Polyamine-DNA liquid crystals may be either cholesteric or 2D columnar hexagonal, as illustrated on Figure 1.18. In the cholesteric phase, molecules are aligned in parallel and their orientation rotate along an axis called the cholesteric axis. In the hexagonal phases, molecules are aligned in parallel and form a hexagonal lattice in section.

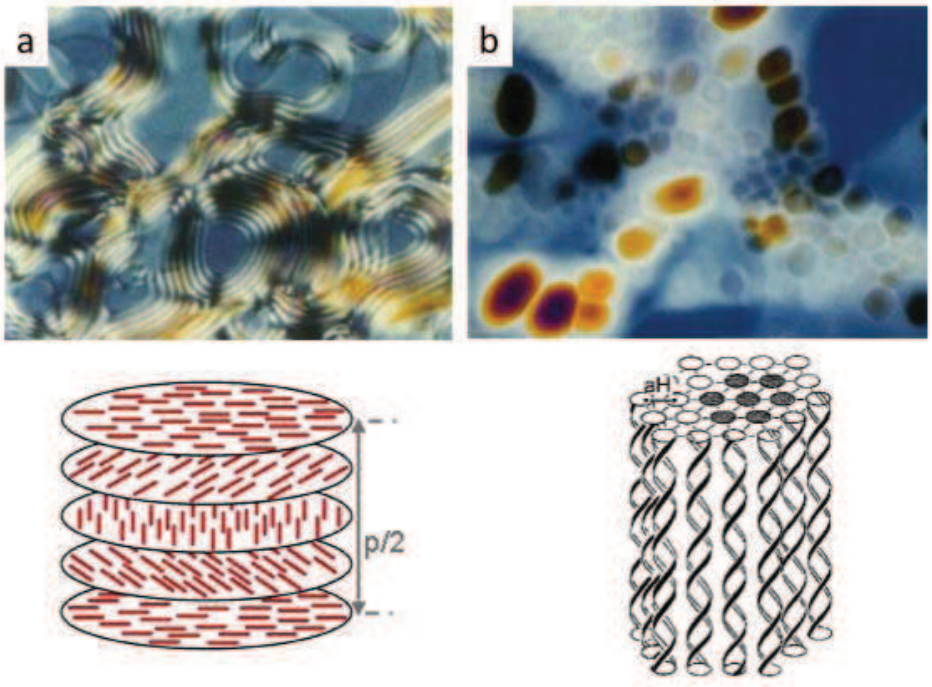

Fig. 1.18: Spermidine-DNA aggregates observed in polarizing microscopy, between crossed polars. a) Fingerprint patterns of the cholesteric phase. The distance between two consecutive lines corresponds to half the helical pitch (180° rotation of the molecular orientations) as drawn below where molecules are represented by red lines in a series of parallel fictive planes. b) domains of the columnar hexagonal phase (as drawn, below) in a planar cholesteric phase.

Measurements of the interhelical spacing (a_H) in the liquid crystalline spermine-DNA condensates have been done by x-ray diffraction (Pelta et al., 1996; Raspaud et al., 2005; Fig. 1.19). When aggregates are prepared from dilute DNA solutions (0.6-3 mM of 146 and 48 kbp DNA), the interhelical spacing stays nearly constant (28.15 ± 0.10 Å) for Csp ≤ 10 mM, and further progressively increases with Csp. The a_H also increases with the monovalent salt concentration. Higher interhelix distances were found in the high concentration regime of DNA (Fig 1.19b)

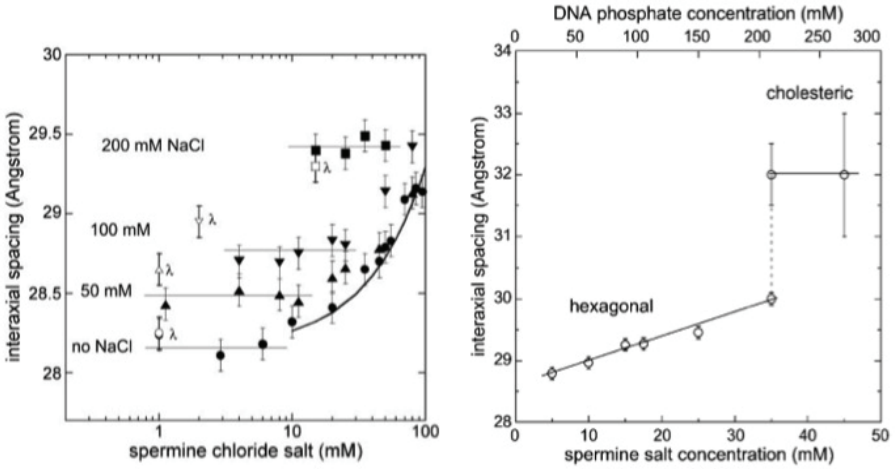

Fig. 1.19: Variation of the interhelix spacing (a_H) in the aggregates of DNA condensed by spermine a) in the low DNA concentration range (experiments performed with $C_{DNA=}$ 0.6 or 3 mM; regime n˚2 in the Fig. 1.17) and b) in the high DNA concentration range (regime n˚1 in the Fig. 1.11) (Raspaud et al., 2005).

Following the work by Hud and Dowing (2001), a few cryo-electron microscopy studies have been done to analyze the structure of polyamine-DNA aggregates formed by long DNA molecules (> 100 kbp). Lambert et al. (2000) used the T5 bacteriophage/FhuA receptor system (to be described in the next chapter) to inject DNA inside vesicles or in the bulk and to condense this DNA with spermine. Using this method they were able to form toroids much larger than usual, some with a tunnel like structure (Figure 1.20).

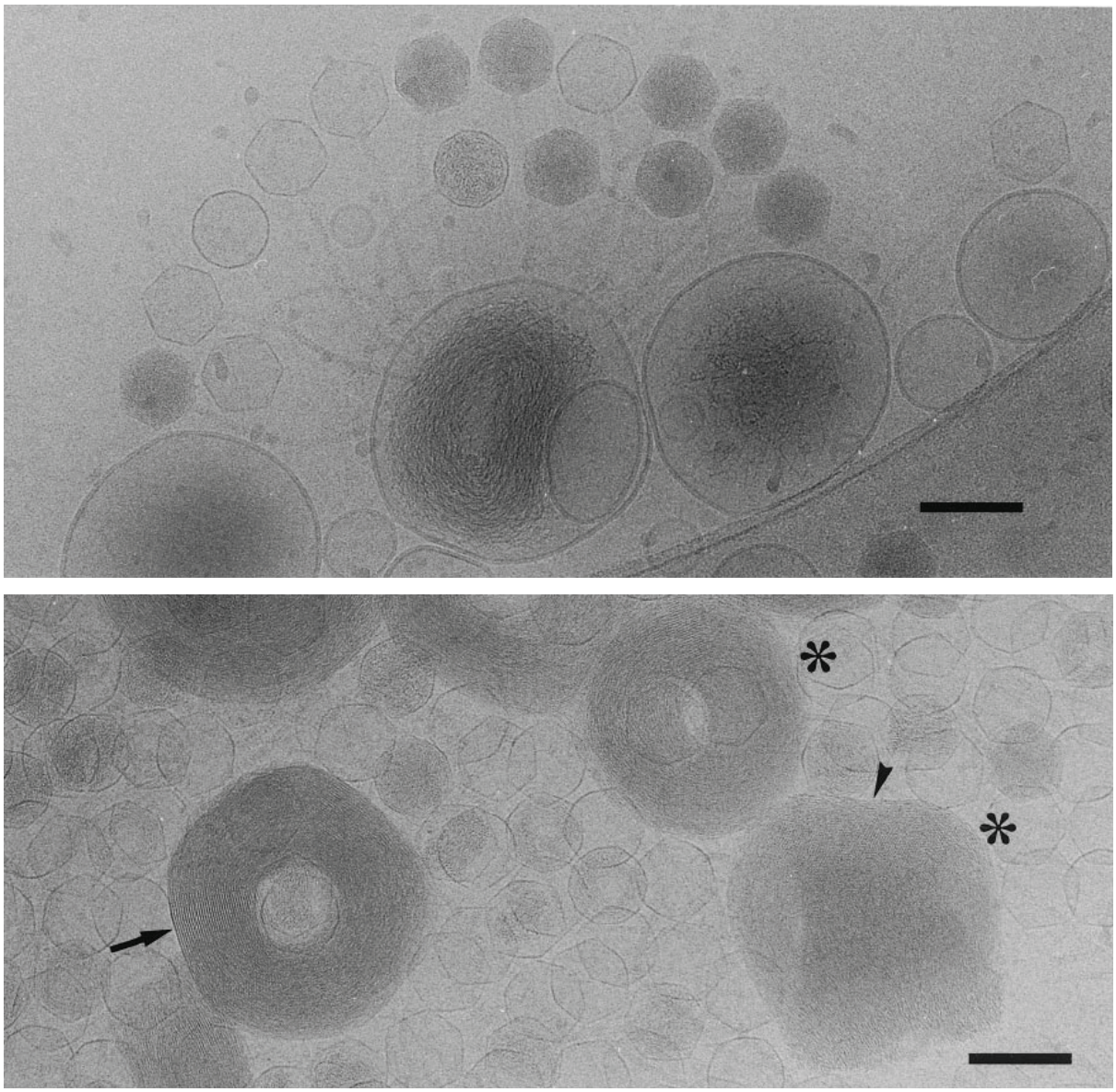

Fig. 1.20: CryoTEM of DNA toroids formed inside vesicles (top) or in the bulk (bottom) upon addition of spermine (Csp = 20-50 mM, 150 mM NaCl, 20 mM Hepes, pH 7). Scale bars = 100 nm. (Lambert et al., 2000)

Using the same bacteriophage system Leforestier and Livolant (2009) focused on the structure of the spermine-DNA toroids resulting from the collapse of a single long chain inside the bacteriophage capsid (~80 nm in diameter) (Fig. 1.21). Under ionic conditions that have been tested (50 mM spermine, with 10 mM NaCl, 1 mM $CaCl_2$, 1 mM $MgCl_2$, or with 10 mM NaCl, 1 mM $CaCl_2$, 10 mM $MgCl_2$, in 10 mM Tris buffer of pH 7.6), DNA is hexagonally packed and the interhelix spacing a_H = 2.8 nm. Details of the toroid structure have been revealed, especially the twist walls caused by the frustration arising from the competition between the chirality of the DNA and its dense hexagonal packing. Moreover, due to the curvature of the toroid, the adjacent and correlated DNA chains present period variations of the pitch of the DNA double helix along the circumference of the toroid (Fig. 1.22).

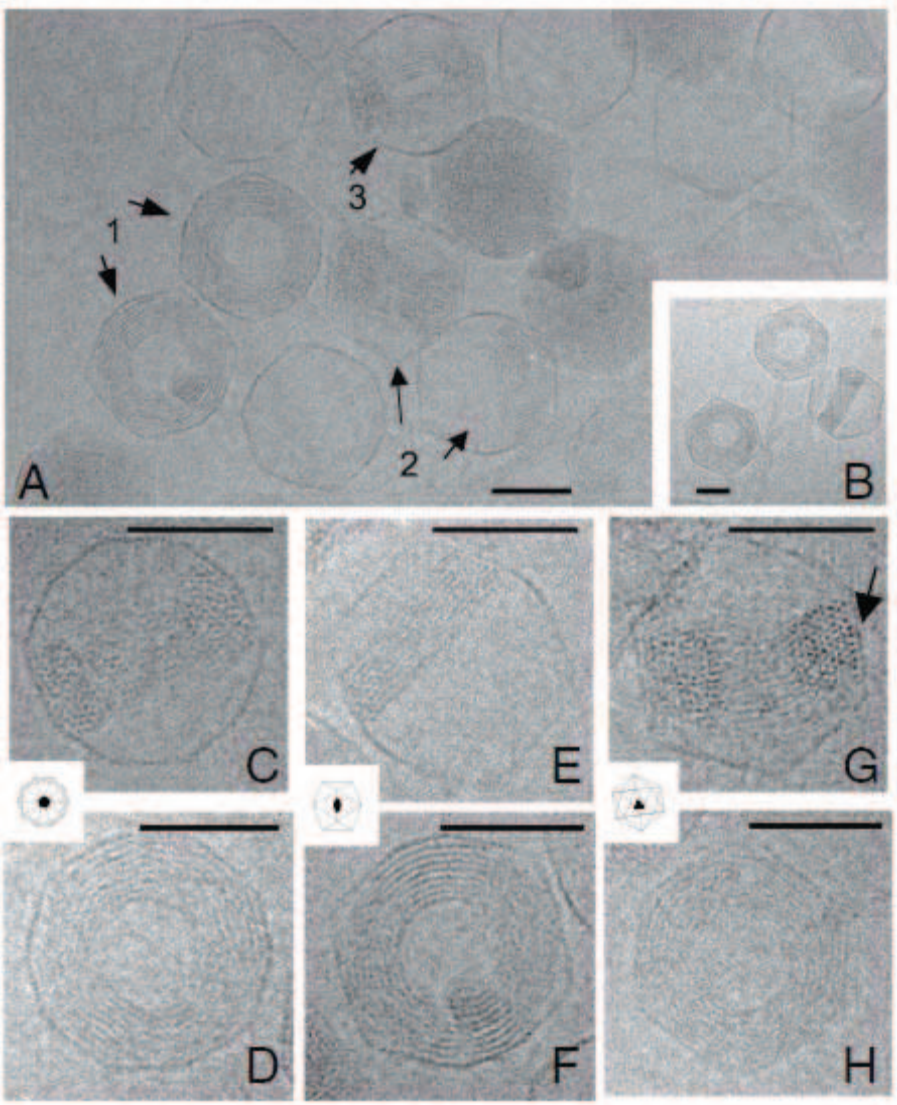

Fig. 1.21: CryoTEM of DNA toroids formed inside the T5 bacteriophage capsid (shortened T5 DNA + spermine) (Leforestier and Livolant, 2009). The images show the hexagonal lattice of a DNA chain (C-G) in the toroid side-view, and its projection (series of parallel striations) in the top-view. Scale bars = 50 nm.

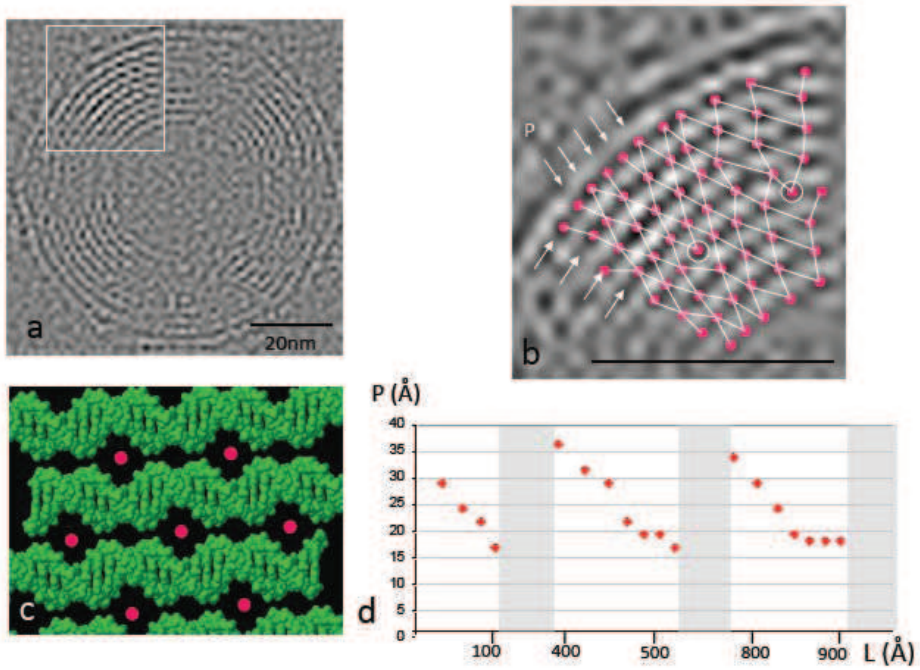

Fig. 1.22: DNA correlations and change of the pitch of the dsDNA helices in the toroids within the T5 phage capsid (Leforestier and Livolant, 2009). (a) Digitized and filtered image of a toroid. (b) Detail of (a) showing the variation of the periodicity P of the DNA helix. (c) DNA helices are shifted by half the helical pitch form one row to the next. (d) Measurement of the pitch along one row.

2. EXPERIMENTAL SYSTEMS AND METHODS

2.1. Preparation of DNA in the bulk solution and in the bacteriophage capsid

2.1.1 Lambda DNA

The genome of the lambda bacteriophage is composed of a long linear DNA molecule (48 kbp), and this purified lambda DNA is commercially available in the form of a dehydrated powder. The solution of DNA is intensively dialyzed against a concentrated NaCl solution, in order to replace as much as possible the cations initially bound to DNA. Then, the solution is dialyzed against 10 mM TE buffer (10 mM Tris, 1 mM EDTA; pH 7.6).

2.1.2 The bacteriophage-receptor system

Tailed bacteriophages (or phages) are a group of viruses that infect bacteria. They have an icosahedral capsid (20-100 nm in diameter) and a tail (short, long contractile or long non-contractile). The capsid is the nanoscale assembly of structural unit proteins and encloses and protects the viral genome. The bacteriophage capsid is connected to a hollow and cylindrical tail with an inner diameter just wide enough to allow the dsDNA chain to be ejected along its length, into the bacteria. At the joint between the capsid and the tail, there is a protein assembly (called “portal complex”) which plays the role of “door” for the DNA ejection and packaging. The bacteriophages are nanomolecular machines designed by nature to recognize the host cell surface and deliver the viral genome to the bacterial cytoplasm (Fig. 2.1). This recognition is accomplished by the specific binding of the tail end to the host receptor which is a membrane protein of the host cell. As soon as the tail binds to the receptor protein, the resulting protein conformation change opens the portal complex, and the DNA confined inside the capsid is ejected through the tail into the bacteria. For the case of T5 bacteriophage, that we have been using in our experiments, the genome is 121 kbp dsDNA (contour length = 41 μm), and the T5 icosahedral capsid has an average diameter of ~80 nm. The T5 tail is a non-contractible and flexible tube 12 nm in diameter and 250 nm in total length. The FhuA protein, localized in the outer membrane protein of *E. coli*, is a receptor for the T5 phage and has been biochemically purified (Boulanger et al., 1996). In vitro experiments are then possible since DNA ejection is triggered after interaction of the phage with its receptor in the absence of the bacteria.

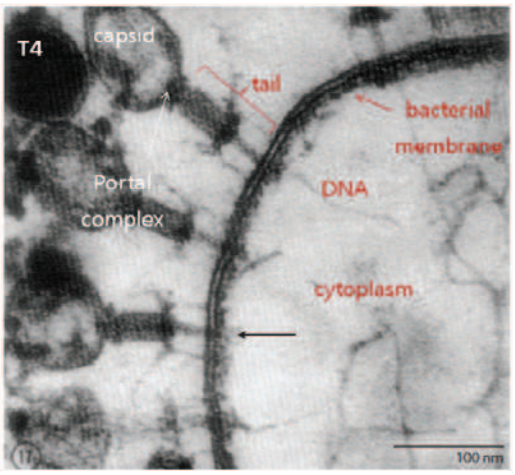

Fig. 2.1: A TEM image of T4 bacteriophages infecting a bacterium *E. coli*. The DNA is ejected from the phage capsid into the cytoplasm through the tail. Note that this image is taken by using conventional TEM in which the structures of the specimens are largely modified (Simon and Anderson, 1967).

Researchers (Evilevitch et al., 2003; Castelnovo and Evilevitch, 2007) have developed a subtle method to control the length of ejected DNA chain from the bacteriophage Lambda by changing the osmotic pressure (acting on the bacteriophages) in the solution. Their experimental method can be summarized as follows: the host receptor, solubilized by a small amount of detergent, is added into the solution of the bacteriophages, diffuses to the phage and binds to the tail and induces whole DNA ejection. If a water-soluble polymer (for example, PEG) is present in the solution, it produces an osmotic pressure resulting in a counterforce to the DNA ejection force. When the two forces are in equilibrium, the DNA ejection process stops and the DNA chain is only partly ejected. The ejected length depends on the applied external pressure, i.e. the polymer concentration in the solution (Fig. 2.2).

DNA ejection from the bacteriophage T5 is more complex. There is not a given length of DNA trapped in the bacteriophage capsid for a given pressure applied in the buffer. Capsids contain a variable fraction of their initial genome (Fig. 2.3) (Leforestier et al., 2008).

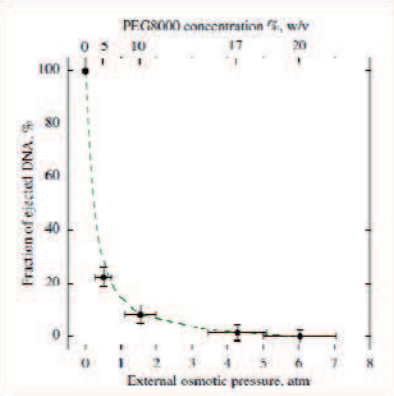

Fig. 2.2: Fraction of DNA ejected from the bacteriophage Lambda as a function of the external osmotic pressure (controlled by the concentration of PEG8000 in the solution). The DNA ejection of the phage is triggered by their binding to the host receptor. Then, with DNase into the solution, the ejected part of DNA chain is digested into nucleotides. Since they can control the osmotic force by varying the polymer concentration and determine the ejected DNA length by measuring the nucleotide concentration with ultraviolet-visible absorbance measurement in the supernatant after centrifugation of the bacteriophages, the correlation between the osmotic pressure and the ejected DNA length can be plotted (Castelnovo and Evilevitch, 2007).

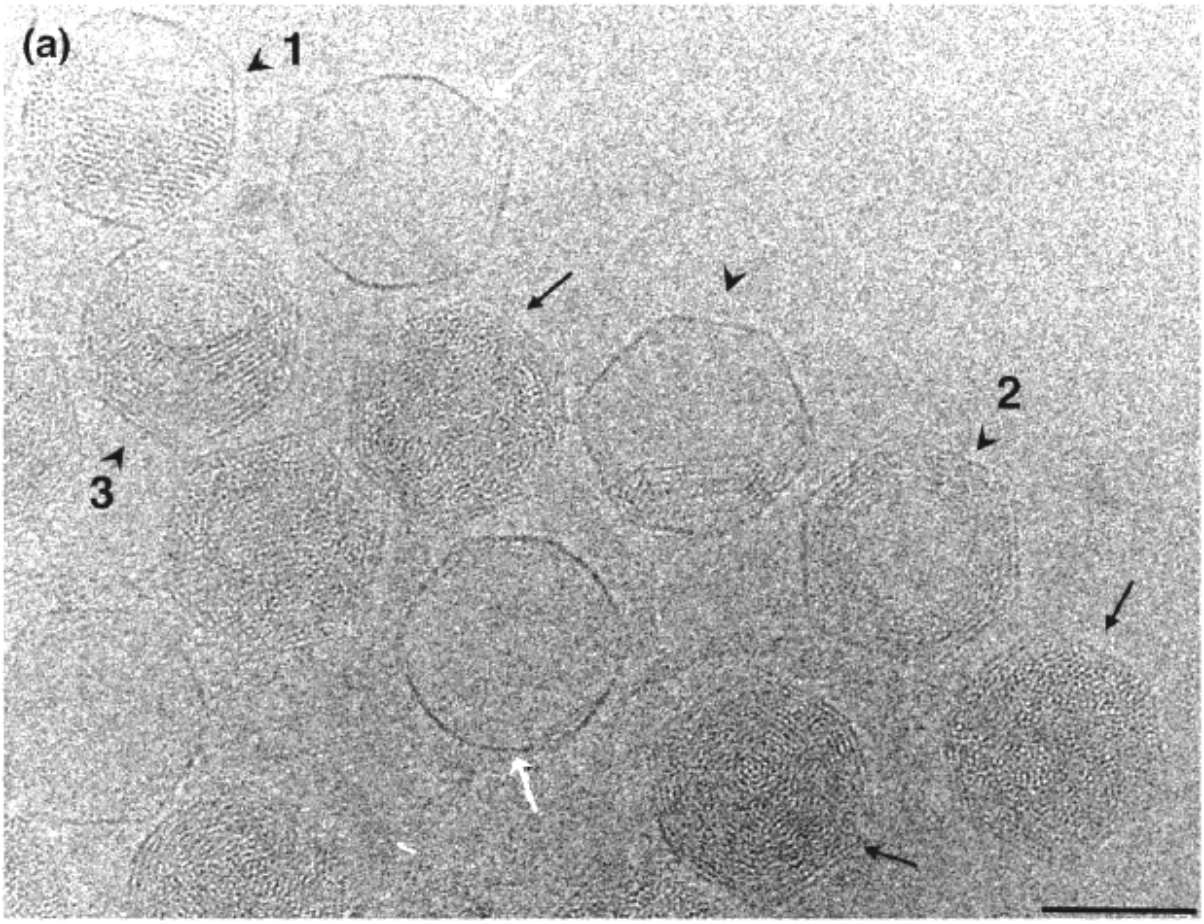

Fig. 2.3: Cryo-EM of T5 bacteriophages after partial ejection of their DNA under pressure, and secondary condensation of DNA with spermine. Empty phages (white arrows), full phages (black arrows), and phages containing intermediate amounts of DNA (arrowheads) are found in coexistence. In the latter case, the conformation of the DNA is torus-like due to the presence of spermine. Side views (1), top views (2), and oblique views (3) of the toroids are visualized. The scale bar represents 50 nm (Leforestier et al., 2008).

The interest of this bacteriophage system is that each DNA chain is kept isolated in each capsid, which prevents any aggregation effect. The protein capsid being permeable to cations, ionic conditions can be tuned and the structure of the DNA in the capsid analyzed under controlled experimental conditions. The specific interest of T5 is that under a given condition, capsids containing fragments with different length can be analyzed at the same time.

2.2 Cryo-electron microscopy

2.2.1 Water in biological systems

The water molecule is extremely abundant on the earth. It is composed of one oxygen and two hydrogen atoms. Each hydrogen is coupled with the oxygen by a covalent bond (bonding distance = 1 Å), and the two bonds form an angle of 104.45°. The water molecules interact with each other by hydrogen bonding due to the electrostatic polarization of each water molecule (Fig. 2.4). When this is done with minimal constrains, the fully hydrogen-bonded water molecule is the center of a tetrahedron. Starting from one oxygen atom, there are four symmetric ways to leave the molecule.

The tetrahedral structure is the basic feature of water structure.

The liquid water plays critical roles in living systems, because ~70 % of the total weight in a cell is composed of water. In biological conditions, all macromolecules, and their associated ions, are in interactions with water molecules in structural manners. Elementary processes of hydration intervene in the structure, stabilization, reaction, and transport of biomolecules *in vivo*. Therefore, if we are interested in the conformation and structure of biological macromolecules, we need to keep the molecules hydrated. Nevertheless, the presence of water is incompatible with electron microscopy studies. Therefore, in classical electron microscopy, the specimens are dehydrated before their introduction in the column under vacuum. However, in cryo-EM (Dubochet et al., 1988), samples can be frozen at low temperature and the water is rapidly transformed into vitreous (amorphous) ice. Vitreous ice keeps as much as possible the conformation and the original molecular environment of the biological macromolecules.

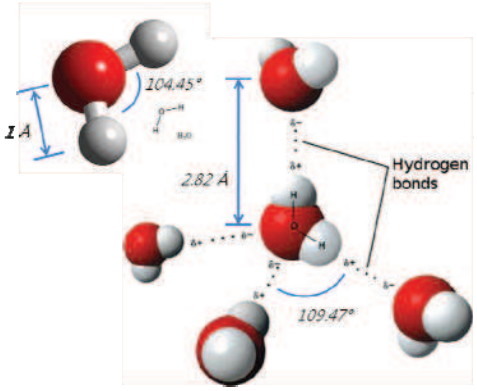

Fig. 2.4: A drawing for the tetrahedral structure of the fully hydrogen-bonded water molecules. The electrically polarized parts (δ+ and δ-) of the molecules interact each other. (from *3dchem.com* and *Wikipedia.com*)

2.2.2 Phase diagram of water

We present on Figure 2.5, the phase diagram of water. Liquid water molecules have great mobility. Their rotation or exchange time at room temperature is of the order of 10^{-12} seconds. Furthermore, liquid water has the same global symmetry as the gas phase.

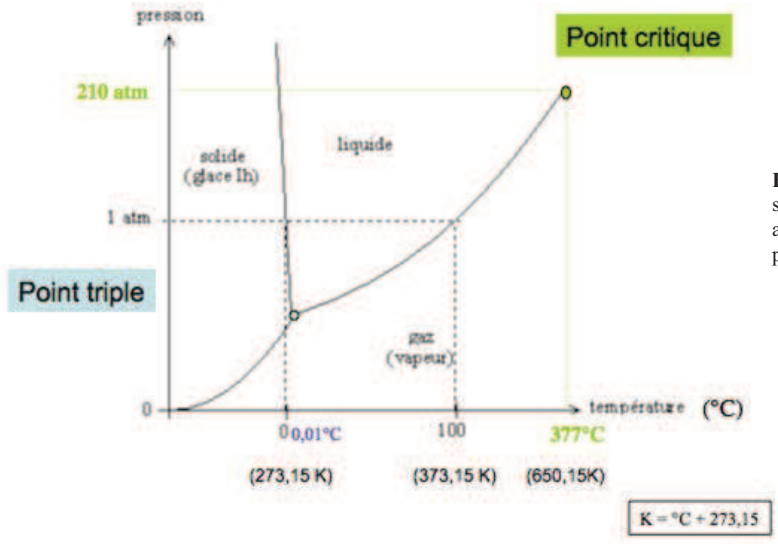

Fig. 2.5: Phase diagram of water showing the three phases (solid, liquid, and gas), a triple point, and a critical point.

When liquid water is cooled slowly (a few degrees per second) under atmospheric pressure, it forms hexagonal crystals of ice (Fig. 2.6). This structure is formed when other water molecules are “frozen”

at each summit of the tetrahedron and the structure is extended infinitely. Other types of ice can be formed depending on the temperature and pressure (Fig. 2.7). For example, cubic ice is very similar to hexagonal ice but it is only stable below -70 °C at normal pressure. Many more ice polymorphs exist at high pressure, when more distortion of the hydrogen bond network becomes possible.

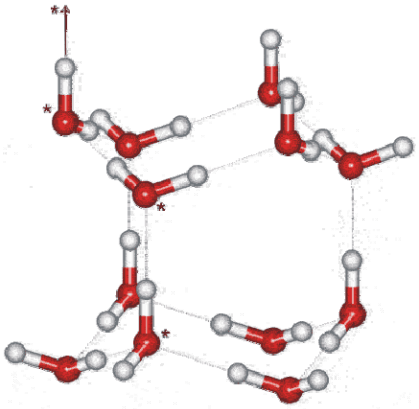

Fig. 2.6: Schematic view of a small part of a hexagonal ice crystal.

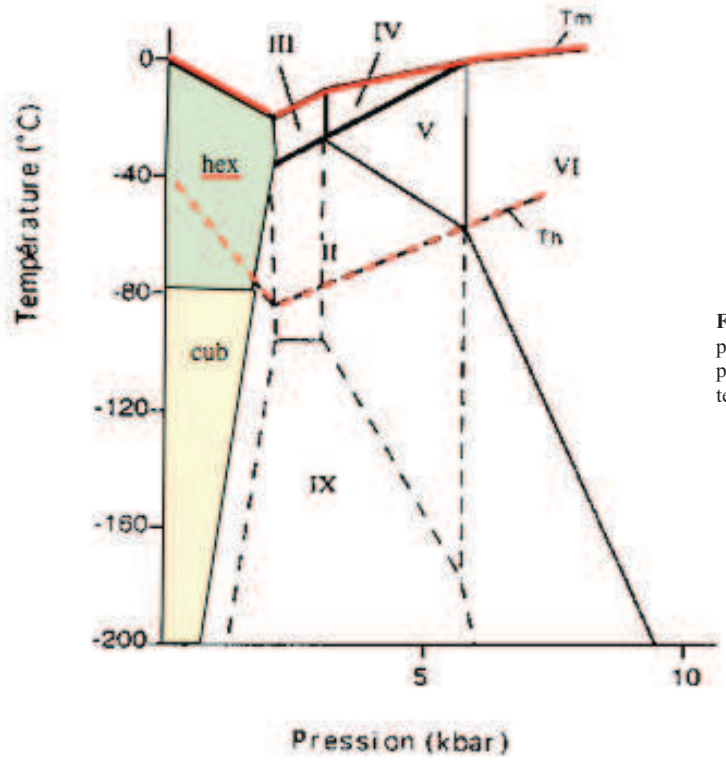

Fig. 2.7: Phase diagram of the solid-phase water (ice), which shows various phases of ice depending on the temperature and the pressure.

2.2.3 Amorphous state of ice

The amorphous states do not have long-range order (hundreds to thousands of atoms), but only possess a short-range order (a few to tens of atoms) (Malenkov, 2009). This amorphous state can be obtained when the material (in its melted phase) is cooled very rapidly (~10^6 degrees per second at atmospheric pressure) to quench its atoms or molecules before they crystallize. It is the state in which immobilization is achieved before nucleation. This leads to a blurred halo pattern in X-ray diffraction, which is totally different from regular dotted diffraction patterns of crystals (Dubochet et al., 1988). The amorphous state is thermodynamically in non-equilibrium, or energetically in a

metastable state. This is schematically drawn in Fig. 2.8.

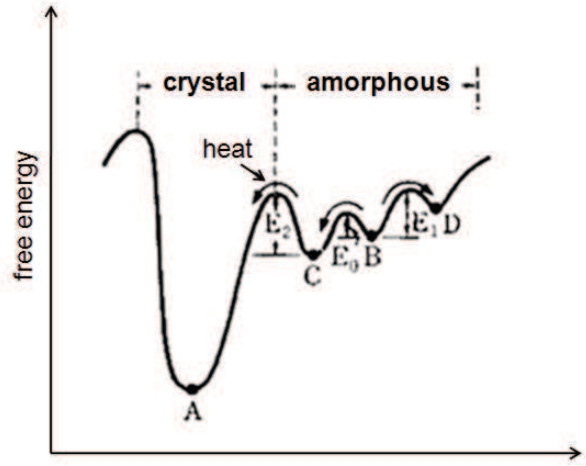

Fig. 2.8: Free energy of crystalline and amorphous states (modified from the reference by Kuwano (1987)). Generally, a thermodynamically equilibrated state takes the globally minimum-energy point among all the free-energy points of the states, for example, point A. However, since the amorphous states are quenched before reaching equilibrium, they take higher energy states, like point B, and this local minimum can be varied by quenching conditions. By external excitations, the point B can be transferred to more stable states (for example, point C), or to higher energy states (for example, point D). If the excitation energy is large enough to exceed the transition barrier (for example, E_2), the amorphous state changes its phase to the crystalline state.

2.2.4 Electron optics for cryo-EM

In TEM, the structure information is obtained from the elastic scattering; the accompanying inelastic scattering causes radiation damage (Saibil, 2000; De Graef, 2003). The cross-section for 0.025 Å electron scattering is 10^5 times greater than that for 1.5 Å X-ray scattering (Saibil, 2000). Because of this large scattering cross-section in EM, the sample must be very thin (less than 200 nm) to avoid multiple scattering that seriously hampers the high-resolution imaging (Saibil, 2000; Elands and Hax, 2004).

There are two contrast mechanisms in TEM – amplitude and phase contrast (Dubochet et al., 1988; Elands and Hax, 2004; Sommerdijk et al., 2010): Amplitude contrast is a scattering-absorption contrast relying on the inhomogeniety of local density and atomic number in the specimen. Phase contrast arises from the coherent interference of the scattered and transmitted electron beams. For the organic specimens (such as DNA), the contribution of the amplitude contrast is very small because of the low atomic numbers of the organic elements (carbon, nitrogen, oxygen, etc). Therefore, phase contrast is the only option for the high-resolution imaging of the non-stained soft materials in cryo-EM

Thin samples of macromolecules or biological nano-particles fulfil the weak phase approximation, the theory of image formation which is used to describe and analyze the phase-contrast images of weakly scattering specimens (Saibil, 2000; Elands and Hax, 2004). Although there is no contrast when the image is in focus, spherical aberration and defocus combine to give a phase-contrast image (Saibil, 2000; De Graef, 2003). The imaging characteristics are described by the contrast-transfer function (CTF), which can be derived from the weak phase approximation (Saibil, 2000; De Graef, 2003). The CTF is the function which modulates the amplitudes and phases of the electron diffraction pattern formed in the back focal plane of the objective lens. The CTF describes the contrast transfer as a function of spatial frequency (Dubochet et al., 1988; Saibil, 2000). It has alternating bands of positive and negative contrast (Saibil, 2000; Sommerdijk et al., 2010). Its real-space equivalent is the point-spread function, the microscope image of a small point object (Saibil, 2000). Defocusing of the image tunes the phase-contrast transfer function to enhance or diminish a given structural detail of the specimen (Fig. 2.9; Dubochet et al., 1988; Sommerdijk et al., 2010).

The electron microscope can be used either as an imaging or a diffraction instrument.

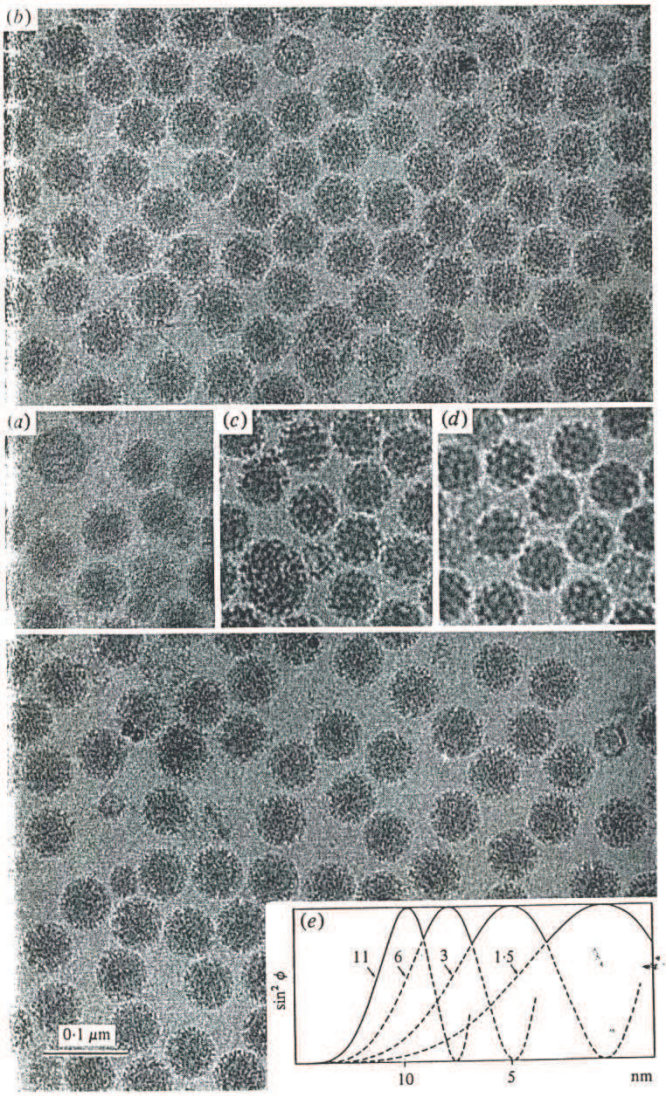

Fig. 2.9: An example showing the relation between the defocusing and the phase contrast function (Dubochet et al., 1988).
Increasing the defocusing from the in-focus (a), the phase contrast function changes (b) to produce images presenting the overall shape of the particle (c and d) instead of their details in (a).

2.2.5 Thin film vitrification method

Nanoscaled specimens below ~100 nm in diameter, such as macromolecular complexes or viral particles, can be frozen in a film of water to be imaged by cryo-EM (Fuller, 1999; Elands and Hax, 2004; Grassucci et al., 2007). This is often accomplished by cooling the sample solution (in which the specimen nano-particles are suspended) extremely quickly (cooling speed > 10^6 Kelvin/second) in a thin layer of vitrified water (i.e., water in a solid glass-like state) (Fuller, 1999; Saibil, 2000; Fig. 2.10). The thinner the better, since the sample film must be thin enough to produce contrasts in the images by transmitting the beam of electrons (Fuller, 1999; Elands and Hax, 2004). Inside the vitrified water film, the specimen nano-particles can tolerate the vacuum environment of the microscope and keep their original shapes without evaporating their bound water ('structure preservation') (van Heel et al., 2000). The vitreous ice layer is formed on perforated carbon films so that regions of ice unsupported by carbon film are imaged.

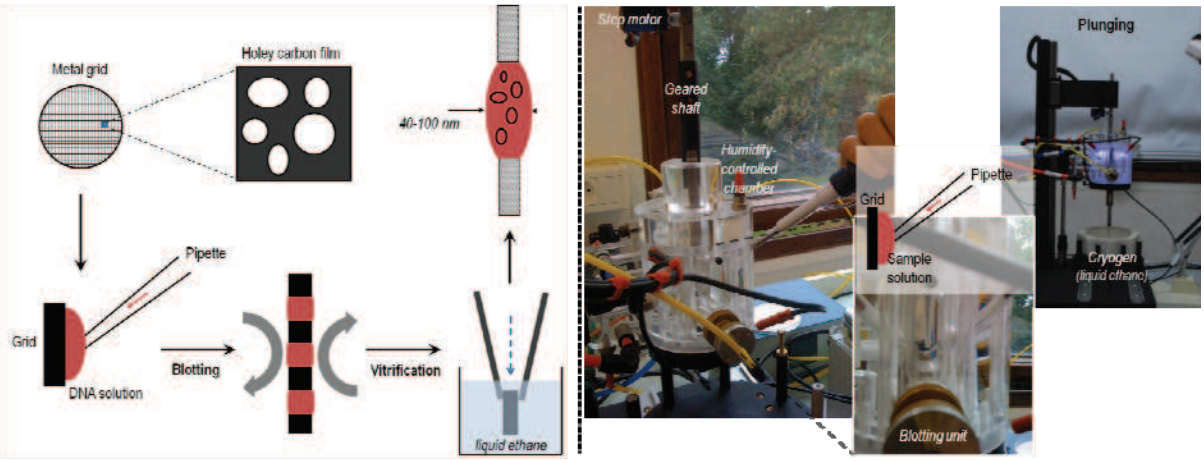

Fig. 2.10: Principle of the formation of thin vitrified water films by cryo-plunging (left) and pictures of the experimental device (right).The chamber where is placed the grid is humidity controlled. A droplet of the sample is deposited on the grid inside the chamber. The grid is then blotted automatically from both sides and immediately dropped into the liquid cryogen.

For the formation of the specimen imbedded in a vitrified water layer, a small aliquot of the specimen in suspension is placed on a holey carbon film, blotted to generate a layer less than ~100 nm thickness and plunged into a bath of liquid ethane (-183˚C) held in a container of liquid nitrogen (~100 K) (Fuller, 1999; Elands and Hax, 2004). Ethane is a very efficient cryogen since (1) it has a high heat conductivity that fits for rapid cooling of the water layer, and (2) unlike nitrogen, it does not boil at the temperatures used for vitrification (Fuller, 1999; Sommerdijk et al., 2010). Nitrogen is not used directly since the formation of gas around the specimen when it is introduced into nitrogen slows the cooling and leads to the formation of crystalline ice (Fuller, 1999). The thin layer of solution in the perforated carbon film has a large surface-to-volume ratio that enables rapid heat exchange and ensures efficient vitrification (Dubochet et al., 1988). However, this large surface-to-volume ratio also can cause fast evaporation of the solvent (water) during the preparation step which will result in a significant change of the ionic concentration in the layered sample solution (Dubochet et al., 1988). For this reason, the solvent saturation in the environment is essential for the cryo-specimen preparation in a humidity and temperature-controlled chamber. A computer interface-controlled chamber has been used to regulate the local atmospheric environment (temperature and humidity) and the blotting conditions (mechanical blotting speed and water absorption rate) before freezing (Figure 2.10).

2.2.6 Conditions of imaging for cryo-EM

The vitrified sample is kept in liquid nitrogen (T < -135˚C), mounted it in a liquid-nitrogen-cooled specimen holder (designed to maintain the low temperature and minimize ice contamination of the grid surface) which is inserted into the microscope (Fuller, 1999; Saibil, 2000). The vitrified sample is maintained at near -170°C during microscopy. The boiling point of liquid nitrogen is -196 °C (and its freezing point -210 °C). Thus, in liquid nitrogen, the specimen is kept at least below the boiling point temperature. The specimen is extremely sensitive to radiation damage from the electron beam of the microscope (Dubochet et al., 1988; Fuller, 1999). For this reason, low dose techniques are required for the electron microscopy. The state of the vitrified water layer can be assessed by electron diffraction (Dubochet et al., 1988; Saibil, 2000; see Fig. 2.11).

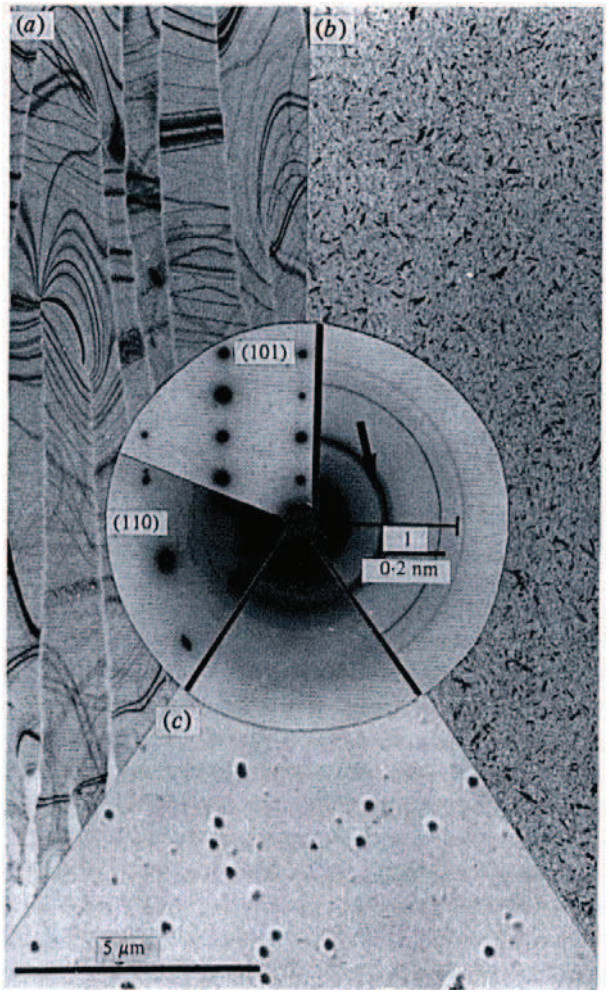

Fig. 2.11: Typical images and electron diffractograms of three forms of solid water observed in the electron microscope. (a) Hexagonal ice obtained by rapid freezing of a water layer on a carbon film. (b) Cubic ice obtained by warming a layer of vitreous water obtained by condensation. (c) Vitreous water obtained in the microscope, by condensation of vapor on a cold carbon film supporting polystyrene spheres. [fig. 5 (p. 142) in Dubochet et al., 1988]

In practice, the specimen is first imaged at low magnification (×200-2000) so that areas of interest can be identified with minimal irradiation (< 0.1 electrons $Å^{-2}$) (Fuller, 1999). The image is then captured at higher magnification with the first electrons to hit the specimen (Dubochet et al., 1988; Fuller, 1999). Typically, the image is formed with a dose of 5-10 electrons/$Å^{-2}$, under underfocus conditions that must be determined for each sample (Fuller, 1999). The image is a superimposition of all the density in the sample (Fuller, 1999; De Graef, 2003). Thus, one should interpret the micrographs in the frame of the projected nature of the image. Moreover, in cryo-EM, high-resolution images can be obtained without any contrasting agents. [In this study, we utilize non-stained specimens and all the images are taken by photographic films, not by CCD cameras.]

2. AIM OF THE THESIS

The fine structure of polyamine-DNA aggregates has been studied a very few ionic conditions (Lambert et al., 2000; Leforestier and Livolant, 2009). In this thesis, it is aimed to study the shape, structure, and coil-globule transition of linear ds DNA chains condensed by the polyamine spermine. We have chosen the cryo-electon microscopy method in order to observe the high resolution structure of the condensates while preserving their ionic environment. The counterion concentration and the reaction time are the parameters that we will vary for controlling the shape, structure and transition. The interhelical distance will be one parameter used to quantify the density of the structures.

Two sets of experiments have been performed:

1) We performed experiments in the bulk, using Lambda DNA (48 kbp) and analyzed how the shape and structure of the condensates formed from a very dilute DNA solution (0.03 mM Ph) depend on the spermine concentration (Csp). We explored a wide range of Csp (from the onset of the precipitation to the redissolution regime) and analysed the samples after 15 minutes of equilibration. All these experiments are done in a large excess of spermine. We also designed a protocol allowing us to trap the objects in the cryofilm at short times after mixing DNA and spermine (6 seconds and more) to get a larger view of the processes involved.

2) In a second set of experiments, we used the bacteriophage /receptor system presented above to analyze the collapse of individual DNA chains (12-54 kbp). The DNA chains are initially confined in the capsid and the initial DNA concentration is therefore much higher than in the first series of experiments. For a given concentration of capsids /DNA, we varied the spermine concentration to explore the coil to globule transition. Experiments are done in conditions where the spermine/DNA charge ratio is significantly lower than in the first set of experiments (close to 1).

References

Allen MJ, Hud NV, Balooch M, Tench RJ, Siekhaus WJ, Balhorn R: Tip-radius-induced artifacts in AFM images of protamine-complexed DNA fibers. *Ultramicrosc.* **42-44**: 1095-1100 (1992)

Allen MJ, Bradbury EM, Balhorn R: AFM analysis of DNA-protamine complexes bound to mica. *Nucl. Acids Res.* **25**: 2221-2226 (1997)

Ames BN and Dubin DT: The role of polyamines in the neutralization of bacteriophage deoxyribonucleic acid. *J. Biol. Chem.* **235**: 769-775 (1960)

Bachrach U, Wang YC, Tabib A: Polyamines: new cues in cellular signal transduction. *News Physiol. Sci.* **16**: 106-109 (2001)

Baeza I, Gariglio P, Rangel LM, Chavez P, Cervantes L, Arguello C, Wong C, Montanez C: Electron microscopy and biochemical properties of polyamine-compacted DNA. *Biochem.* **26**: 6387-6392 (1987)

Baigl D and Yoshikawa K: Dielectric control of counterion-induced single-chain folding transition of DNA. *Biophys. J.* **88**: 3486-3493 (2005)

Battle C, van der Broek B, Noom MC, van Mameren J, Wuite GJL, MacKintosh FC: Unraveling DNA tori under tension. *Phys. Rev. E* **80**: 031917 (2009)

Baumann CG, Smith SB, Bloomfield VA, Bustemante C: Ionic effects on the elasticity of single DNA molecules. *Proc. Natl. Acad. Sci. U.S.A.* **94**: 6185-6190 (1997)

Baumann CG, Bloomfield VA, Smith SB, Bustemante C, Wang MD, Block SM: Stretching of single collapsed DNA molecules. *Biophys. J.* **78**: 1965–1978 (2000)

Besteman K, van Eijk K, Lemay SG: Charge inversion accompanies DNA condensation by multivalent ions. *Nature Phys*. **3**: 641-644 (2007)

Bloomfield VA: DNA condensation. *Curr. Opin. Struct. Biol*. **6**: 334-341 (1996)

Boulanger P, LeMaire M, Bonhivers M, Dubois S, Desmadril M, Letellier L: Purification and structural and functional characterization of FhuA, a transporter of the Escherichia coli outer membrane. *Biochemistry* **35**: 14216–14224 (1996)

Brewer LR, Corzett M, Balhorn R: Protamine-induced condensation and decondensation of the same DNA molecule. *Science* **286**: 120-123 (1999)

Bötcher C, Endish C, Fuhrhop JH, Catterall C, Eaton M: High-yeild preparation of oligomeric c-type DNA toroids and their characterization by cryoelectron microscopy. *J. Am. Chem. Soc.* **120**: 12-17 (1998)

Castelnovo M and Evilevitch A: DNA ejection from bacteriophage: Towards a general behavior for osmotic-suppression experiments. *Eur. Phys. J. E* **24**: 9-18 (2007)

Chattoraj DK, Gosule LC, Schellman JA: DNA condensation with polyamines. II. Electron micorscopy Studies. *J. Mol. Biol.* **121**: 327-337 (1978)

Cherstvy AG: Collapse of highly charged polyelectrolytes triggered by attractive dipole-dipole and correlation-induced electrostatic interactions. *J. Phys. Chem. B* **114**: 5241-5249 (2010)

Conwell CC, Vilfan ID, Hud NV: Controlling the size of nanoscale toroidal DNA condensates with static curvature and ionic strength. *Proc. Natl. Acad. Sci. USA* **100**: 9296-9301 (2003)

Damaschun H, Damaschun G, Becker M, Buder E, Misselwitz R, Zirwe D: Study of DNA-spermine interactions by use of small-angle x-ray scattering and circular dichroism. *Nucl. Acid. Res*. **5**: 3801-3809 (1978)

De Graef M: *Introduction to Conventional Transmission Electron Microscopy* (Cambridge University Press, Cambridge, 2003)

Dias RS and Pais AACC: Polyelectrolyte condensation in bulk, at surfaces, and under confinement. *Adv. Colloid Interface Sci.* **158**: 48-62 (2010)

Dubochet J, Adrian M, Chang JJ, Homo JC, Lepault J, McDowall AW, Schultz P: Cryo-electron microscopy of vitrified specimens. *Q. Rev. Biophys.* **21**: 129-228 (1988)

Elands J and Hax W: CryoEM as a complement to current techniques in protein structural analysis. *Curr. Drug Discov.* October, pp. 15-20 (2004)

Endlich N and Greulich KO: Observation and manipulation of different structural variants of individual cation-DNA complexes in the light microscope. *J. Biotech.* **41**: 149-153 (1995)

Evilevitch A, Gober JW, Phillips M, Knobler CM, Gelbart WM: Measurements of DNA lengths remaining in a viral capsid after osmotically suppressed partial éjection. *Biophys. J.* **88**: 751-756 (2005)

Fang Y and Hoh JH: Early intermediates in spermidine-induced DNA condensation on the surface of mica. *J. Am. Chem. Soc.* **120**: 8903-8909 (1998)

Fazli H and Golestanian R: Aggregation kinetics of stiff polyelectrolytes in the prescence of multivalent salt.

Phys. Rev. E **76**: 041801 (2007)
Fixman M: The flexibility of polyelectrolyte molecules. *J. Chem. Phys.* **76**: 6346-6353 (1982)
Frank-Kamenetskii MD: Biophysics of the DNA molecule. *Phys. Rep*. **288**: 13-60 (1997)
FranklinRE and Gosling RG: Molecular configuration in sodium thymonucleate. *Nature* **171**: 740-741 (1953)
Friedrich H, Frederik PM, de With G, Sommerdijk NAJM: Imaging of self-assembled structures: Interpretation of TEM and cryo-TEM images. *Angew. Chem. Int. Ed.* **49**: 7850-7858 (2010)
Fuller S: Cryo-electron microscopy: taking back the knight. *Microbiol. Today* **26**: 56-58 (1999)
Gelbart WM, Bruinsma RF, Pincus PA, Parsegian VA: DNA electrostatics. *Physics Today*, September 2000, pp. 38-44
Golan R, Pietrasanta LI, Hsieh W, Hansma HG: DNA toroids: stages in condensation. *Biochem*. **38**: 14069-14076 (1999)
Gosule LC and Schellman JA: Compact form of DNA induced by spermidine. *Nature* **259**: 333-335 (1976)
Grason GM and Bruinsma RF: Chirality and equilibrium biopolymer bundles. *Phys. Rev. Lett.* **99**: 098101 (2007)
Grassucci RA, Taylor DJ, Frank J: Preparation of macromolecular complexes for cryo-electron microscopy. *Nature Protocols* **2**: 3239-3246 (2007)
Grosberg AU and Khokhlov AR: *Statistical Physics of Macromolecules*. (American Institute of Physics, NY, USA, 1994)
Grønbech-Jensen N, Mashl RJ, Bruinsma RF, Gelbart WM: Counterion-Induced Attraction between Rigid Polyelectrolytes. *Phys. Rev. Lett.* **78**: 2477–2480 (1997)
Ha BY and Liu AJ: Counterion-mediated attraction between two like-charged rods. *Phys. Rev. Lett.* **79**: 1289-1292 (1997)
Ha BY and Liu AJ: Effect of non-pairwise-additive interactions on bundles of rodlike polyelectrolytes. *Phys. Rev. Lett.* **81**: 1011-1014 (1998)
Ha BY and Liu AJ: Kinetics of bundle growth in DNA condensation. *Europhys. Lett.* **46**: 624-630 (1999)
Haley J and Geng Y: Role of DNA in condensation and combinative self-assembly. *Chem. Comm.* **46**: 955-957 (2010)
Hansma HG: Surface biology of DNA by atomic force microscopy. *Annu. Rev. Phys. Chem.* **52**: 71-92 (2001)
Haynes M, Garrett RA, Gratzer WB: Structure of nucleic acid-poly base complexes. *Biochem.* **9**: 4410-6 (1970)
He S, Arscott PG, Bloomfield VA: Condensation of DNA by multivalent cations: experimental studies of condensation kinetics. *Biopolymers* **53**: 329-341 (2000)
Henle ML and Pincus PA: Equilibrium bundle size of rodlike polyelectrolytes with counterion-induced attractive interactions. *Phys. Rev. E* **71**: 060801 (2005)
Hizume K, Nakai T, Araki S, Prieto E, Yoshikawa K, Takeyasu K: Removal of histone tails from nucleosome dissects the physical mechanisms of salt-induced aggregation, linker histone H1-induced compaction, and 30-nm fiber formation of the nucleosome array. *Ultramicrosc.* **109**: 868-873 (2009)
Hsiang MW and Cole RD: Structure of histone H1-DNA complex: effect of histone H1 on DNA condensation. *Proc. Natl. Acad. Sci. U.S.A.* **74**: 4852-4856 (1977)
Huang CI and Olvera de la Cruz M: Polyelectrolytes in multivalent salt solutions: monomolecular versus multimolecular aggregation. *Macromol.* **35**: 976-986 (2002)
Hud NV, Allen MJ, Downing KH, Lee J, Balhorn R: Identification of the elemental packing unit of DNA in mammalian sperm cells by atomic force microscopy. *Biochem. Biophys. Res. Comm.* **193**: 1347-1354 (1993)
Hud NV, Downing KH, Balhorn R: A constant radius of curvature model for the organization of DNA in toroidal condensates. *Proc. Natl. Acad. Sci. USA* **92**: 3581-3585 (1995)
Hud NV and Downing K: Cryoelectron microscopy of lambda phage DNA condensates in vitreous ice: the fine structure of DNA toroids. *Proc. Natl. Acad. Sci. USA* **98**: 14925-14930 (2001)
Igarashi K and Kashiwagi K: Polyamines: mysterious modulators of cellular functions. *Biochem. Biophys. Res. Comm.* **271**: 559-564 (2000)
Iwaki T, Makita N, Yoshikawa K: Folding transition of a single semiflexible polyelectrolyte through toroidal bundling of loop structures. *J. Chem. Phys.* **129**: 065103 (2008)
Iwataki T, Kidoaki S, Sakaue T, Yoshikawa K, Abramchuk SS: Competition between compaction of single chains and bundling of multiple chains in giant DNA molecules. *J. Chem. Phys.* **120**: 4004-4011 (2004)
Jary D : *Etude des propriétés statiques et dynamiques de longues chaines d'ADN sur deux exemples : rhéologie de solutions semi-diluées et cyclisation d'une chaine globulaire*. PhD Thesis, Orsay University, 1998 (France)
Jary D and Sikorav JL: Cyclization of globular DNA. Implications for DNA-DNA interactions *in vivo. Biochemistry* **38**: 3223-3227 (1999)

Jayaram B, Sharp KA, Honig B: The electrostatic potential of B-DNA. *Biopolymers* **28**: 975-993 (1989)
Klimenko SM, Tikchonenko TI, Andreev VM: Packing of DNA in the head of bacteriophage T2. *J. Mol. Biol.* **23**: 523-533 (1967)
Korolev N, Lyubartsev AP, Laaksonen A, Nordenskiöld L: On the competition between waster, sodium ions, and spermine in binding to DNA: a molecular dynamics computer simulation study. *Biophys. J.* **82**: 2860-2875 (2002)
Korolev N, Lyubartsev AP, Nordenskiöld L: Cation-induced polyelectrolyte-polyelectrolyte attraction in solutions of DNA and nucleosome core particles. *Adv. Colloid Interface Sci.* **158**: 32-47 (2010)
Kundagrami A and Muthukumar M: Effective charge and coil-globule transition of a polyelectrolyte chain. *Macromolecules* **43**: 2574-2581 (2010)
Kwoh DY, Coffin CC, Lollo CP, Jovenal J, Banaszczyk MG, Mullen P, Phillips A, Amini A, Fabrycki J, Bartholomew RM, Brostoff SW, Carlo DJ: Stabilization of poly-L-lysine/DNA polyplexes for in vivo gene delivery to the liver. *Biochim. Biophys. Acta* **1444**: 171-190 (1999)
Lambert O, Letellier L, Gelbart WM, Rigaud JL: DNA delivery by phage as a strategy for encapsulating toroidal condensates of arbitrary size into liposomes. *Proc. Natl. Acad. Sci. USA* **97**: 7248-7253 (2000)
Le Bret M: Electrostatic contribution to the persistence length of a polyelectrolyte. *J. Chem. Phys.* **76**: 6243-6255 (1982)
Le Bret M and Zimm BH: Monte Carlo determination of the distribution of ions about a cylindrical polyelectrolyte. *Biopolymers* **23**: 271-285 (1984)
Lee LK, Mount CN, Shamlou PA: Characterisation of the physical stability of colloidal polycation-DNA complexes for gene therapy and DNA vaccines. *Chem. Eng. Sci.* **56**: 3163-3172 (2001)
Leforestier A, Brasilès S, de Frutos M, Raspaud E, Letellier L, Tavares P, Livolant F: Bacteriophage T5 DNA ejection under pressure. *J. Mol. Biol.* **384**: 730-739 (2008)
Leforestier A and Livolant F: Structure of toroidal DNA collapsed inside the phage capsid. *Proc. Natl. Acad. Sci. USA* **106**: 9157-9162(2009)
Leforestier A and Livolant F: The bacteriophage genome undergoes a succession of intracapsid phase transitions upon DNA ejection. *J. Mol. Biol.* **396**: 384-395 (2010)
Lepault J, Dubochet J, Baschong W, Kellenberger E: Organization of double-stranded DNA in bacteriophages: a study by cryo-electron microscopy of vitrified samples. *EMBO J*. **6(5)**: 1507-1512 (1987)
Lucius H, Haberland A, Zaitsev S, Dallüge R, Schneider M, Böttger M: Structure of transfection-active histone H1/DNA complexes. *Mol. Biol. Rep.* **28**: 157-165 (2002)
Malenkov G: Liquid water and ices: understanding the structure and physical properties. *J. Phys. Condens. Matter* **21**: 283101 (2009)
Manning GS: Polyelectrolytes. *Ann. Rev. Phys. Chem.* **23**: 117-140 (1972)
Manning GS: The molecular theory of polyelectrolyte solutions with applications to the electrostatic properties of polynucleotides. *Q. Rev. Biophys.* **11**: 179-246 (1978)
Marko JF and Siggia ED: Stretching DNA. *Macromolecules* **28**: 8759-8770 (1995)
Marx KA and Reynolds TC: Spermidine-condensed phi X174 DNA cleavage by micrococcal nuclease: torus cleavage model and evidence for unidirectional circumferential DNA wrapping. *Proc. Natl. Acad. Sci. USA* **79**: 6484-6488 (1982)
Marx KA and Ruben GC: Evidence for hydrated spermidine-calf thymus DNA toruses organized by circumferential DNA wrapping. *Nucl. Acids Res.* **11**: 1839–1854 (1983)
Martin AL, Davies MC, Rackstraw BJ, Roberts CJ, Stolnik S, Tendler SJ, Williams PM: Observation of DNA-polymer condensate formation in real time at a molecular level. *FEBS Lett.* **480**: 106-12 (2000)
Minagawa K, Matsuzawa Y, Yoshikawa K, Matsumoto M, Doi M: Direct observation of the biphasic conformational change of DNA induced by cationic polymers. *FEBS Lett.* **295**: 67-69 (1991)
Miyazawa N, Sakaue T, Yoshikawa K, Zana R: Rings-on-a-string chain structure in DNA. *J. Chem. Phys*. **122**: 044902 (2005)
Noguchi H and Yoshikawa K: Morphological variation in a collapsed single homopolymer chain. *J. Chem. Phys.* **109**: 5070-5077 (1998)
Odijk T: Polyelectrolytes near the rod limit. *J. Polymer Sci.: Polymer Phys. Edit.* **15**: 477-483 (1977)
Ono MY and Spain EM: Dynamics of DNA condensates at the solid-liquid interface by atomic force microscopy. *J. Am. Chem. Soc.* **121**: 7330-7334 (1999)
Oosawa F: *Polyelectrolytes* (Dekker, New York, 1971)
Ou Z and Muthukumar M: Langevin dynamics of semiflexible polyelectrolytes: rod-toroid-globule-coil

structures and counterion distribution. *J. Chem. Phys.* **123**: 074905 (2005)
Ouameur AA and Tajmir-Riahi HA: Structural analysis of DNA interactions with biogenic polyamines and Cobalt(III) hexamine studied by Fourier transform infrared and capillary electrophoresis. *J. Biol. Chem.* **279**: 42041-42054 (2004)
Pegg AE and McCann PP: Polyamine metabolism and function. *Am. J. Physiol.* **243**: C212-C221 (1982)
Pelta J, Livolant F, Sikorav JL: DNA aggregation induced by polyamines and cobalthexamine. *J. Biol.Chem.* **271**: 5656-5662 (1996)
Philippova OE, Akitaya T, Mullagaliev IR, Khokhlov AR, Yoshikawa K: Salt-controlled intrachain/interchain segregation in DNA complexes with polycation of natural origoin. *Macromolecules* **38**: 9359-9365 (2005)
Pinto MFV, Morán MC, Miguel MG, Lindman B, Jurado AS, Pais AACC: Controlling the morphology in DNA condensation and precipitation. *Biomacromol*. **10(6)**: 1319-1323 (2009)
Porschke D: Dynamics of DNA condensation. *Biochem.* **23**: 4821-4828 (1984)
Post CB and Zimm BH: Light-scattering study of DNA condensation: Competition between collapse and aggregation. *Biopolymers* **21**: 2139-2160 (1982)
Raspaud E, Olvera de la Cruz M, Sikorav JL, Livolant F: Precipitation of DNA by polyamines: a polyelectrolyte behavior. *Biophys. J*. **74**: 381-393 (1998)
Raspaud E, Durand D, Livolant F: Interhelical spacing in liquid crystalline spermine and spermidine-DNA precipitates. *Biophys. J.* **88**: 392-403 (2005)
Rau DC and Parsegian VA: Direct measurement of temperature-dependent solvation forces between DNA double helices. *Biophys. J.* **61**: 260–271 (1992)
Record MT, Anderson CF, Lohman T: Thermodynamic analysis of ion dffects on the binding and conformational equilibria of proteins and nucleic acids: the role of ion association and release, screening and ion effects on water activity. *Q. Rev. Biophys.* **11**: 103-178 (1978)
Rädler JO, Koltover I, Salditt T, Safinya CR: Structure of DNA-cationic liposome complexes: DNA intercalation in multilamellar membranes in distinct interhelical packing regimes. *Science* **275**: 810-814 (1997)
Rouzina I and Bloomfield VA: Macroion attraction due to electrostatic correlation between screening counterions. 1. Mobile surface-adsorbed ions and diffuse ion cloud. *J. Phys. Chem.* **100**: 9977–9989 (1996)
Saito T and Yoshikawa K: Finite-width bundle is most stable in a solution with salt. *J. Chem. Phys.* **133**: 045102 (2010)
Saminathan M, Thomas T, Shirahata A, Pillai CKS, Thomas TJ: Polyamine structural effects on the induction and stabilization of liquid crystalline DNA: potential applications to DNA packaging, gene therapy and polyamine therapeutics. *Nucl. Acids Res.* **30**: 3722-3731 (2002)
Sarkar T, Vitoc I, Mukerji I, Hud NV: Baterial protein HU dictates the morphology of DNA condensates produced by crowding agents and polyamines. *Nucl. Acids Res.* **35(3)**: 951-961 (2007)
Saibil HR: Macromolecular structure determination by cryo-electron microscopy. *Acta Cryst.* **D56**: 1215-1222 (2000)
Simon LD and Anderson TF: The infection of Escherichia coli by T2 and T4 bacteriophages as seen in the electron microscope I. Attachment and penetration. *Virology* **32**: 279-297 (1967)
Skolnick J and Fixman M: Electrostatic persistence length of a wormlike polyelectrolyte. *Macromolecules* **10**: 944-948 (1977)
Smith SB, Finzi L, Bustamante C: Direct mechanical measurement of the elasticity of single DNA molecules by using magnetic beads. *Science* **258**: 1122-1126 (1992)
Smith DE, Tans SJ, Smith SB, Grimes S, Anderson DL, Bustamante C: The bacteriophage f29 portal motor can package DNA against a large internal force. *Nature* **413** 748-752 (2001)
Stevens MJ: Simple simulations of DNA condensation. *Biophys. J.* **80**: 130-139 (2001)
Strick T, Allemand JF, Croquette V, Bensimon D : Twisting and stretching single DNA molecules. *Prog. Biophys. Mol. Biol.* **74**: 115-140 (2000)
Stukan MR, Ivanov VA, Grosberg AY, Paul W, Binder K: Chain length dependence of the state diagram of a stiff-chain macromolecules: theory and Monte Carlo simulation. *J. Chem. Phys.* **118**: 3392-3400 (2003)
Tabor CW and Tabor H: Polyamines in microorganisms. Microbiol. Rev. 49(1): 81-99 (1985)
Takahashi M, Yoshikawa K, Vasilevskaya VV, Khokhlov AR: Discrete coil-globule transition of single duplex DNAs induced by polyamines. *J. Phys. Chem. B* **101**: 45, 9396-9401 (1997)
Takenaka Y, Yoshikawa K, Yoshikawa Y, Koyama Y, Kanbe T: Morphological variation in a toroid generated from a single polymer chain. *J. Chem. Phys.* **123**: 014902 (2005)
Tang MX and Szoka FC: The influence of polymer structure on the interactions of cationic polymers with DNA

and morphology of the resulting complexes. *Gene Therapy* **4**: 823-832 (1997)
Thomas T and Thomas TJ: Polyamines in cell growth and cell death: molecular mechanisms and therapeutic applications. *Cell. Mol. Life Sci.* **58**: 244-258 (2001)
Todd BA and Rau DC: Interplay of ion binding and attraction in DNA condensed by multivalent cations. *Nucl. Acid. Res.* **36**: 501-510 (2008)
Todd BA, Parsegian AV, Shirahata A, Thomas TJ, Rau DC: Attractive forces between cation condensed DNA double helices. *Biophys. J.* **94**: 4775-4782 (2008)
Toma AC: *DNA condensation by a basic protein, the salmon protamine.* (Ph.D. thesis, Université Paris-Sud XI, Orsay, 2008)
Trubetskoy VS, Wolf JA, Budker VG: The role of a microscopic colloidally stabilized phase in solubilizing oligoamine-condensed DNA complexes. *Biophys. J.* **84**: 1124-1130 (2003)
Tzlil S, Kindt JT, Gelbart WM, Ben-Shaul A: Forces and pressures in DNA packaging and release from viral capsids. *Biophys. J.* **84**: 1616-1627 (2003)
Ueda M and Yoshikawa K: Phase transition and phase segregation in a single double-stranded DNA molecule. *Phys. Rev. Lett.* **77(10)**: 2133-2136 (1996)
Van der Broek B, Noom MC, van Mameren J, Battle C, MacKintosh FC, Wuite GJL: Visualizing the formation and collapse of DNA toroids. *Biophys. J.* **98**: 1902-1910 (2010)
Vasilevskaya VV, Khokhlov AR, Kidoaki S, Yoshikawa K: Structure of collapsed persistent macromolecule: toroid vs. spherical globule. *Biopolymers* **41**: 51-60 (1997)
Verma R, Crocker JC, Lubensky TC, Yodh AG: Etropic colloidal interactions in concentrated DNA solutions. *Phys. Rev. Lett.* **81**: 4004-4007 (1998)
Vilfan ID, Conwell CC, Sarkar T, Hud NV: Time study of DNA condensate morphology: implications regarding nucleation, growth, and equilibrium populations of toroids and rods. *Biochem.* **45**: 8174-8183 (2006)
Wan L, Manickam DS, Oupický D, Mao G: DNA Release dynamics from bioreducible poly(amido amine) polyplexes *J. Phys. Chem. B* **113**: 13735–13741 (2009)
Watson JD and Crick FHC: Molecular structure of nucleic acids: a structure for deoxyribose nucleic acid. *Nature* **171**: 737-738 (1953)
Widom J and Baldwin RL: Cation-induced toroidal condensation of DNA studies with $Co^{3+}(NH_3)_6$. *J. Mol. Biol*. **144**: 431-453 (1980)
Widom J and Baldwin RL: Molecular condensation of λ-DNA induced by cobalt hexamine. *Biopolymers* **22**: 1595-1620 (1983)
Wilson RW and Bloomfield VA: Counterion-induced condensation of deoxyribonucleic acid. A light scattering study. *Biochem*. **18**: 2192-2196 (1979)
Williams LD and Maher III LJ: Electrostatic mechanisms of DNA deformation. *Annu. Rev. Biophys. Biomol. Struct.* **29**: 497-521 (2000)
Yamada A, Kubo K, Nakai T, Yoshikawa K, Tsumoto K: All-or-none switching of transcriptional activity on single DNA molecules caused by a discrete conformation transition. *Appl. Phys. Lett.* **86**: 223901 (2005)
Yamasaki Y, Teramoto Y, Yoshikawa K: Disappearance of the negative charge in giant DNA with a folding transition. *Biophys. J.* **80**: 2823-2832 (2001)
Yamasaki Y, Katayose S, Kataoka K, Yoshikawa K: PEG-PLL blok copolymers induce reversible large descrete coil-globule transition in a single DNA molecule through cooperative complex formation. *Macromol.* **36**: 6276-6279 (2003)
Yang J and Rau DC: Incomplete ion dissociation underlies the weakened attraction between DNA helices at high spermidine concentrations. *Biophys. J.* **89**: 1932-1940 (2005)
Yoshikawa Y, Emi N, Kanbe T, Yoshikawa K, Saito H: Folding and aggregation of DNA chains induced by complexation with lipospermine: formation of a nucleosome-like structure and network assembly. *FEBS Lett.* **396**: 71-76 (1996)
Zhang C, Shao PG, van Kan JA, van der Maarel JRC: Macromolecular crowding induced elongation and compaction of single DNA molecules confined in a nanochannel. *Proc. Natl. Acad. Sci. USA* **106**: 16651-16656 (2009)
Zinchenko ZA, Sergeyev VG, Murata S, Yoshikawa K: Controlling the interchain segregation on a single DNA molecule. *J. Am. Chem. Soc.* **125**: 4414-4415 (2003)

Cryo-electron microscopy of the spermine-DNA condensates

INTRODUCTION

Multivalent cations, proteins and molecular crowding agents can cause DNA to collapse from solution into well-defined nanometer scale particles. This phenomenon has been studied for years as a model of high density DNA packing in living systems, particularly in viruses. More recently, efforts to develop artificial gene delivery have renewed the interest for theoretical and experimental studies, with the hope to control size and shape of condensed DNA. This collapse often results in the formation of toroids, rods or spherical globules.

To our knowledge there is no systematic morphological analysis of DNA condensed in the bulk by the polyamines spermidine (3+) and spermine (4+) despite the ubiquity and highest biological interest of these cations involved in many biological processes and also in DNA condensation in vivo and in vitro. Raspaud et al. (1998) elaborated a complete phase diagram and defined ionic conditions where short DNA fragments (146 bp) are partially or totally aggregated, by exploring a large range of spermine and added salt (NaCl) concentrations. The aggregates collected by centrifugation have been analyzed by X-ray diffraction (Raspaud et al., 2005). At low DNA concentration, the smaller interhelix spacings are obtained for the lowest salt and spermine concentrations. The interhelix distance increases from 28.2 Å (no salt) up to 29.4 Å at 200 mM NaCl. A similar range of variation is measured in the absence of NaCl by increasing the spermine concentration from 1 to 100 mM spermine.

Cryo electron microscopy permits now precise measurements of the interhelix spacing together with the visualization of the shape of the collapsed DNA but only few ionic conditions have been tested. Hud and Downing (2001) studied Lambda DNA condensed by $Co(NH_3)_6Cl_3$ (in 10 mM Tris, 1 mM EDTA, pH 7.0) and visualized the hexagonal packing of the chain inside the toroid together with the facetting of their section. Considering the polyamines, only a few conditions have been tested but slight changes were shown to modify significantly the structure of DNA into toroids confined into vesicles (Lambert et al., 2000) or into bacteriophage capsids (Leforestier and Livolant, 2009). Otherwise, Carnerup and Ainalem et al. (2009) reported cryoEM observations of multiple morphologies of linearized T7 DNA (4331 bp) condensed by [ethylenediamine core]-PANAM dendrimers (z= 8, 16 and 64+) in 10 mM NaBr at charge ratio NH3+/PO4- <1. They performed time-resolved cryoTEM, by freezing the samples during the time of condensation, as already reported by others (Frederik and Sommerdijk, 2005), after 1 min or more. They reported how the size, composition and morphology of the aggregates are affected by dendrimer size and charge. They also explored the effect of salt on the morphology of the aggregates (Carnerup et al., 2011). The interhelix distance is much larger in the aggregates formed with dendrimers (3.1-3.4 nm) than in CoHex or polyamine-DNA aggregates.

Our first goal is here to use cryoEM to analyze in parallel the structure and morphology of DNA condensed by spermine. We explored a vertical line in the phase diagram between the onset of precipitation at low spermine concentration (0.05 mM) up to above the resolubilization limit (400 mM spermine). All experiments have been done in low salt conditions (10 mM Tris HCl, 1 mM EDTA, pH 7.6). By varying the spermine concentration, we expect to change the interhelix distance and to monitor in parallel changes of the conformation of the DNA globule. The concentration of DNA has been fixed to 0.03 mM phosphate to favour the collapse of individual chains and to limit their aggregation.

Another important aspect of DNA condensation deals with the kinetics of the process. Widom and Baldwin (1980) reported how the condensation of DNA is a slow process (about 1-3 hours) and how

the rate decreases with increasing DNA concentration. Later on, Porschke (1984) demonstrated the existence of two different condensation reactions which are clearly separated on the time scale. The intramolecular condensation (≤ 1 µM DNA) is a very fast process that occurs in two steps, the condensation of the ligands onto DNA that is the limiting step of the reaction followed by the very fast collapse of the DNA chain. For higher DNA concentrations (≥ 5 µM) an intermolecular association takes place identified as a "very slow" reaction that would correspond to a very broad ensemble of time constants. The kinetic aspects of the transitions have been considered experimentally these last years, using AFM methods. Interesting planar morphologies such as "flower-shaped" structures have been described as transition steps between rods and toroids (Fang and Hoh, 1998). Despite the high interest of this approach, the limitation of AFM – and other related near field microscopy methods - comes from the fact that the DNA condensation occurs on the surface of the supporting charged film and not in the bulk, which more likely introduces non negligible effects on DNA condensation. According to theory, the globule-toroid transition would be first order-like (Grosberg and Khokhlov, 1994). Nevertheless, this discontinuous change in topology would be associated to a continuous progression from disordered to ordered internal structure (Cooke and Williams, 2004). It has been proposed that, in this two steps process, the first one would correspond to the formation of the dense toroidal aggregate, and the second one to the transition to a twisted entangled state (Kulic et al., 2004). Therefore the kinetics appears to be also an important parameter to take into account, together with small internal structural changes in the collapse DNA globule. The liquid crystalline state of the DNA globule would be an essential point to allow this reorganization of DNA inside the globule. In the second part of the article we tentatively followed the kinetics of the DNA collapse at a given spermine concentration that was fixed to 0.05 mM.

MATERIAL AND METHODS

DNA Preparation

Lambda bacteriophage DNA (48,500 bp) (Invitrogen Inc., Carlsbad, Canada) was extensively dyalized in 2 M NaCl and then in 10 mM Tris-Cl^-, 1 mM EDTA, pH 7.6 to replace all counterions bound to DNA by monovalent ions (mostly Na+ with some Tris+) and stored at 4°C at a concentration of 370 µg/ml.
Samples were prepared at a final 10 µg/ml DNA concentration (0.03 mM Phosphates) by mixing equal volumes of 20 µg/ml DNA and 0.1, 2, 200, 400, and 800 mM spermine 4HCl (Sigma) prepared in the same buffer. After gentle stirring with a pipette, sample are left at 20-21°C for 16 min before preparation for cryoEM.
In a second set of experiments, a modification was added to the procedure: 1.5 µl of the 20 µg/ml Lambda DNA solution was deposited on the carbon-coated surface of the holey-carbon grid which was vertically fixed in the temperature-humidity controlled chamber. Then, the 0.1 mM spermine solution was deposited on the opposite face of the grid, as drawn on Figure 1. From this moment (t = 0), spermine immediately diffuses into the DNA solution on the opposite side of the grid, to induce DNA condensation. CryoEM plunging was done as described below after t = 6 s, 9 s, 20 s, and 60 s. Final concentration were 10 µg/ml DNA and 0.05 mM spermine.

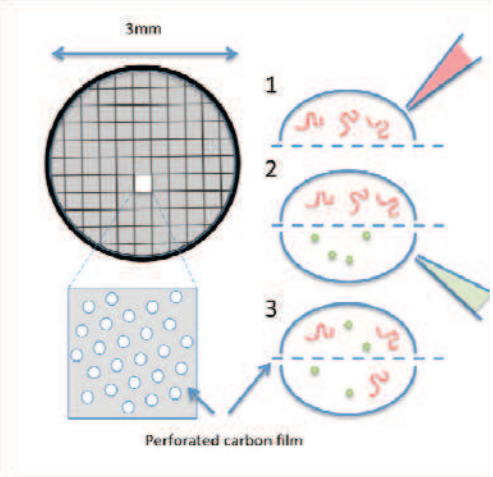

Figure 1. Protocol for time resolved cryoEM observation of DNA aggregates formation. The DNA solution (red) was deposited on one side (step 1). At t = 0, the spermine solution was added on the other side of the grid (step 2). The two solutions mix up through the holes (diameter 2 µm) of the carbon film covering the EM grid.

Electron Microscopy

3 µL of the solution are deposited on a glow-discharged holey carbon grid (Quantifoil R2/2, Jena, Germany). The grid is blotted with a filter paper for 2-3 seconds to remove the excess of the solution, and directly plunged into liquid ethane cooled down by liquid nitrogen. During the preparation of the samples, the temperature and relative humidity of the environment are kept at 20-21°C and 89-96 %, respectively, in a home-made device. Frozen samples are transferred into a Gatan 626 cryostage (Gatan, Warrendale, USA) and observed in a transmission electron microscope (JEM-2010, JEOL, Japan) operated at 200 kV. All images are recorded on Kodak SO163 negative films under low dose conditions at a magnification of 50000X. Micrographs were taken at two underfocus values to get information on the overall shape of the objets (-3000 nm) and to image details of the DNA structure (- 850 nm). The films are developed in full strength Kodak D19 for 12 min, and scanned with a Nikon Coolscan 9000 at a resolution of 4000 pixels/inch. DNA interhelix spacings were measured on scanned images using ImageJ.

RESULTS

1. Morphology of the DNA aggregates as a function of the spermine concentration

We analyzed by cryoelectron microscopy the structure of DNA condensates using Lambda DNA (48.5 kbp) and the tetravalent polycation spermine (sp, 4+) mixed in the bulk in 10 mM Tris buffer. The final DNA concentration was fixed to 0.03 mM phosphates, and the spermine concentration adjusted to 0.05, 1, 100, 200 and 400 mM to explore a large range of conditions, starting at the onset of precipitation up to above the re-solubilization limit. The phase diagram elaborated for short DNA fragments (50 nm) and long DNA chains (Lambda) condensed by spermine (Raspaud et al., 1998) is given in Figure 2. The region where DNA is partly or fully precipitated from the supernatant (2 phases domain) is limited by the precipitation and resolubilization lines. Experimental points correspond to the low concentration regime and are indicated along a vertical line on Figure 2. All experiments are done in excess of positive charges, with charge ratio ($r = NH3^{+}/PO4^{-}$) being respectively 1.6, 33.3, 3300, 6660 and 13300.

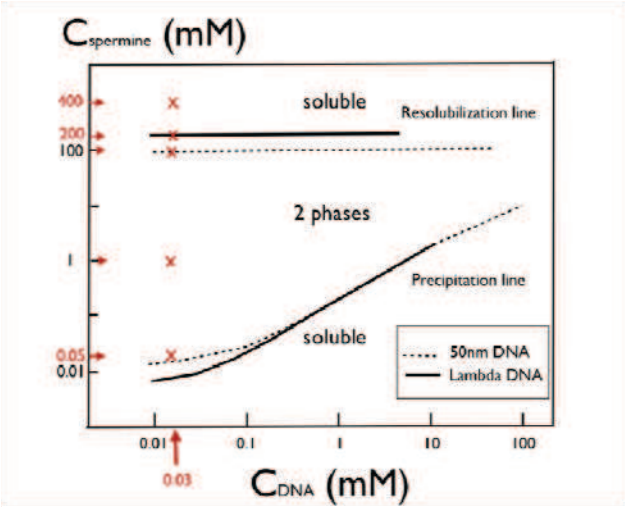

Figure 2. Schematic phase diagram of short DNA fragments (----) and long Lambda chains (—) precipitated by spermine (4+) in 10 mM TE buffer. DNA is partly or fully precipitated from the supernatant (2 phases) between the precipitation and redissolution lines and soluble outside of this domain. (Redrawn from Raspaud et al., 1998). For cryoEM observations, we fixed the lambda DNA concentration to C_{DNA} = 0.03 mM Ph, and analyzed samples prepared at $C_{spermine}$ = 0.05, 1, 100, 200, and 400 mM, as indicated in red on the diagram.

λ-DNA is a worm like chain with a contour length L = 48500 bp x 3.4 Å = 16.5 µm. The overlap concentration C* between the dilute and the semi-dilute regime can be defined as ~ M_w/R_g^3 with M_w the molecular weight and R_g the radius of gyration of the chain. In our buffer conditions (10 mM Tris buffer, 1 mM EDTA, pH 7.6), λ-DNA has a persistence length of 50 nm (Taylor and Hagerman, 1990) and a radius of gyration R_g ~ 500 nm (Pernodet and Tinland, 1997). The C* concentration was determined experimentally as ~ 50 µg/ml by Verma et al. (1998) which corresponds to ~ one λ coil/µm (Hud and Downing, 2001). Our λ-DNA stock solution prepared at C = 20 µg/ml is a dilute solution (not far below the C* concentration) with about one coil/0.4µm (Lambert et al., 2000). At this salt concentration the Debye screening length is ~ 3 nm. We did not collect images of the initial 0.03mM Lambda DNA solution before addition of spermine. These images are not so easy to obtain and we did not focus our effort on this.

In the precipitation domain ($0.05 \leq C_{spermine} \leq 100$ mM), DNA chains mostly form large aggregates that are presented on Figure 3 a,c,d. Nevertheless, DNA toroids usually keep their individuality and can be recognized in the aggregates. The toroids are stuck on top of each other and they may be flattened or distorted by the stacking. Isolated rods or toroids are rarely found, only at 0.05 and 100 mM spermine concentrations, never at 1 mM spermine. DNA bundles are also found under a large range of ionic conditions. They are predominant at Csp = 200 mM (the upper limit of the precipitation domain). At 200 mM, these bundles (up to 50 nm in diameter) are straight. The smallest ones that consist of only a few molecules are called fibers. We notice a large dispersion of their dimensions as illustrated on Figure 3e.

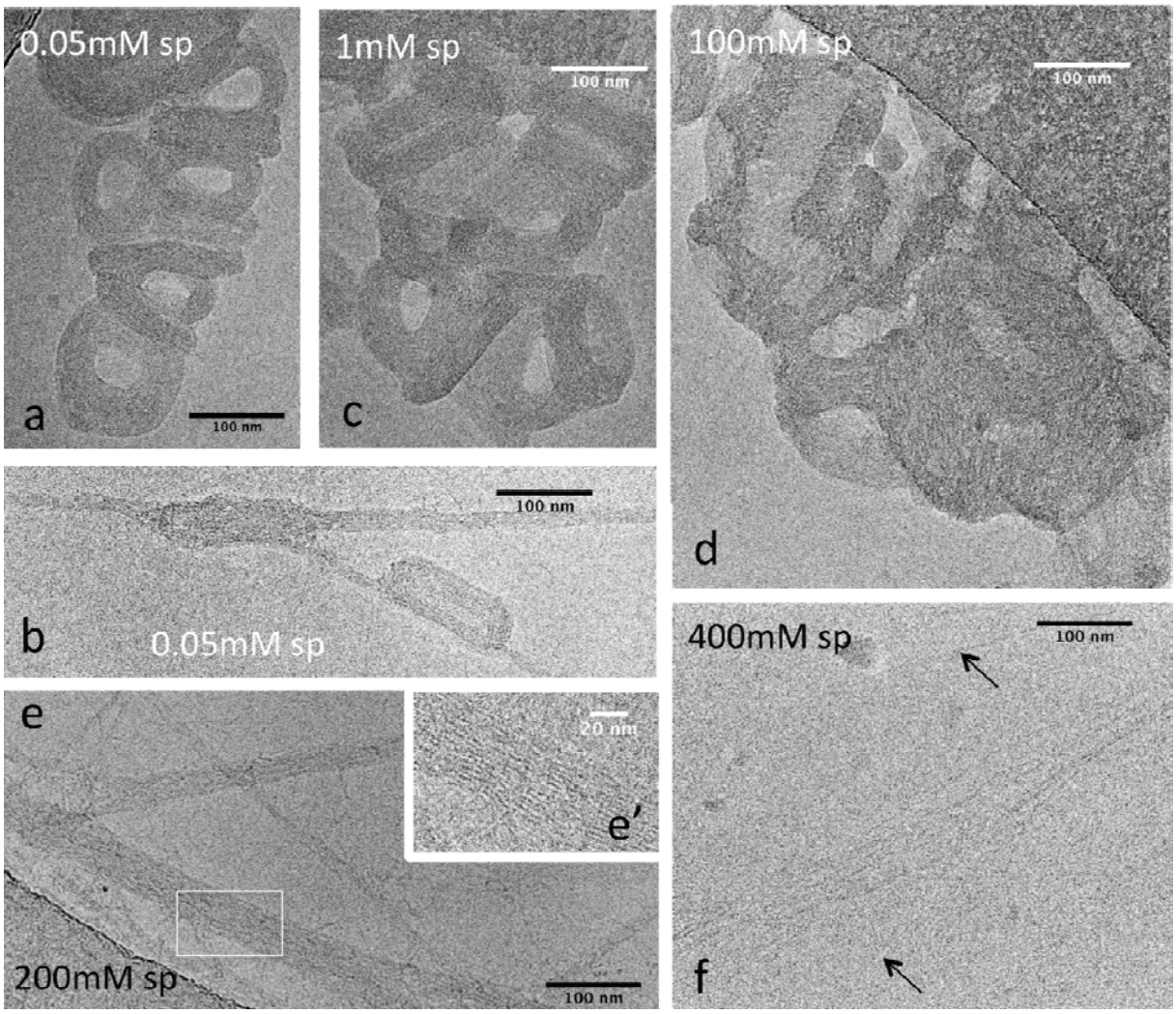

Figure 3. Morphology of the aggregates as a function of the spermine concentration. Aggregated toroids are found at 0.05 mM (a) together with bundles and rods (b). At Csp = 1 mM (c) and Csp = 100 mM (d) large aggregates are formed, made of toroids that are fusing together. Bundles are predominant at 200 mM sp (e, e'). Only very thin bundles are seen at 400 mM spermine (f). CryoEM micrographs recorded at -3000 nm defocus.

Outside of the precipitation domain (Csp = 400 mM), DNA chains form a network of thin fibrils 4-6 nm in diameter (Figure 3f). Their aspect differs from a dilute Na-DNA solution, where chains are kept apart (not shown). They are thicker, more rigid and not completely isolated the ones from the others.

2. Morphology of the aggregates at different times after addition of spermine

In a second set of experiments, the spermine concentration was fixed to 0.05 mM and we analyzed the condensation process at short times after addition of spermine (6, 9, 20 and 60 s). The DNA concentration was fixed to 0.03 mM Ph as in the first series of experiments but the DNA and spermine were not manually mixed. Spermine was deposited on the opposite side of the grid and let to diffuse through the holes of the carbon grid into the DNA solution, as drawn in Figure 1. By this process we were able to reduce to the minimum the delay between the addition of spermine and the time of freezing. We also reduced artefactual stretching of the DNA fibers that may be induced by vortexing or mixing with the tip of a pipette.

An overview of the structures is given in Figure 4.

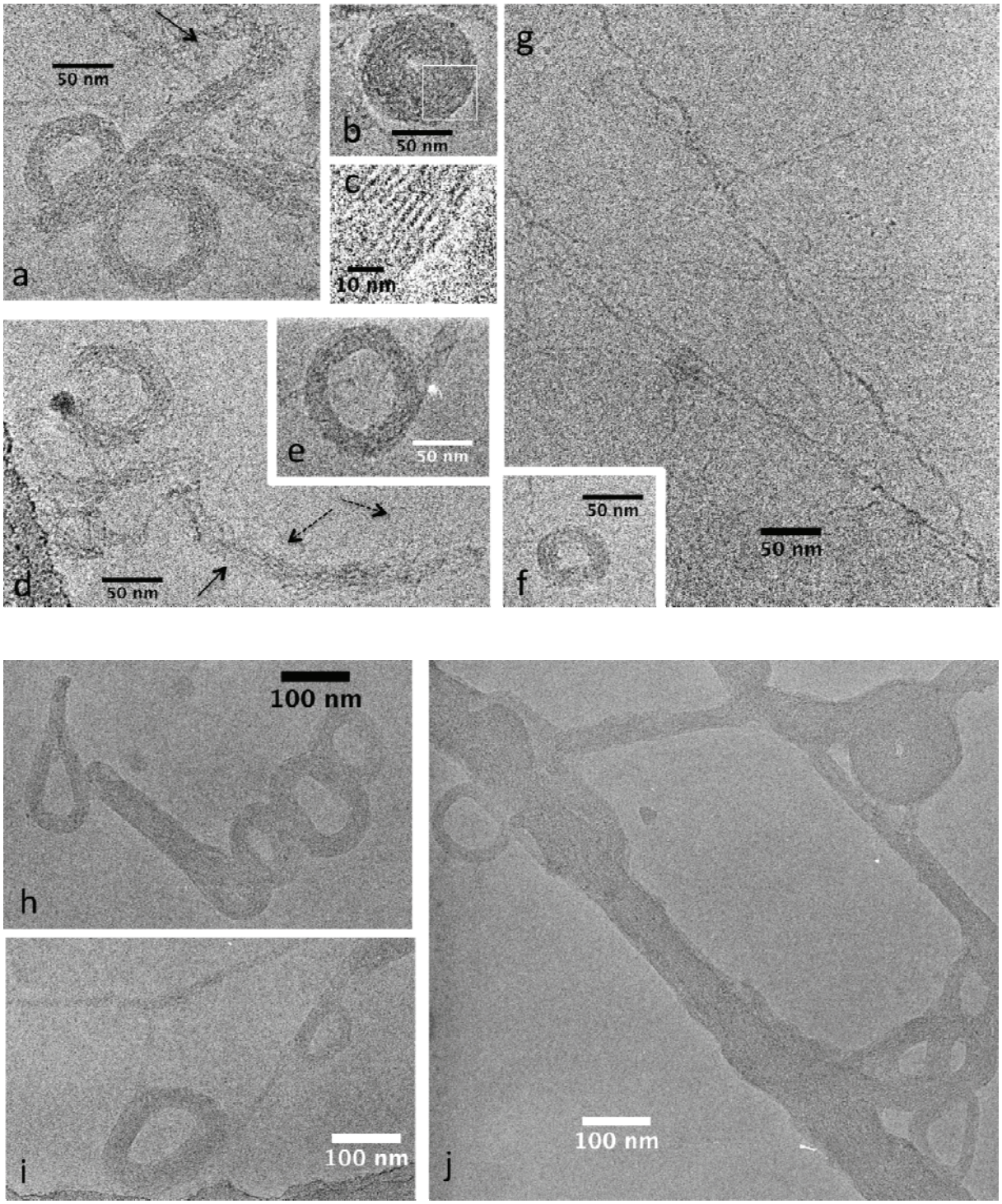

Figure 4: General aspect of the aggregates after 9 sec (a-g), 20 sec (h-i) and 60 sec (j). Samples were prepared as described in Material and Methods. CryoEM micrographs are recorded at -3000 nm defocus except in (c) that corresponds to a detail of (h) (-880 nm). Arrows in (a) and (d) point to partially collapsed objects connected to toroids and bundles, with uncondensed fibres around (dotted arrow).

6 sec after addition of spermine, we do not observe any condensed form of DNA: no globules, toroids, rods, bundles, fibers, or aggregates. We did not visualized uncondensed DNA either, probably

because of the difficulties mentionned above in the visualization of dilute Na-DNA. A few seconds later (t = 9 s), we mostly observe fibers, about 4-6 nm in diameter, usually made of 1-5 DNA chains aligned in parallel. These are well visible at 3000 nm underfocus. They are often stretched and highly networked, and sometimes aligned along preferred orientations. Some of them wiggle and twist with a pseudo period of 30-60 nm, along distances as long as 1 µm (Figure 4g). Many globules, toroids, and rods are also found. Often connected to toroids and bundles are seen loosely condensed objects and uncondensed chains pointing out (arrows in Figure 4a,b). Toroids are usually smaller and thinner than those formed after 16min in the first set of experiments (Figure 4a-f). The smallest one (Figure 4f) has an external diameter of about 50 nm, close to the value measured for the smallest G4 dendrimer/DNA toroids (Carnerup et al., 2009). The rods may be straight or curved with DNA loosely packed inside (Figure 6a,d). Small isolated globules were found occasionnally. A close examination reveals that at least some of them are toroids with a very small central hole (Figure 4b). Large aggregates are extremely rare.

At t = 20 s, thin fibers are not seen anymore and are replaced by bundles. Globules, toroids, rods are found isolated and, more often, aggregated by groups of 2 to 5 or stuck to the bundles (Figure 4h-i). Compared to data collected at t = 9 sec, toroids and rods are generally larger. Their boundaries are better defined and the DNA ordering inside present more striated patterns which suggests a higher DNA organization. Objects with shapes intermediate between toroids and rods (rackets) that are found here (Figure 4h) were never observed under other conditions in our experiments.

At t = 60 s, there are numbers of toroids and rods that are mostly stuck to large bundles. A typical example is given in Figure 4j. The diameter of these bundles is irregular, and in many places it seems to be made of merging rods and toroids. Their diameter is also larger than at t = 20 s. Thin fibers observed at t = 9 sec are not found anymore.

3. Structure of spermine-DNA aggregates

We present on Figure 5 aggregates of toroids formed at 0.05, 1 and 100 mM spermine, and imaged with low underfocus values (-850 nm) to visualize the details of the structure. Many of these toroids are easy to identify (underlined with different colours on Figure 5a). Figure 5b presents two toroids, one in top view (on the left) and one in side view (on the right). As schematically drawn on Figure 6, the side view shows the section profiles of the toroid, in which we recognize the DNA segments seen along their axis and organized into a hexagonal lattice (double arrow on Figure 5b). In the aggregates, a few toroids are more difficult to identify, apparently engaged into a process of fusion and reorganization (Figure 5a) that will be detailed below. Aggregates where toroids cannot be recognized are also found, especially at 1 mM spermine (Figure 5c), and present beautiful top and side views of the hexagonal lattice from which can be measured the distance (d) between the reticular planes and the interhelix distance (a_H), with $d = a_H\sqrt{3}/2$.

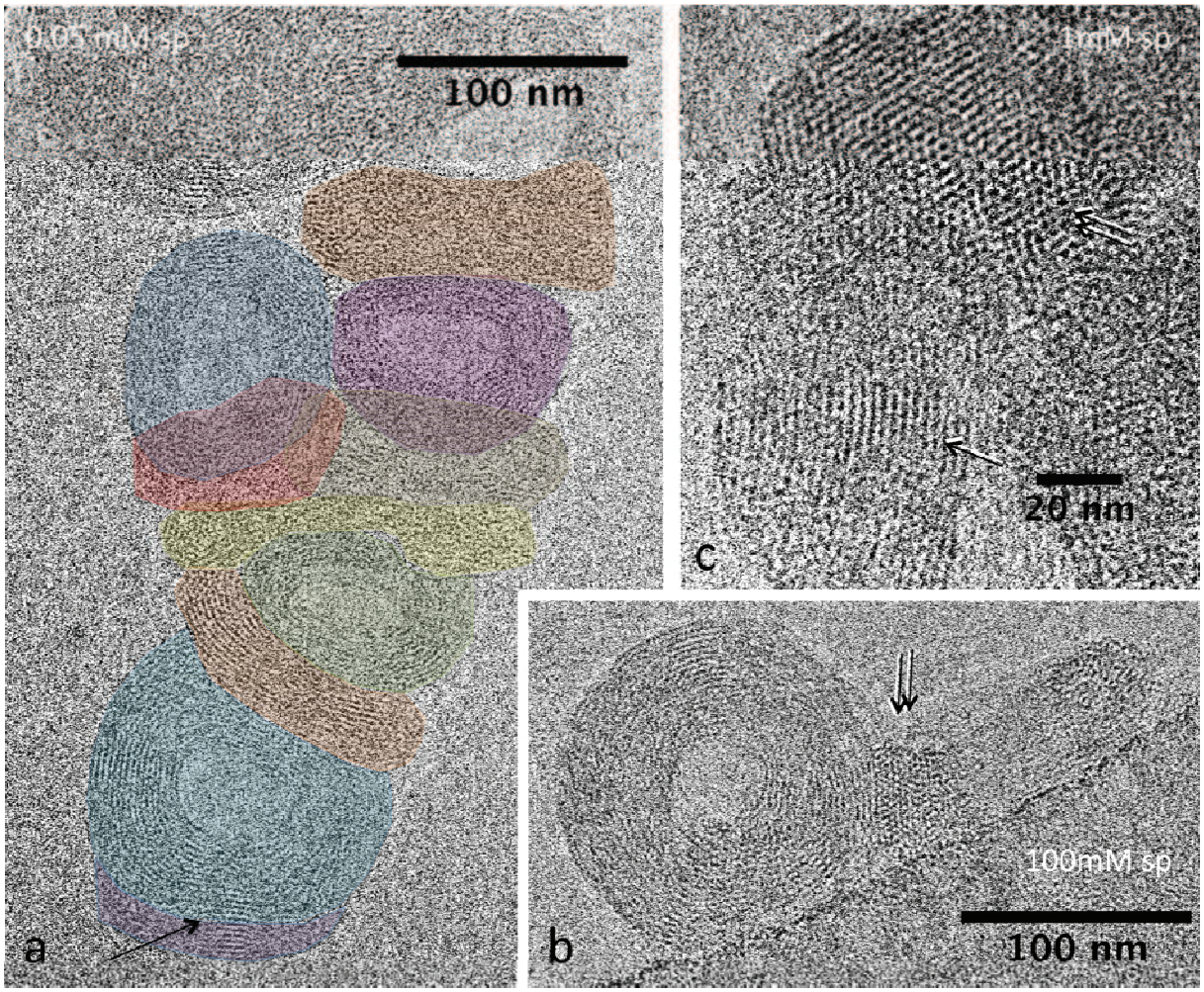

Figure 5. Aggregates of toroids with details of their local hexagonal DNA structure (a: 0.05 mM sp, b: 100 mM sp; c: 1 mM sp). CryoEM micrographs are recorded at -850 nm underfocus. Details of the structure are visible under favourable orientations, either striated patterns (simple arrows) or hexagonal lattice (double arrows).

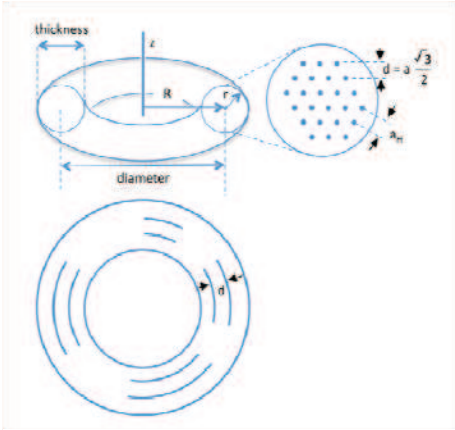

Figure 6: Characteristics of the toroids of radius *r* and *R*, with the *thickness* and *diameter* parameters that have been measured on the micrographs. Top views of the hexagonal lattice let us measure a_H, the interhelix spacing or *d*, the distance separating the reticular planes, easily measured on oblique and side views of the lattice.

We present on Figures 7 and 8 a collection of patterns characteristic of the hexagonal packi ng of DNA helices in toroids, bundles and aggregates. Striations correspond to side views of the hexagonal lattice, and reveal that the reticular planes are perfectly oriented along the direction of the

electron beam. These striated domains are seen in elongated bundles as well as in toroids. As illustrated on Figure 7, the alternation of striated and unresolved patterns is found at all spermine concentrations. The striated domains can extend laterally over distances are small as a few nm (Figure 8d) up to 80-100 nm in a few cases. Their limits can be very sharp with an abrupt transition from the striated to unresolved patterns (Figure 8b). Nevertheless, in many cases, a careful observation reveals that these striations are scarce but can nevertheless be followed outside of these domains (Figure 8a,b - arrows). Regions devoid of clear striations are found frequently in the striated domains. These unresolved domains can be extremely thin (Figure 8c) or more extended. In the toroids, there are generally from 1 to 4-5 striated domain (Figure 5a, Figure 7b) with a large range of lateral extension. The periodicity is well defined and stays constant from the inside to the outside of the toroid. Interestingly, it is extremely rare to detect dislocation lines in these striated patterns.

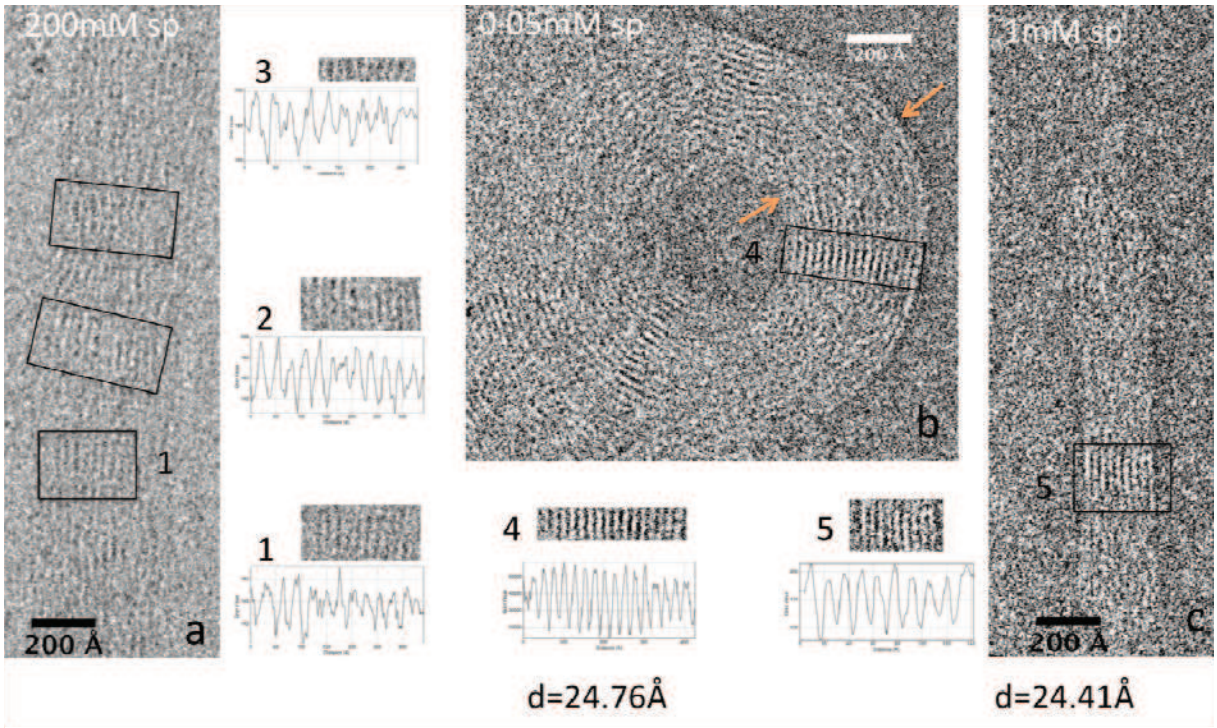

Figure 7: Examples of striated domains observed for three different spermine concentrations (0.05, 1 and 200 mM). The preriod d is measured from the profiles of the selected regions, and averaged over a large number of measurements.

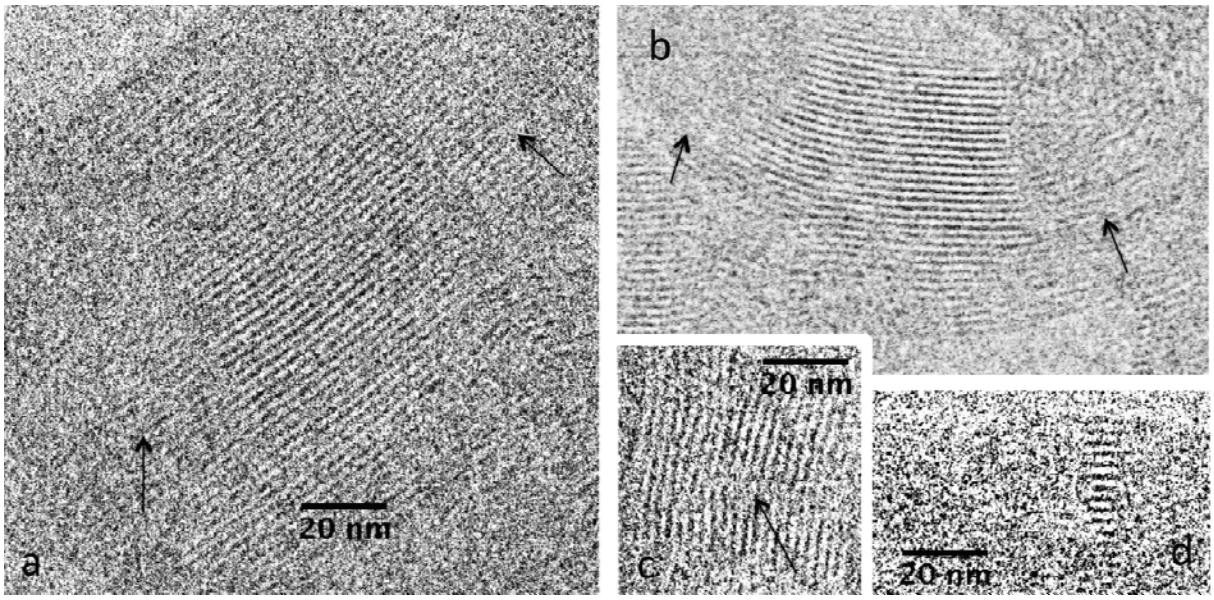

Figure 8: Striated patterns of the hexagonal DNA lattice inside the aggregates formed in 0.05 mM spermine. Arrows indicate lines extending laterally outside of the "striated domain" (in a and b) and a domain with no striation inside a striated domain (in c).

4. Variation of the interhelix distance a_H

The a_H values given in Table 1 have been measured on toroids and aggregates directly on top views of the lattice or by measuring the distance (d) separating the reticular planes ($a_H = (2/\sqrt{3})d$).

aH values (nm)	Average values	globules	toroids	rods	undefined	aggregates	bundles
0.05mM (t=9sec)	**2.98** ±0.02 (90)	3.15±0.01 (3)	2.95±0.02 (79)	2.97±0.1 (3)	3.40±0.11(5)		
0.05mM (t=20sec)	**2.98**±0.01 (134)	3.02±0.14 (3)	2.97±0.01(70)				2.98±0.02 (56)
0.05mM (t=60sec)	**2.91**±0.02 (67)	3.09±0.04 (10)	2.91±0.02 (61)	2.98±0.03 (16)			2.96±0.01(44)
0.05mM (t=16min)	**2.93**±0.01 (64)	2.97 (1)	2.93±0.01 (46)			2.93±0.02 (15)	3.21 (1)
1mM (t=16min)	**2.88**±0.01 (67)		2.88±0.01(45)			2.88±0.02 (21)	
100mM (t=16min)	**2.95**±0.02 (42)		2.95± 0.02(31)				
200mM (t=16min)	**3.32**±0.04 (11)						3.32±0.04 (11)

Table 1: The a_H values measured for each set of experiments. Each averaged value corresponds to the number of measurement indicated in brackets.

Data collected at 1 and 100 mM spermine are in correct agreement with data collected previously by X-ray diffraction analysis of pellets in the 0.1-100 mM sp concentration range in comparable buffer conditions (10 mM TE or 13 mM NaCl) (Raspaud et al., 2005) (Figure 9). It was also shown previously in CoHex-DNA aggregates that values of the interhelix spacing were comparable when measured by X-ray (2.83 nm; Rau and Parsegian, 1992) or by cryoEM (2.8 nm; Hud and Downing, 2001). Our measurements extend to lower and larger spermine concentrations the explored range of spermine-DNA conditions of condensation. We notice a significant increase of the interhelix spacing at Csp = 200 mM. There is no available data to which we can make comparisons at Csp = 0.05 and

200 mM.

For each set of data, we compared the interhelix spacing a_H in globules, toroids, rods, bundles and aggregates.

Toroids may be isolated or aggregated. Aggregates specify that isolated objets cannot be identified anymore. The a_H values are identical in toroids and aggregates, which means that the fusion of toroids and their reorganization into larger objects happens without any change in the interhelix spacing. Only bundles formed at 200 mM show a significant larger interhelix spacing, and interestingly no toroids are formed ar this high spermine concentration. We cannot see bundles in apical views, but we suspect that the DNA chains are not hexagonally packed anymore because the striated patterns are not as regular as in 0.05 and 1 mM spermine (Figure 7). In bundles found at 0.05 mM sp (only at short time, 20 and 60 s), a_H values do not differ from the values measured in toroids. The structure is the same. There are therefore two types of bundles, those that correspond to a transient step before toroids are formed at 0.05 mM spermine, and those that correspond to stable conformations where no toroids are formed at 200 mM spermine.

The a_H values measured at 9, 20, 60 sec (respectively 2.98 ± 0.02, 2.98 ± 0.01, 2.91 ± 0.02 nm) are not significantly different from the values measured after 16 minutes (2.93 ± 0.01 nm).

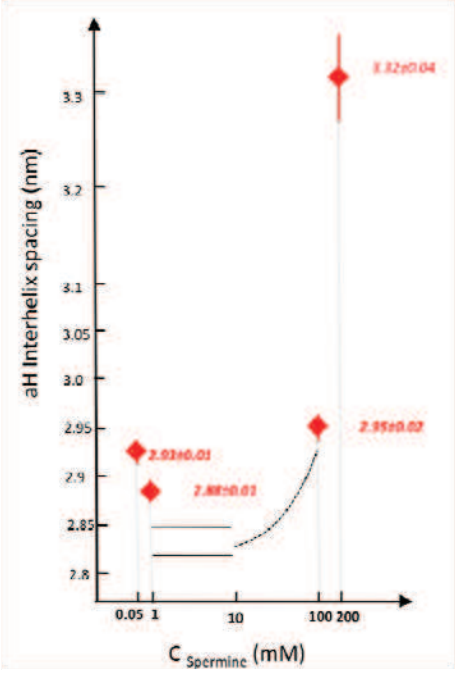

Figure 9: Graph reprenting the measured a_H values in Lambda toroids and aggregates at 0.05, 0.1, 100 and 200 mM spermine concentration in 10 mM monovalent salt (Tris+ and Na+) after 16 minutes of equilibration. For comparison, X-ray data measured with short DNA fragments with no salt and 50 mM NaCl are indicated by the two horizontal lines up to 10 mM sp and by the dotted line between 10 and 100 mM sp where the distance does not depend on the salt environment. (X-ray data from Raspaud et al., 2005).

5. Correlations between DNA helices

In many regions showing the striated patterns, we observed an undulated aspect of the successive series of DNA rows (or reticular planes) (Figure 8a,b). Density profiles have been recorded on selected regions of interest, as illustrated on Figure 10. We have chosen in this example a domain that presents striations almost everywhere around a +π disclination line (Figure 10a). (This type of rotation defect is frequent in lamellar liquid crystalline phases such as hexagonal ones). Their presence reveals that the phase is fluid. Nevertheless, the intensity of the striations fluctuates. The domain with the best striations was selected and density profiles were recorded i) perpendicular to the striations to determine the periodicity d of the hexagonal lattice (d = 25.27 Å in this case) (Figure

10b) and ii) along the rows (Figure 10c). From the periodic patterns recorded along selected rows, we measured a periodicity p ~ 34 Å that corresponds to the helical pitch of the DNA helices. This means that in the thickness of the bundle, a series of helices are correlated and aligned perfectly in register, so that their pitches superimpose and become visible and measurable in 2D projection.

In addition, we compared the scans from successive rows and noticed the relative orientation of the helices from one row to the next. In this particular region, we observe that helices are out of register, as illustrated by the orange spots deposited on top of the highest density spots along the rows, just by blinking the eye to better visualize the visible periodicity. The alignment of the profiles also reveals locally this out of register alignment of the helices. Our observations are in agreement with the report of DNA correlations in spermine-DNA aggregates by X-ray diffraction (Raspaud et al., 2005), and by cryoEM in spermine-DNA bundles and toroids formed inside the bacteriophage capsid (Leforestier and Livolant, 2009). Such correlations of DNA helices have been initially reported in dense Na-DNA hexagonal phases (Durand et al., 1992). Theoretical approaches predicted such DNA correlations and calculated possible relationships between helices in 3D space (Kornyshev, 2010). An improvement in the signal to noise ratio of the images would be needed to perform systematic analyses and to determine whether helices are always shifted from one row to the next, whether it depends on the interhelix spacing, and whether DNA correlations are linked to possible variations of the DNA helical pitch.

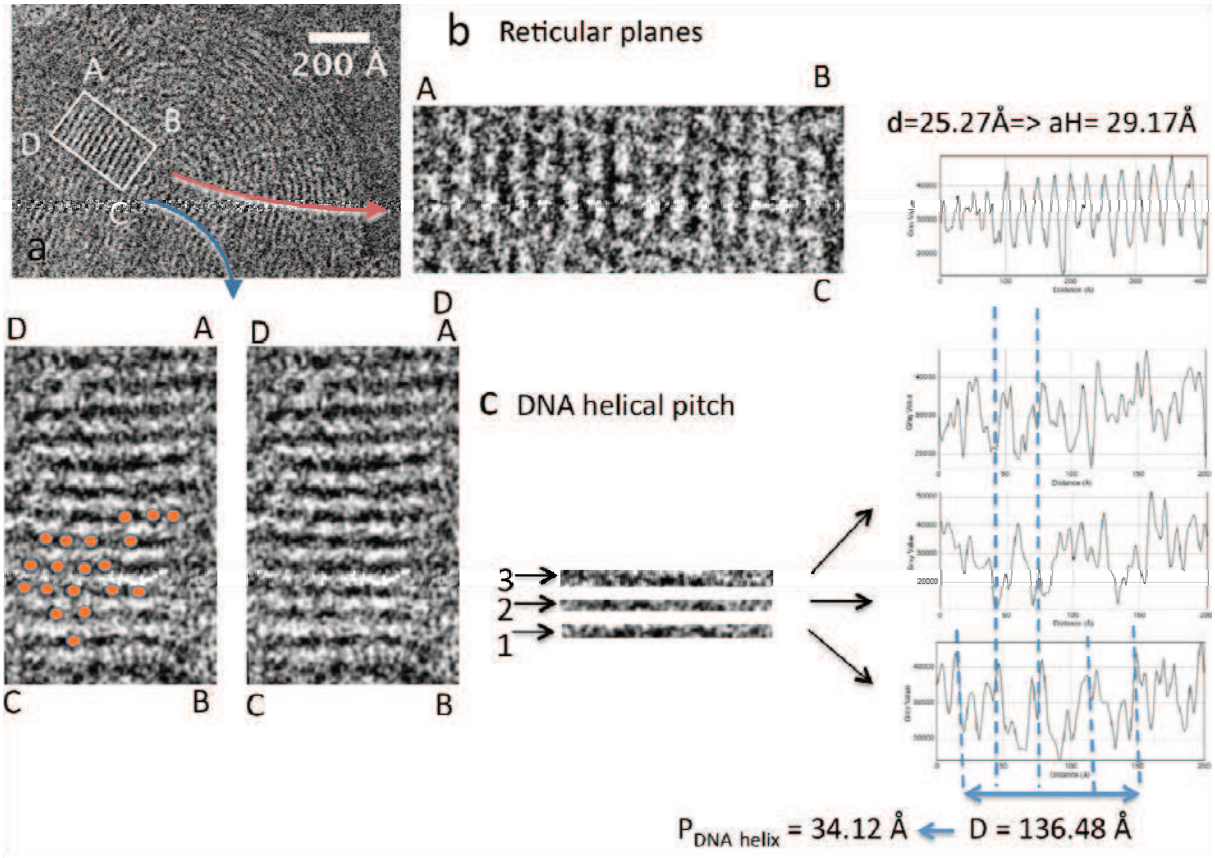

Figure 10: From a selected striated domain (ABCD) are analyze in (b) the periodicity between the reticular planes along AB direction (here d = 25.2 Å) and in (c) the periodicty in the DNA rows along DA direction. The profiles recorded for three successive rows let us meausre a periodicity P = 34 Å that corresponds to the DNA helical pitch. The denser spots along the rows are underlined by orange dots on a copy of the same micrograph.

6. Deviations from a perfect hexagonal structure

Top views of the hexagonal lattice are not rare and enable us distinguish individual helices and measure directly the interhelix distance a_H. This hexagonal lattice does not extend perfectly over large distances. We observe instead a lot of deviations from a perfect hexagonal ordering of parallel helices (Figure 5c, Figure 11). For example, we note the presence of configurations with a few DNA segments seen in perfect top view, surronded by segments that draw lines around them (encircled in Figures 11c). Such patterns are reminiscent of the so-called “double twist” configurations. A small tilt of DNA orientation underlines one of the three main directions of the hexagonal lattice (Figure 11b) or disturb the lattice when the directions of tilt are not correlated. Interestingly, we note here that these lines draw successively different orientations encircling the central molecules. This means that there are different directions of twist around a given molecule, which is the signature of a “double twist” configuration, frequent in bundles formed by helical molecules (Figure 11e). It is more surprising to see their presence inside large aggregates, as described here. Their occurrence reveals the presence of frustration between the dense hexagonal packing of helices and their intrinsic properties of twist. Many examples of structures resulting from this competition have been reported so far (Leforestier et al., 2008) and predicted theoretically (Harris et al., 1999). The presence of domains with double twist configurations inside macroscopic aggregates has not been reported yet to our knowledge. We also observe distortions of the lattice with zig-zag or more complex patterns that we did not analyze in detail yet.

These deviations from the perfect hexagonal structure together with the occasional lack of hexagonal lattice (right part of the side-view toroid in Figure 5b) may be related to side views of the lattice showing the transitions from the strong to the faint and to unresolved striated patterns. Except in one particular case (Figure 7b), there is no significant variation of the diameter of the bundle between striated and unresolved patterns, which cancels out in almost all cases the occurrence of density fluctuations in the aggregates. We assume that the lack of striations arises either from the presence of defects such as those seen along the hexagonal axis or to unfavourable orientations of the reticular planes. Images with a higher signal to noise ratio (for example in thinner sample or tilted images) would be necessary to go further in the analysis of these structural details. These observations can be understood as clues that reveal the complexity of the hexagonal structure at the local scale and how it has to account for the competition arising between close packing and tendency to twist of DNA helices.

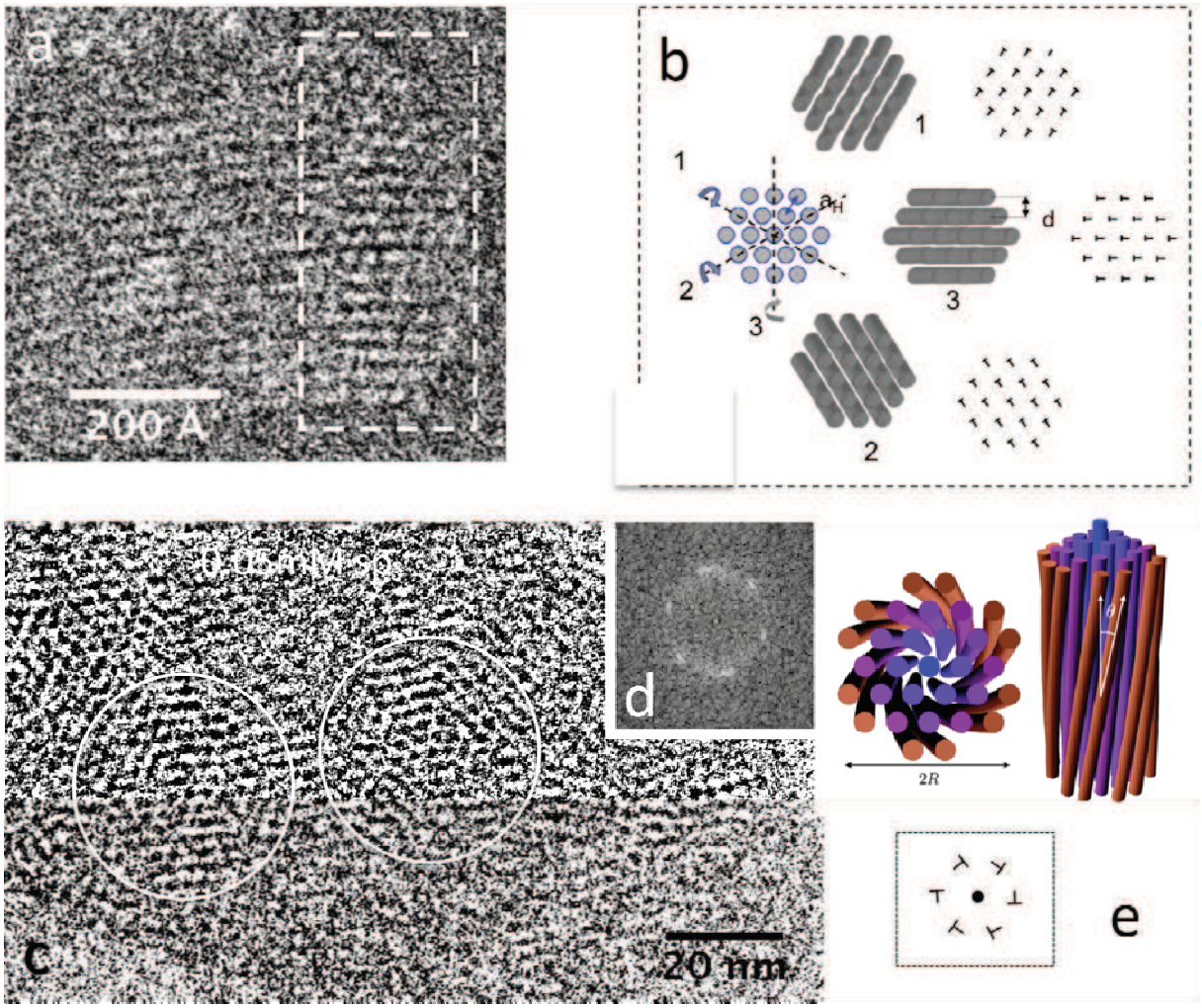

Figure 11: (a-b) Hexagonal lattice of DNA helices almost normal to the observation plane (in the region limited by the dotted line), with a slight tilt of the network that underlines one of the three main directions of the hexagonal lattice, as explained in (b) (redrawn from Leforestier et al, *J. Mol Biol. (2010) 396, 384-395*). A slight tilt of DNA helices along the direction 1, 2 or 3, leads to the formation of striations along one of the three main directions of the hexagonal lattice. Together with each perspective view is given the same pattern using the nail convention: the nail indicates that the chain is oblique to the observation plane, with the tip pointing to the observer; the longer the nail, the higher the obliquity. Here, all chains present the same obliquity with respect to the observation plane. In (c) is presented a top view of a hexagonal domain showing "double-twist" configurations (in encircled domains) revealed by striations drawing a hexagonal box around a few central molecules seen in perfect top view. These patterns arise, as above, from a slight tilt of helices, but the tilt occurs in all directions around the central helices, as drawn in (e) (redrawn from Grason and Bruinsma (2007) *Phys. Rev. Lett.* **99**, 098101) and in (f) according to the nail convention.

7. Fusion and re-organization of DNA aggregates in their liquid crystalline state

Although most toroids present a more or less spherical section profile (usually facetted), a few larger barrel-like toroids have been found. This kind of toroids was described earlier in solutions of bacteriophages ejecting simultaneously their DNA in the presence of spermine (Lambert et al., 2000). Here these barrel-like toroids seem to be made of several superimposed small toroids that fuse together secondarily. Indeed, Figure 12a and b let us recognize a few toroids seen in side view. Those are stuck on top of each other, with their axes aligned along the same direction. At least two toroids can be recognized on Figure 6a and the faceting of the lower one is still visible (bracket n°1). A closely related situation is seen on Figure 12b, with several superimposed domains (toroids) still visible,

especially on the right side that is not straight. We may hypothesize that toroids seen on Figure 12c and d were made of several toroids that cannot be identified anymore.

Such patterns reveal that aggregation does not correspond to a simple sticking of toroids. This initial aggregation step would be followed by a fusion and reorganization of DNA to form larger toroids or larger aggregates. Such a process reveals a necessary fluidity of the sample based on a liquid like behaviour of DNA, with molecules probably sliding along one another in the aggregate. Pelta et al. (1996) already described the fluidity of the liquid crystalline phases of polyamine-DNA aggregates in optical microscopy. We are visualizing here what happens at higher resolution. In other aggregates, the toroids cannot be recognized anymore (Figure 5c). Those may correspond to a later stage of the secondary aggregation process.

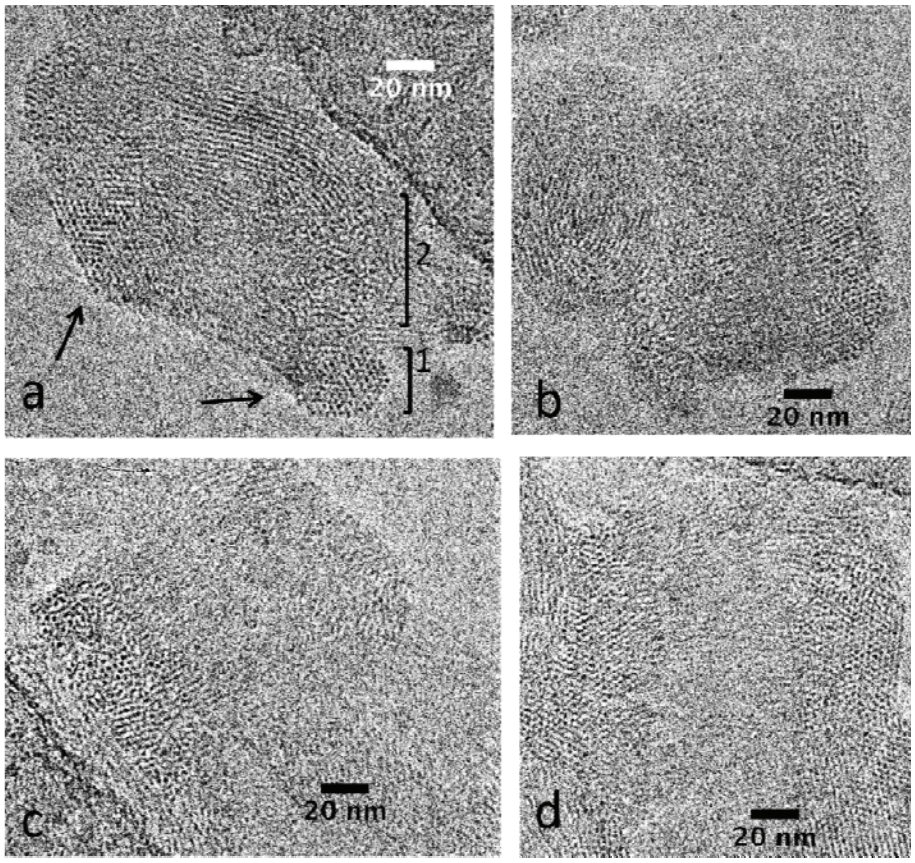

Figure 12. Fusion of toroids into larger aggregates in 0.05 mM spermine.

Other examples of this liquid crystalline fluidity and reorganization of DNA in the aggregates comes form the observation of the striated patterns. There are many examples showing how striations are in continuity between two aggregated toroids that are still recognizable, as for example in the region indicated by the arrow on Figure 5a.

8. DNA toroids, bundles, spheroids, rods and rackets

We tried to quantify the relative amounts of DNA conformations in the two series of experiments (Figure 13). Toroids are predominant at low and moderate spermine concentration (0.05, 1 and

100 mM). A sharp transition from toroids to bundles is observed between 100 and 200 mM spermine. For higher spermine concentrations, bundles disassemble into thin elongated fibers (called here fibres of type 1) (Figure 3f). For the 0.05 mM spermine concentration, the toroidal shapes are predominant. Nevertheless, they are exceptionnally observed at 9 s and become more numerous at 20 s. Instead we found many thin fibers (type 2) at very short times that are still present after 20 s in coexistence with bundles, toroids, rods and rackets (Figure 4). Bundles of type 2 as well as rods and rackets (Figure 4h) can be considered as transient states in the process of toroid formation since they are never found under other conditions. Thin elongated fibers observed just below and above the resolubilisation line at high spermine concentration (type 1) or at very short time close to the precipitation line (type 2) should not be confused. They share the particularity to be thin, stretched and elongated but for different reasons that we will discuss below.

Effect of spermine concentration (t=16min)	Rods and rackets	Toroids	Bundles	Fibres
400mM	-	-	-	+++ (type 1)
200mM	-	-	++++	+
100mM	-	++++	-	-
1mM	-	+++	ε	-
0.05mM	-	+++	+	-
Effect of time after mixing (Csp= 0.05mM)				
6 sec	-	-	-	-
9 sec	-	+	-	+++ (type2)
20 sec	++	++	++	++
60 sec	-	++	++	-
16 min	-	+++	+	-

Figure 13: Semi-quantitative evaluation of the relative frequency of identified DNA shapes (rods, bundles, toroids, and fibers) as a function of the spermine concentration (after 16 min) and as a function of time (for Csp = 0.05 mM).

We focus now on bundle and toroid morphologies that were found under all experimental conditions.

i) Toroids

All identified toroids were measured and their diameter plotted with respect to their thickness (Figure 14). As in Conwell et al. (2003), toroid diameter and thickness correspond to twice the respective radii R and r, as drawn in Figure 6. For each set of data, we plotted the correlation line. All correlations are slightly positive, as illustrated in the inserts of Figure 14. Toroids have a mean diameter of 87 ± 2, 80 ± 4 and 88 ± 2 nm and a mean thickness of 40 ± 2, 46 ± 4 and 47 ± 2 nm, when observed after 16 min at 0.05 , 1 and 100 mM spermine respectively. For the 0.05 mM spermine concentration, we note that toroids formed at short time are significantly smaller and thinner (diameter D = 65 ± 3 nm and thickness Th = 6 ± 2 nm at 9 s) than toroids observed at longer time (D = 90 ± 4 nm and Th = 36 ± 2 nm at t = 20 s; D = 85 ± 6 nm and Th = 32 ± 2 nm at t = 60 s).

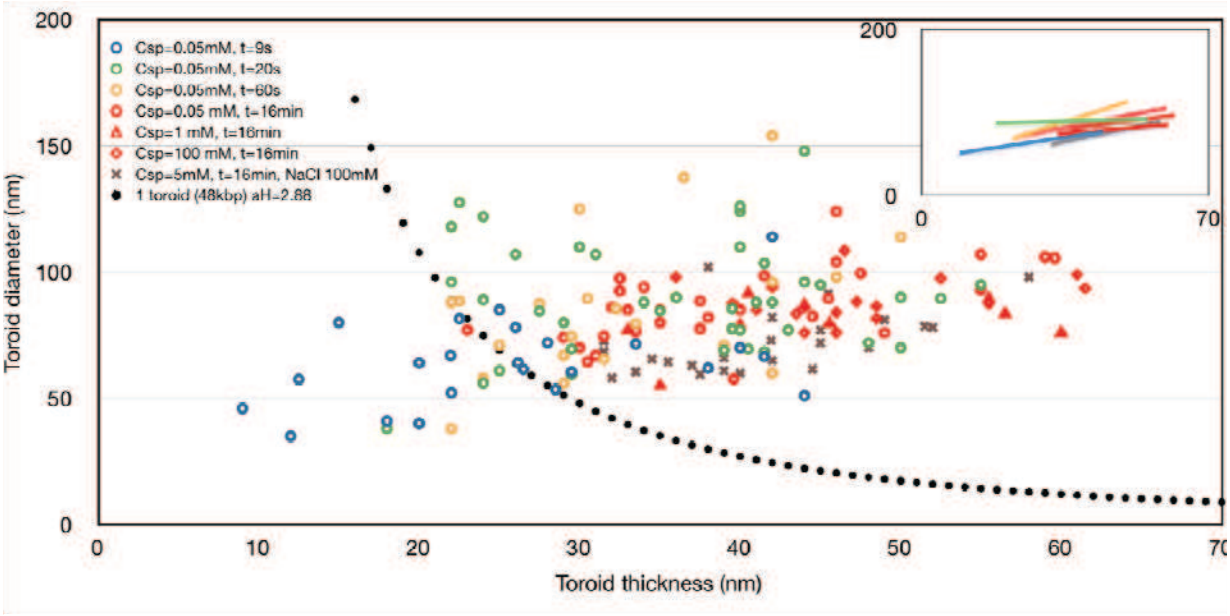

Figure 14: Comparison of toroids diameter and thickness as a function of the spermine concentration and as a function of time for the given spermine concentration (Csp = 0.05 mM). The black dots correspond to possible dimensions of a toroid made of a unique Lambda DNA chain (48 kbp) with interhelix distances aH = 2.88 nm (the volume of a lambda chain is 1.1 x 10^5 nm^3). All measurements are collected in 10 mM Tris-Cl^-, 1 mM EDTA, pH 7.6 except one set of data (x symbols) (collected in 5 mM sp, 100 mM NaCl, 10 mM tris-Cl-, after 15 min). The insert presents the regression lines calculated for each set of data, using the same color code. All points below the black dotted line are made of less than one Lambda chain.

The black dots drawn on Figure 14 correspond to the possible dimensions of a toroid made of a single 48 kbp DNA chain. This curve, plotting the diameter versus the thickness, was obtained from a calculation assuming that a single DNA chain forms a torus in keeping constant interhelical spacing (a_H). By equating the torus volume ($V = 2\pi^2Rr^2$) to the volume of a cylinder of diameter a_H containing the DNA molecule of length L ($\pi a_H^2 L/4$), we obtain the following relation: *diameter* = $a_H^2 L/\pi(thickness)^2$. In our case, we put L = 16320 nm (for lambda DNA) and a_H = 2.88 nm (for Csp = 0.05 nm).

Interestingly, all toroids (except one) measured 16 min after addition of spermine contain more than one λ-DNA chain. Conversely, toroids made of less DNA than expected for one λ-DNA chain are found only at short time after addition of spermine (half of the toroids observed after 9 s, and a few other at 20 and 60 s). These data include a few barrel-like toroids presented on Figure 12c,d.

The Figure summarizing the dimensions of toroids can be compared to the observations of Conwell et al. (2003) with 3 kbp DNA chains condensed with Cobalt hexamine (3+) in various ionic environments. They showed that the diameter and the thickness of the toroid show proportional relations in general.

ii) Bundles

As reported above, bundles are rare at Csp = 1 mM and absent at Csp = 100 mM (Figure 13). When bundles exist, their thickness depends on the ionic conditions. Figure 15a compares the histograms of the thickness of bundles formed at 0.05, 1 and 200 mM spermine. A bell curve is observed at 200 mM spermine (with a mean value of 19.3 ± 0.6 nm) whereas bundles formed at 0.05 mM spermine present an asymmetric distribution with a majority of very thin bundles (made of the lateral interaction of 1-3 DNA chains). The tail distribution of larger bundles leads to a mean value of 9.4 ± 0.6 nm. It can be noted that the symmetric distribution is found when bundles present a large interhelix distance (3.3 nm in 100 mM) and do not coexist with toroids. Conversely asymmetric

distributions are found for bundles with small interhelix spacing, coexisting with toroids.

For a given spermine concentration, the thickness of the bundles also increases with time (Figure 15b), with a mean value of 4.8 ± 0.4 nm at t = 9 sec, compared to 28.8 ± 2.3 nm at t = 20 sec and 39.2 ± 2.1 nm at t = 60 sec. This increase illustrates the aggregation process. Surprisingly, their thickness was reduced to 9.4 ± 0.8 nm after 16 min when samples are prepared in the bulk.

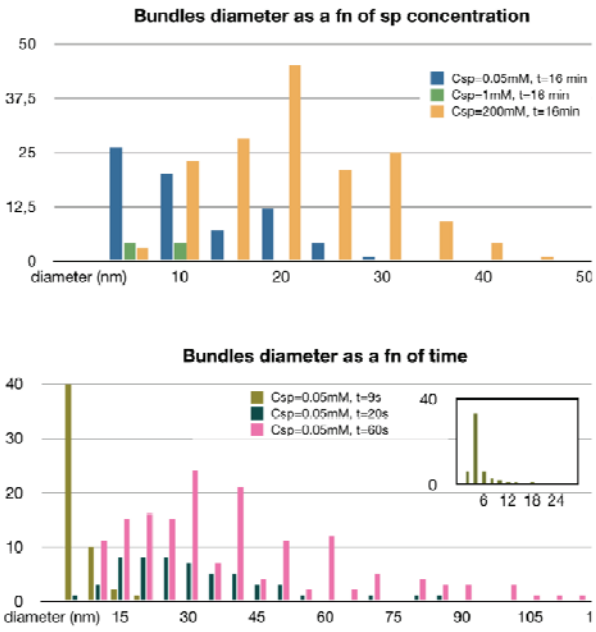

Figure 15: Thickness of the bundles as a function of spermine concentration (a) and as a function time (b).

The thickness of the bundles was also compared to the thickness of the toroids for ionic conditions where both morphologies coexist (at Csp = 0.05 mM for several condensation times and at Csp = 5 mM, with 100 mM added NaCl after 16 min) (Figure 16). The thicknesses distribution in toroids looks more or less symmetric in all conditions whereas in bundles the distribution is asymmetric and skewed to the right which suggests that their dimensions did not reach an equilibrium state (even after 16 min) probably because of a competition between the formation of bundles and toroids that coexist under these ionic conditions.

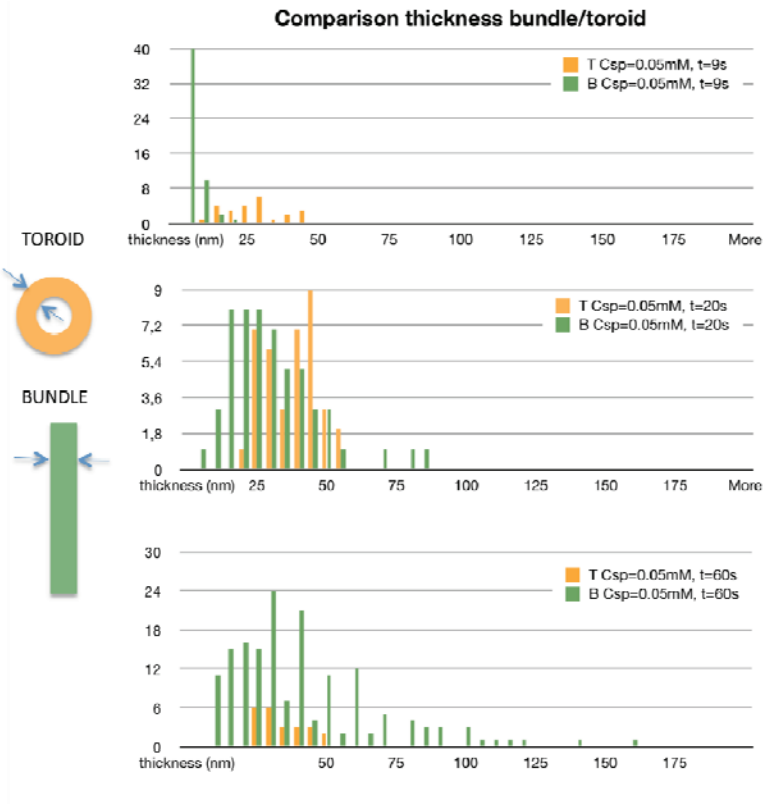

Figure 16: Histograms illustrating the comparison between the thickness of bundles (B) and toroids (T) measured for Csp=0.05 mM after 9, 20 and 60 sec.

The broad distribution of the thicknes of DNA bundles may be discussed in relation with theoretical predictions. According to some authors (Ha and Liu, 1998; Huang et al., 2002) the formation of bundles was predicted to be a macroscopic phase separation, that would result in a bundle with large thickness. For others, the equilibrium distribution of bundle sizes should be sharply peaked, all bundles having approximately the same thickness for a given ionic condition (Henle and Pincus, 2005; Fazli and Golestanian, 2007; Saito and Yoshikawa, 2010). However, a model by Grason and Bruinsma (2007) has considered the chirality as a core thermodynamic parameter for the aggregation to produce a stable disperse phase of hexagonal bundles. According to their result, the free energy curve versus the bundle radius shows a flat continuous minimum for multimolecular bundle formation, which represents a broad dispersion of the bundle width. This may imply that the DNA bundles could have structural chirality with columnar hexagonal order, as already discussed in a previous cryo-EM study (Leforestier and Livolant, 2009).

iii) Other shapes

In addition to toroids and bundles that represent the two main categories of DNA condensates, we also observed a few spheroids and rods (less than 10), only at low spermine concentration (0.05 mM sp), more often after short condensation times. Those are only exceptionnally found isolated. They are usually stuck to form aggregates. Rackets are transient objects observed only 20 sec after addition of 0.05 mM spermine (Figure 4h).

DISCUSSION

1. Collapse versus aggregation

Widom and Baldwin (1983) reported how it was impossible to separate the collapse and aggregation of Lambda DNA chains condensed by spermine and spermidine, although this separation was possible when using Cobalt hexamine as the condensing agent at low DNA concentration (Lambda DNA, 200 µg/ml). Nevertheless, the single molecular collapse seems to be possible at even lower DNA concentration (< 1 µM T4 DNA; 166 kbp) with polyamines after equilibration times of 1-2 h, in 10-30 mM Tris (pH 6-8), sometimes with 10 mM NaCl (Takahashi et al., 1997; Iwataki et al., 2004). However, in these fluorescence microscopy experiments, each DNA chain is tagged by fluorescent dye molecules, usually DAPI (4' 6-diamidino-2-phenylindole) that binds to the major groove of DNA. Although it is reported that DAPI does not significantly change the persistence and contour lengths of the DNA chain, its presence (usually 0.1 µM) may modify the electrostatic property of the DNA chain in some degree. Another DNA-intercalating fluorescent dye (YOYO-1) was shown to induce the collapse of a DNA chain (Kuyper et al., 2003). In addition, any detail of the structure of the DNA cannot be reached by these optical microscopy methods.

In our cryoEM experiments, we tried to prevent the initial aggregation of DNA by working at low DNA concentration and to prevent the secondary aggregation either by keeping the objects isolated the ones from under ionic conditions where they repulse each other, and by freezing the objects at short time after addition of the condensing agent.

Nevertheless, in our experimental condition (C_{DNA} = 0.03 mM), the calculation on the number of chains in the DNA toroids implies that the DNA condensation is usually not a single-molecular collapse, but mostly corresponds to multimolecular aggregation even when isolated toroids are formed. Lower DNA concentrations would have been more favourable to separate collapse from aggregation but it would have become difficult to find the objects in the glassy water film.

Besteman et al. (2007) measured the electrophoretic mobility of DNA (8 kbp, 5mg/ml) condensed by varying amounts of spermine. In 10 mM Tris, the measured values turn form negative to positive when the spermine concentration is increased and it is equal to zero for Csp = 1 mM. This explains why the total DNA is aggregated at Csp = 1 mM since there are no repulsive interactions to keep the chains isolated the ones from the others. For Csp values above and below 1 mM, the spermine-DNA complexes are respectively negatively and positively charged and conditions are more favorable to find isolated collapsed DNA chains in solution. In our experiments, we indeed favour the formation of smaller aggregates by lowering the spermine concentration to Csp = 0.05 mM and found under these conditions a few isolated globules and toroid. Conversely, we did not observe a significant decrease of the aggregation when increasing the spermine concentration up to 100 mM. On the contrary, the number of chains in a condensate shows a tendency to increase as the spermine concentration becomes higher. In future experiments, considering the mobility measurements of Besteman et al. (2007) recorded at lower Tris concentration, we could think of decreasing the molarity of the Tris buffer to 1 mM to favor te formation of isolated condensed chains.

2. Kinetic effects

Porschke found that, when the DNA concentration is around 1 µM, there are "fast" (milliseconds range) and "slow" (minutes range) processes in the DNA condensation, that represent the intramolecular and the intermolecular associations, respectively. In our experimental conditions, we

had no chance to catch the fast processes. Surprisingly, we did not observe any DNA condensation at t = 6 s. After t = 9 s, the intramolecular and intermolecular DNA condensation is at work to form small globules, toroids, rods, and fine networks of fibers. We observed toroids smaller than expected for one Lambda chain but our DNA concentration is rather high (0.03 mM) compared to that of Porschke. Therefore, the discrimination between intra- and inter-molecular condensations is not clear. Our small toroids may be made of DNA segments belonging to one or several chains. Freezing the samples at early stages of the process was necessary to trap these small objects, but our method may have introduced inhomogeneities in the ionic conditions. Let us comment the experimental set up. The chain has a contour length of 16.5 µm, with a radius of gyration (before addition of spemine *i.e. in good solvent conditions*) significantly larger than the diameter of the holes in the carbon film (2 µm). DNA chains can then only marginally cross the carbon surface. Ions instead, are in large excess (0.05 mM spermine x 4 (valency of the cation) = 0.2 mM positive charges) compared to 0.03 mM negative phosphate charges and they can diffuse freely. They migrate through the holes to condense onto DNA. If we consider an ideal diffusion of a spermine molecule by Brownian motion in a static fluid, the process is governed only by Fick's law, which describes the relation between the mean displacement of the motion (l) and its requiring time (t) as $l^2 = 2Dt$, where D is the diffusion coefficient. When we take $D = 4 \times 10^{-10}$ m^2/s, which is a value measured from a dye-labeled derivative of spermine (Ware et al., 1988), we find t = 5000 s (1h 40 min) for a spermine molecule to travel 2 mm distance. This is a very long time compared to the time scale of our experimental conditions, and cannot explain the DNA condensation in 9-60 s. Now, if we take into account the possible micro-turbulent mixing of the solutions through the micropores, caused by the osmotic pressure of the concentrated spermine, a sub-millimeter range of active diffusion (let us take 100 µm) is enough to make the spermine molecules diffuse to all the volume of the solution in 12.5 s, which is a value in reasonable agreement with our experimental results. Another effect that could decrease the diffusion time of spermine into the DNA solution is that DNA may be attracted to the surface either by the negatively charged surface of the mica (carbon coated grids are glow discharged to facilitate the spreading of the DNA solution) or/and by the spermine cations which should also attract the DNA chains close to the carbon film. The two effects may increase locally the DNA concentration close to the carbon surface and favor aggregation versus collapse of the chains. To conclude, our time resolved experiments let us trap the formation of very small toroids containing only part of one (or a few) Lambda DNA chain(s), usually connected to uncondensed DNA molecules around. Besides toroids, we also noticed at shorter times after mixing DNA and spermine another interesting effect: the stretching of the thin visible fibers. We cannot rule out the possibility that DNA stretching occurs during the preparation of the thin cryofilm but our observations rely on the observation of grids prepared using the same protocol. This stretching of the fibers reminds us of the macroscopic stretching phenomenon that was coupled to DNA aggregation of short DNA fragments upon addition of spermine to a solution of 50 nm DNA fragments (unpublished observations). We also relate such observations to the remark by Porschke (1984) noticing that "it is remarkable how fast the DNA is packed from a disordered wormlike coil to an apparently well-ordered condensed state. It seems that the DNA can be compared with a string which is kept under tension by electrostatic repulsion; upon release of this tension, the string collapses almost immediately". We hypothesize that the helical fibers presented on Figure 4g correspond to events that occur very rapidly (and are therefore rarely trapped by freezing) during the transition between the extended fiber and the collapsed toroid.

Experiments have been designed by others to follow the kinetics of a single DNA chain collapse, by keeping a single DNA chain attached to a surface at one extremity, and by elongating the chain under flow before addition of the condensing agent (protamine in this case) (Corzett and Balhorn, 1999). In these experiments, DNA condensation starts always from the end of the stretched DNA, a consequence of the non uniform tension distribution in such a configuration. Later on it has been shown that DNA fixed to two beads is reeled in from the both ends at the same time upon addition of spermine (van der Broek et al., 2010), in good agreement with the finding that the onset of DNA

condensation is the formation of a DNA loop due to random fluctuations of the polymer (Besteman et al., 2007). The design of experiments following this DNA chain collapse in the absence of any stretching of the chain, and with the resolution of electron microscopy remains to be done. We will show in the second chapter of this thesis that keeping DNA chains isolated the ones from the others inside the protein bacteriophage capsid (see Leforestier and Livolant, 2009) is a strategy that may resolve some of our experimental difficulties.

The overall increase of the sizes of the DNA condensates with time is consistent with previous reports (Porschke, 1984; He et al., 2000; Lee et al., 2001). At t = 20 s, the intramolecular or intermolecular (among 3-5 chains) condensation is completed to form larger condensates with clear boundaries and ordered internal structures. According to the TEM data by He et al. (2000) thick networks of the toroids and bundles are formed after long condensation time (t = 30 min), and the tendency of forming such large aggregates becomes stronger as the DNA concentration increases. Therefore, we can imagine that, in our condition, the sizes of the aggregates would be even larger with longer condensation time.

We observed that the a_H values do not significantly change as time goes on (Csp = 0.05 mM). Nevertheless, the degree of order seems to increase and this may be a consequence of the stabilization and optimization process, the charge (spermine) redistribution along the DNA helix. According to a Monte Carlo simulation by Porschke, the degree of spermine binding to DNA gradually increases with time (up to seconds range), when the spermine-DNA association/disassociation rate and the charge redistribution process (including sliding and/or hopping) are taken into the consideration (Porschke, 1984). Furthermore, this charge redistribution can be a critical factor to determine the morphology of a condensed DNA structure. For example, according to the simulation report by Stevens, in a DNA condensate, a few sharper turns require less energy than many slight bends, and the Coulomb energy also reduces when two segments of a DNA chain lie parallel (Stevens, 2001). Since the charge redistribution rate can be a major factor that determines the degree of bending (and move from sharp turns into parallel configurations) of a semiflexible DNA chain, the fine kinetics of charge association and redistribution can change the structure and morphology of a DNA condensate even with a constant interhelical spacing.

From our observations, we hypoythesize that the events follow the sequence drawn on Figure 16: 1) DNA chains are first stretched. Thin fibers (type 2) made of 2-5 chains aligned in parallel and observed after 9 sec may be due to a combination of kinetic and ionic effects. The fibers would correspond to DNA chains onto which spermine are condensed at amounts lower than the critical concentration required to induce the collapse. This sub-threshold concentration of spermine (due to inhomogeneous distribution of spermine ions) along the DNA would transiently increase tremendously the persistance length of DNA. 2) The chain would secondarily coil into toroids with intermediate undulation instabilities. The smallest toroids seen after 9 s (in coexistence with the stretched fibers) are sometimes uncompletely formed, with part of the Lambda chain still outside of it (and visible in a few cases). Rods and rackets also correspond to intermediate (or alternative) steps in the process of toroids formation. Fibers also aggregate laterally to form bundles, and we hypothesize that their formation is favoured by the extension of the DNA chains. Their width increases with time to form bundles that remain usually straight. Individualized toroids and rods are seen in coexistence with the fibers at all steps of the process and they are most of the time sticked to the fibers/bundles. In some cases, they seem to become part of them. The diameter of the toroids also increases with time. The transient formation of these bundles may slow down but apparently does not prevent the formation of the toroids. Toroids may contain more than one chain but they remain individualized in the aggregates. We conclude that a transition occurs from fibers to bundles and to toroids. Concomitantly, the internal organization of the condensates is often quite loose at the initial steps of the process with visible fluctuations of the molecular orientations inside the fibers, rods and toroids

although, in a few cases, striated domains are already visible after 9 s. The hexagonal structure is usually well established after 20 sec as revealed by the striations that become frequent in most bundles and toroids. The occurrence of the striated domains further increases with time. DNA chains are thus almost immediately organized into a 3D hexagonal lattice. Since the macroscopic reorganization of the aggregates still goes on, this means that the chains continue to reorganize and move the ones with respect to the others. Striated and non striated domains correspond to a fluid liquid crystalline state in a continuous process of reorganization. When time goes on, the DNA hexagonal ordering is further improved and seen almost everywhere under favourable orientations of the lattice, either in side or top views. For longer equilibration time (16 min), bundles are almost completely retracted. Aggregates are mostly formed by toroids that were mostly individualized but can secondarily fuse together to form cylindrical toroids (Figure 5). We present a schematic drawing summarizing the different steps of this evolution of Figure 17.

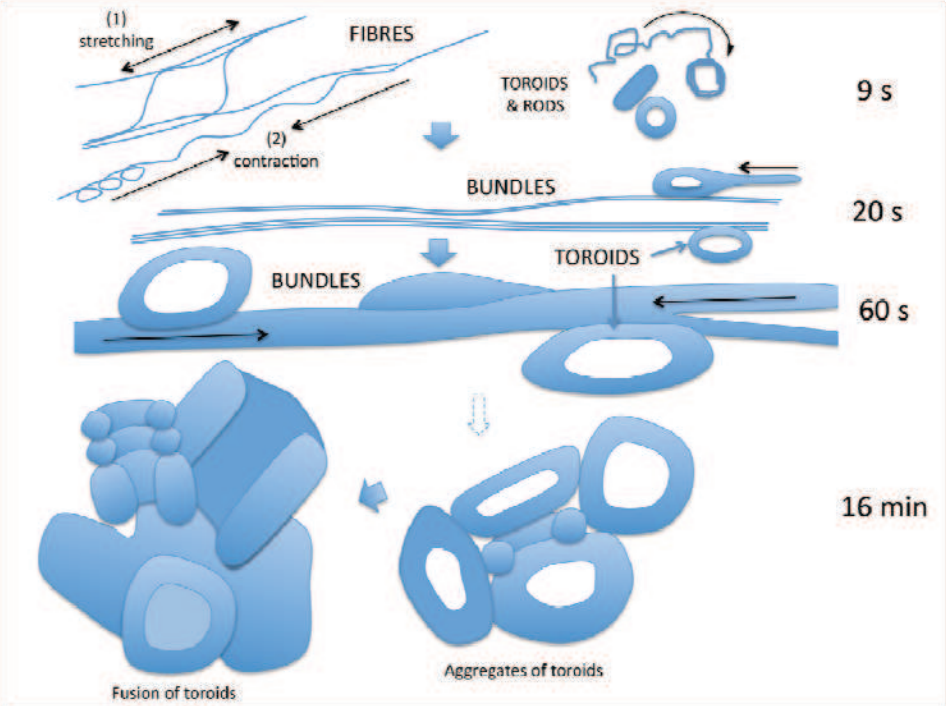

Figure 17: Schematic drawing of the observed condensed objets at different times after addition of spermine (for a final 0.05 mM spermine concentration). 9, 20 and 60 s correspond to identical protocols (addition of spermine on the opposite side of the grid) whereas observations at 16 min were done after mixing the samples in test tubes. Arrows indicate possible transitions between these different conformations.

3. Relationship between the shape of the aggregates and their internal structure

We observed that:

i) the morphology of the aggregates is related to their local structure and depends on the spermine concentration.

The objects with the higher density are toroids, either isolated or aggregated, formed at low spermine concentration, with a_H values close to 2.88 nm. Bundles characterized by a larger interhelix spacing (3.3 nm) are formed at higher spermine concentration. Based on previous observation

(Durand et al., 1992; Pelta et al., 1996), we know that the hexagonal liquid crystalline state turns cholesteric for interhelix distances a_H above 31.5 Å. According to Raspaud et al (2005), the cohesive energy E/kT ≈ 0.05 for a_H = 2.9 nm (hexagonal phase) is over 3.3 times larger than E/kT ≈ 0.015 for a_H = 3.3 (cholesteric phase). Such a decrease of the interchain cohesive energy unpon increase of the spermine concentration follows the overcharging of the chains since the aggregates turn from negative to positive upon increase of the spermine concentration (Besteman et al., 2007). The decrease of the interchain cohesive energy, together with the overcharging of the chains that occurs upon increase of the spermine concentration and leads to the hexagonal-cholesteric transition may not be enough anymore to overcome the bending energy of the semiflexible DNA chains. Straight DNA chains would aggregate laterally to form a multimolecular bundle with larger a_H, probably in a liquid crystalline cholesteric state. This toroid-bundle transition that we report here at 200 mM spermine may correspond to a general behaviour since it was was also observed with CoHex (Conwell et al., 2003). The authors report that the transition happened at approximately two times the ionic strength when $MgCl_2$ was added instead of NaCl but they did not go further in the analysis of this phenomenon.

Nevertheless, the existence of straight elongated bundles with short interhelix distances (a_H = 2.88 nm) has been reported (Leforestier and Livolant, 2009). They were formed with long DNA chains ejected from SPP1 viruses in the presence of 10 mM spermidine in a 10 mM Tris (pH 7.6) solution at a DNA concentration much higher than in our experiments. Iwaki et al., using T4 DNA chains, also reported how, for an identical spermidine (3+) concentration, toroids were preferentially produced at low DNA concentration and bundles at higher DNA concentration (Iwataki et al., 2004). High DNA concentration of course favours the aggregation of the DNA chains and the consequent formation of bundles. Under our experimental conditions, we have been able to differentiate the formation of toroids and bundles as a function of spermine concentration, which is a completely different phenomenon.

ii) DNA solubilized in excess of spermine forms a loose network

The networks of thin fibers observed above the redissolution line (Figure 3f; Csp = 400 mM) differ from a classical solution of Na-DNA chains in the absence of spermine (not shown). The persistence length of these fibers looks significantly larger than the 50 nm of isolated DNA chains. The conformation of DNA in this high spermine concentration region has not been investigated yet experimentally except by Trubetskoy et al. (2003). These authors proposed that the DNA redisolution at high spermine concentration is due to the formation of small (< 100 nm) colloidal condensed DNA particles that are suspended in the solution. They described bead-on-a-string structures that we never observed. However, their experimental observations are done in a conventional TEM with silver-enhancement and gold-labeling, which can modify significantly the electrostatic interactions of the spermine-DNA system. On the other hand, Iwataki et al. (2004) also have reported the generation of network structure by mixing T4 DNA (5 μM) solution with a large excess of spermidine (0.5 mM) on a glass plate by using fluorescence microscopy that they interpret as a kinetically “frozen” state due to very strong effective attraction between the DNA chains (caused by the excess of spermidine). We instead consider the phenomenon as a consequence of the decrease of the interchain attractive interaction. The structure of the DNA condensate may evolve from the initial (precipitated) hexagonal phase to the (precipitated) cholesteric phase, and finally to the soluble phase, accompanying the corresponding morphological transitions from the toroids, globules, rods, and bundles, to the dominantly bundles, and finally to the fibrous network, respectively.

As a conclusion, we analyzed by cryoEM the shape and the structure of DNA condensed by spermine from the onset of precipitation up to above the resolubilization limit. We showed how the toroids are

always hexagonal inside as opposed to bundles that may be hexagonal under conditions where they coexist with toroids, and cholesteric (with a larger interhelix distance) at higher spermine concentration, when toroids are not found anymore. The transition from toroids to bundles seems therefore to be the consequence of a decrease of the cohesive energy resulting from the excess of spermine cations. Hexagonal bundles coexisting with toroids may correspond instead to unstable shapes that should ultimately transform into toroids. We extended the domain explored previously by X-ray diffraction analysis of the DNA packing, and analyzed local scale deviations from a perfect hexagonal packing of helices that we relate to a competition between helical twist and dense hexagonal packing. We also analyzed the process of aggregation of toroids inside larger aggregates and how different objects can merge together thanks to the fluidity of their liquid crystalline state and to the necessary redistribution of condensed cations. In addition, helical instabilities of the spermine-DNA chains together with toroids made of less than one DNA chain were trapped by working with microvolumes and by freezing samples at very short times after the addition of the condensing agent.

References

Ainalem ML, Carnerup AM, Janiak J, Alfredsson V, Nylander T, Schillen K: Condensing DNA with poly(amido amine) dendrimers of different generations: means of controlling aggregate morphology. *Soft Matter* **5**: 2310-2320 (2009)

Besteman K, van Eijk K, Lemay SG: Charge inversion accompanies DNA condensation by multivalent ions. *Nature Phys*. **3**: 641-644 (2007)

Carnerup AM, Ainalem ML, Alfredsson V, Nylander T: Watching DNA condensation induced by Poly'(amido amine) dendrimers with time-resolved cryo-TEM. *Langmuir Lett.* **25**: 12466-12470 (2009)

Carnerup AM, Ainalem ML, Alfredsson V, Nylander T: Condensation of DNA using poly(amido-amine) dendrimers: effects of salt concentration on aggregate morphology. *Soft Matter* **7**: 760-768 (2011)

Conwell CC, Vilfan ID, Hud NV: Controlling the size of nanoscale toroidal DNA condensates with static curvature and ionic strength. *Proc. Natl. Acad. Sci. USA* **100**: 9296–9301 (2003)

Cooke IR and Williams DRM: Condensed states of a semiflexible homopolymer: ordered globules and toroids. *Physica A: Statistical Mechanics and its Applications* **339**: 45-52 (2004)

Corzett M and Balhorn R: Protamine-Induced Condensation and Decondensation of the Same DNA Molecule. *Science* **286**: 120-123 (1999)

Durand D, Doucet J, Livolant F: A study of the structure of the highly concentrated phases of DNA by X-ray diffraction. *J Phys. II* **2**: 1769-1783 (1992)

Fang Y and Hoh JH: Early intermediates in spermidine-induced DNA condensation on the surface of mica. *J. Am. Chem. Soc* **120**: 8903-8909 (1998)

Fazli H and Golestanian R: Aggregation kinetics of stiff polyelectrolytes in the presence of multivalent salt. *Phys. Rev. E* **76**: 041801 (2007)

Frederik PM and Sommerdijk N: Spatial and temporal resolution in cryo-electron microscopy – a scope for nano-chemistry. *Current Opin. Colloid Interface Sci.* **10**: 245-249 (2005)

Grason GM and Bruisna RF: Chirality and Equilibrium Biopolymer Bundles, *Phys. Rev. Lett.* **99**: 098101 (2007)

Grosberg AY and Khokhlov AR, in *Statistical Physics of Macromolecules* (AIP Press, New York, 1994)

Ha BY and Liu AJ: Effect of non-pairwise-additive interactions on bundles of rodlike polyelectrolytes. *Phys. Rev. Lett.* **81**: 1011-1014 (1998)

Harris AB, Kamien RC, Lubensky TC: Moleular chirality and chiral parameters. *Rev. Mod. Phys.* **71**: 1745-1757 (1999)

He S, Arscott PG, Bloomfield VA: Condensation of DNA by multivalent cations: experimental studies of condensation kinetics. *Biopolymers* **53**: 329–341 (2000)

Henle ML and Pincus PA: Equilibrium bundle size of rodlike polyelectrolytes with counterion-induced attractive interactions. *Phys. Rev. E* **71**: 060801(R) (2005)

Huang CI and Olvera de la Cruz M: Polyelectrolytes in multivalent salt solutions: monomolecular versus multimolecular aggregation. *Macromolecules* **35**: 976-986 (2002)

Hud NV and Downing KH: Cryoelectron microscopy of λ phage DNA condensates in vitreous ice: The fine structure of DNA toroids. *Proc. Nat. Acad. Sci. USA* **98**: 4925-14930 (2001)

Iwataki T, Kidoaki S, Sakaue T, Yoshikawa K, Abramchuk SS: Competition between compaction of single chains and bundling of multiple chains in giant DNA molecules. *J. Chem. Phys.* **120**: 4004-4011 (2004)

Kornyshev AA: Physics of DNA: Unravelling hidden abilities encoded in the structure of "the most important molecules" *Phys. Chem. Chem. Phys.* Doi10.1039/C004107F (2010)

Kulic IM, Andrienko D, Deserno M: Twist-bend instability for toroidal DNA condensates. *Europhys. Lett.* **67**: 418-424 (2004)

Kuyper CL, Brewood JP, Chiu DT: Initiating Conformation Transitions of Individual YOYO-Intercalated DNA Molecules with Optical Trapping, *Nano Lett.* **3**: 1387-1389 (2003)

Lambert O, Letellier L, Gelbart W, Rigaud JL: DNA delivery by phage as a strategy for encapsulating toroidal condensates of arbitrary size into liposomes. *Proc. Natl. Acad. Sci. USA* **97**: 248-7253 (2000)

Lee LK, Mount CN, Shamlou PA: Characterisation of the physical stability of colloidal polycation-DNA complexes for gene therapy and DNA vaccines. *Chem. Eng. Sci.* **56**: 3163-3172 (2001)

Leforestier A, Bertin A, Dubochet J, Richter K, Livolant F: Expression of chirality in columnar phases of DNA and nucleosomes. *C. R. Acad. Sci.* **11**: 229-244 (2008)

Leforestier A and Livolant F: Structure of toroidal DNA collapsed inside the phage capsid *Proc. Natl. Acad. Sci. USA* **23**: 9157-9162 (2009)

Pelta J, Durand D, Doucet J, Livolant F: DNA mesophases induced by spermidine: structural properties and biological implications, *Biophys. J.* **71**: 48-63 (1996)

Pernodet N and Tinland B: Influence of λ-DNA concentration on mobilities and dispersion coefficients during agarose gel electrophoresis. *Biopolymers* **42**: 471-478 (1997)

Porschke D: Dynamics of DNA condensation. *Biochemistry* **23**: 4821-4828 (1984)

Raspaud E, Olvera de la Cruz M, Sikorav JL, Livolant F: Precipitation pf DNA by polyamines: A polyelectrolyte behavior. *Biophys. J*. **74**:381-393 (1998)

Raspaud E, Durand D, Livolant F: Interhelical spacing in liquid crystalline spermine and spermidine-DNA precipitates. *Biophys. J.* **88**: 392-403 (2005)

Rau DC and Parsegian VA: Direct measurement of the intermolecular forces between counterion-condensed DNA double helices. *Biophys. J.* **61**: 246-259 (1992)

Saito T and Yoshikawa K: Finite-width bundle is most stable in a solution with salt. *J. Chem. Phys.* **133**: 045102 (2010)

Stevens MJ: Simple simulations of DNA condensation. *Biophys. J.* **80**: 130-139 (2001)

Takahashi M, Yoshikawa K, Vasilevskaya VV, Khokhlov AR: Discrete coil-globule transition of single duplex DNAs induced by polyamines. *J. Phys. Chem. B* **101**: 45, 9396-9401 (1997)

Taylor WH and HagermanPJ: Application of the method of phage T4 DNA ligase-catalyzed ring-closure to the study of DNA structure: II. NaCl-dependence of DNA flexibility and helical repeat. *J. Mol. Biol.* **212**: 363-376 (1990)

Trubetskoy VS, Wolf JA, Budker VG: The role of a microscopic colloidally stabilized phase in solubilizing oligoamine-condensed DNA complexes. *Biophys. J.* **84**: 1124-1130 (2003)

Van den Broek B, Noom MC, van Mameren J, Battle C, MacKintosh FC: Visualizing the formation and collapse of DNA toroids. *Biophys. J*. **98**: 1902-1910 (2010)

Verma R, Crocker JC, Lubensky TC, Yodh AG: Entropic Colloidal Interactions in Concentrated DNA Solutions. *Phys. Rev. Lett.* **81**: 4004-4007 (1998)

Ware BR, Klein JW, Zero K: Interaction of a fluorescent spermine derivative with a nucleic acid polyion. *Langmuir* **4**: 458-463 (1988)

Widom J and Baldwin RL: Cation-induced toroidal condensation of DNA studies with Co3+(NH3)6, *J. Mol. Biol.* **144**: 431-453 (1980)

Widom J and Baldwin RL: Monomoleular condensation of Lambda-DNA induced by Cobalt Hexammine. *Biopolymers* **22**: 1595-1620 (1983)

66

Collapse of single DNA chains confined in protein bacteriophage capsids: a cryoelectron microscopy study

ABSTRACT

The conformation of individual double stranded DNA macromolecules is monitored at the collapse transition by cryoelectron microscopy. Unique DNA chains confined in the volume of the T5 bacteriophage capsid (80 nm in diameter) are collapsed by varying amounts of the polyamine spermine (4+) that diffuses through the protein shell. In the coexistence region, between the region where all chains are in a coil conformation, and the region where all chains are collapsed into toroids, we show that intermediate states exist between the coil and the globule. “Hairy toroids” have been imaged with part of the chain condensed in a toroid and the other part uncondensed around. The measured interhelix distance is smaller in these uncomplete toroids than in the fully organized toroids formed at higher spermine concentrations. We show that in the coexistence region two parameters may adjust the global density of each chain: i) the balance between the condensed (toroïdal) and uncondensed segments along a given DNA chain and ii) the packing density in the toroid.

INTRODUCTION

The DNA molecule is a semiflexible polyelectrolyte and exists in a coil conformation in “good solvent” conditions because of its high charge density. As other polyelectrolytes, the molecule can be collapsed into a globule. Numerous agents can produce the condensation of DNA *in vitro* (Bloomfield, 1996): the addition of alcohol that changes the quality of the solvent (80% alcohol in water is commonly used), the addition of neutral crowding agents such as PolyEthylene Glycol (PEG) through an excluded volume mechanism or the addition of multivalent cations (spermine, spermidine, CoHex), cationic polypeptides and basic proteins. DNA condensation can also be obtained by interaction with cationic amphiphilic liposomes.

The morphology of the DNA condensed particles has drawn much interest especially after the first electron microscopy observation of the DNA globules (Gosule and Schellman, 1976; Chattoraj et al., 1978) showing the frequent toroidal conformation of DNA, although spheres and rods were found sometimes (Marx and Ruben, 1983). This interest has been renewed in the last years with the hope to be able to control the size and charge of the genetic material for potential gene delivery applications. Nevertheless, classical electron microscopy methods that require to dehydrate the sample and to add contrasting agents ruled out high resolution studies. These limitations can be overcome now by cryoelectron microscopy that keeps unchanged the water and ionic environments of the molecule. Hud and Downing (2001) revealed how this method is powerful and well suited to analyze details of the DNA chain conformation. Nevertheless, the systematic analysis of the globular DNA conformations encounters other limitations. The collapse transition of individual chains must be separated from the aggregation that involves several chains. Widom and Baldwin (1983) were able to get rid of the aggregation effect by using $Co^{3+}(NH_3)_6$ as the condensing agent and by working at very low concentrations of λ-DNA concentration (below 0.2 μg/ml). Nevertheless, when spermine and spermidine were used as condensing agents, it has not been possible to separate the collapse from

the aggregation in conditions that were successful for $Co^{3+}(NH_3)_6$. Jary and Sikorav were able to analyze the coil-globule transition before aggregation starts, by working at shorter times with extremely low concentrations of DNA (50 ng/ml) (Jary, 1998). Nevertheless, such experimental constraints prevent any systematic structural analysis of the DNA chain conformation.

Very little was thus known about the morphological changes of individual DNA chains during the coil-globule transition until the development of high sensitivity methods of fluorescence microscopy that were designed to follow the coil-globule transition of "giant" T4 DNA chains confined between slide and coverslip. It happens that the addition of condensing agents –many have been tested– does not modify the extended coil conformation of the chain up to a critical concentration where a few chains start to collapse. Above a second critical concentration of the condensing agent, all DNA chains are compacted in a globular condensed state. In the intermediate range between these two critical concentrations, both coil and globule states coexist. In this coexistence region, and at low salt concentration, the chain may stay in the coil conformation for a long period of time and suddenly collapse, making possible to follow this transition at the level of individual chains. We described earlier a method to perform high resolution cryoEM observations of individual DNA chains at a reasonable DNA concentration, without aggregation (Leforestier et al., 2008; Leforestier and Livolant, 2009). We use the bacteriophage T5 and trigger its DNA ejection *in vitro* upon interaction of the phage with its receptor. The ejection can be stopped before the ejection is complete. Fragments of the chains, whose length ranges from a few hundreds of base pairs to the full genome (121000 bp) are thus kept in each capsid (80 nm in diameter) and cannot interact with each other. The capsid being permeable to water and ions, each chain is entrapped in its own dialysis bag and ionic conditions can be reversibly modified. The conformation of the DNA chain changes accordingly. Using this method, the aim of the present paper is to monitor the changes of the conformation of individual double stranded DNA macromolecules at the collapse transition. We tested three concentrations of the condensing multivalent ion spermine, 0.05, 0.1 and 0.5 mM. We show how the tetravalent cation spermine induces the collapse of the chain inside the capsid, and how the conformation of the chain depends on the concentration of the condensing agent. Not only toroids with varying interhelix distances but also more complex conformations of the DNA chains are observed, that may raise new questions on the underlying mechanisms.

MATERIALS AND METHODS

T5 *wt* bacteriophages were produced in *E. coli* Fsub+ and purified as described by Bonhivers et al. (Boulanger et al., 1996). They were suspended at a concentration of 1×10^3 phages/ml in 10 mM Tris pH 7.6, 1 mM $MgCl_2$, 1 mM $CaCl_2$. The protein receptor FhuA was purified as described earlier 오류! 책갈피가 정의되어 있지 않습니다. (Boulanger et al., 1996) and stored in 250 mM NaCl, 1% (w:v) octyl glucoside and 10 mM Tris, pH8, at a concentration of 2.6 mg/ml. During the experiments, the detergent concentration was kept constant at all steps of the procedures (either octyl glucoside (OG) 1% or lauryldimethyl-amine N-oxide (LDAO) 0.03%).

Partial ejection of DNA and condensation of the DNA chain inside the capsid. The preparation of the samples is detailed in Figure 1. A concentrated solution of T5 bacteriophages ($4.4x10^{12}$ phages/ml) is maintained at 4°C in the presence of the receptor FhuA at a final T5:FhuA ratio of 1:500 (to permit the DNA ejection), 15% PEG 6000 (to apply an external osmotic pressure of 3.2 Atm that blocks the ejection at intermediate steps, see (Leforestier and Livolant, 2010) and DNAse (Amersham Bioscience, 5 units/ml) to digest the ejected DNA. After 4h at 37°C, most phages have ejected a fraction of their DNA. Each capsid contains a unique DNA fragments. A few other capsids are full or completely empty.

A negligible volume of spermine solution is then added. Spermine diffuses through the protein capsid and initiates the conformation change of the DNA chain in the confined volume of the capsid. The sample is then diluted 4 times without changing the spermine and ionic concentrations and equilibrated for 1h to a few days at 4°C before preparation of thin vitrified films.

To summarize, cryoEM observations of DNA chains inside bacteriophage capsids are done in 10 mM Tris buffer pH 7.6, 7 mM NaCl, 1mM $MgCl_2$ and 1mM $CaCl_2$. The concentration of bacteriophages is equal to $1.1x10^{12}$ phages/ml (0.45 mM DNA Phosphates). We tested three concentrations of spermine (0.05, 0.1 and 0.5 mM). Are also present in the buffer the protein receptor FhuA (0.07 mg/ml), PEG 6000 (3.75%) and DNAse (1.25 units/ml).

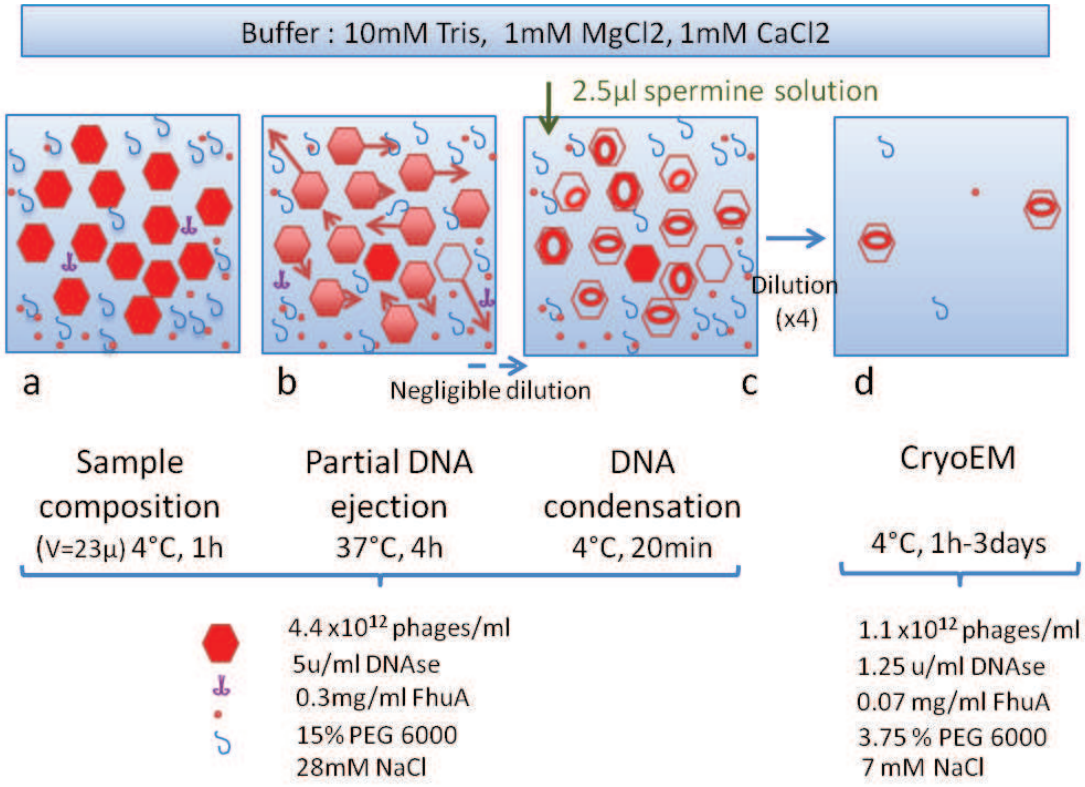

Figure 1: Schematic drawing of the 4 steps experimental protocol. a) Composition of the sample incubated for 1 h at 4°C containing T5 bacteriophages, FhuA receptor, PEG 6000 and DNase. b) Ejection proceeds at 37°C during 4 hours under conditions where DNA is not condensed. c) the addition of spermine induces the condensation of DNA inside the capsids. The low temperature and the DNA condensation block the DNA ejection. d) A dilution of the samples is done before the preparation of thin films for cryoEM observations. CryoEM observations are done in 10 mM Tris, 7 mM NaCl, 1 mM $MgCl_2$ and 1 mM $CaCl_2$. Traces of divalent cations are required to maintain the integrity of the capsids at the initial steps of the experiments.

Cryoelectron microscopy. 3 µL of the solution are deposited on a glow-discharged holey carbon grid (Quantifoil R2/2, Jena, Germany). The grid is blotted with a filter paper for 2-3 seconds to remove the excess of the solution, and directly plunged into liquid ethane cooled down by liquid nitrogen. During the preparation of the samples, the temperature and relative humidity of the environment are kept at 20-21°C and 89-96%, respectively, in a home-made device. Frozen samples are transferred into a Gatan 626 cryostage (Gatan, Warrendale, USA) and observed in a transmission electron microscope (JEM-2010, JEOL, Japan) operated at 200 kV. All images are recorded on Kodak SO163 negative films under low dose conditions at a magnification of X50000 and 880 or 3000 nm underfocus, to image

DNA packing and the overall shape of the objects, respectively. The films are developed in full strength Kodak D19 for 12 minutes, and scanned with a Nikon Coolscan 9000 at a resolution of 4000 pixels/inch.

RESULTS

Imaging conditions have been chosen to optimize the contrast of DNA inside the capsid. DNA is densely packed in full capsids and multiple domains can be recognized; they can be punctuated, striated or uniformly grey. In the punctuated domains, where each point corresponds to a DNA segment seen in top view, the hexagonal lattice can be recognized and the interhelix distances a_H measured directly (example of capsid 5 in Figure 2a that is full of DNA). In striated domains, the interdistance *d,* with $d = a_h\sqrt{3}/2$, corresponds to the reticular planes of the DNA hexagonal lattice. A detailed analysis of the full capsid has been detailed elsewhere (Leforestier and Livolant, 2010).

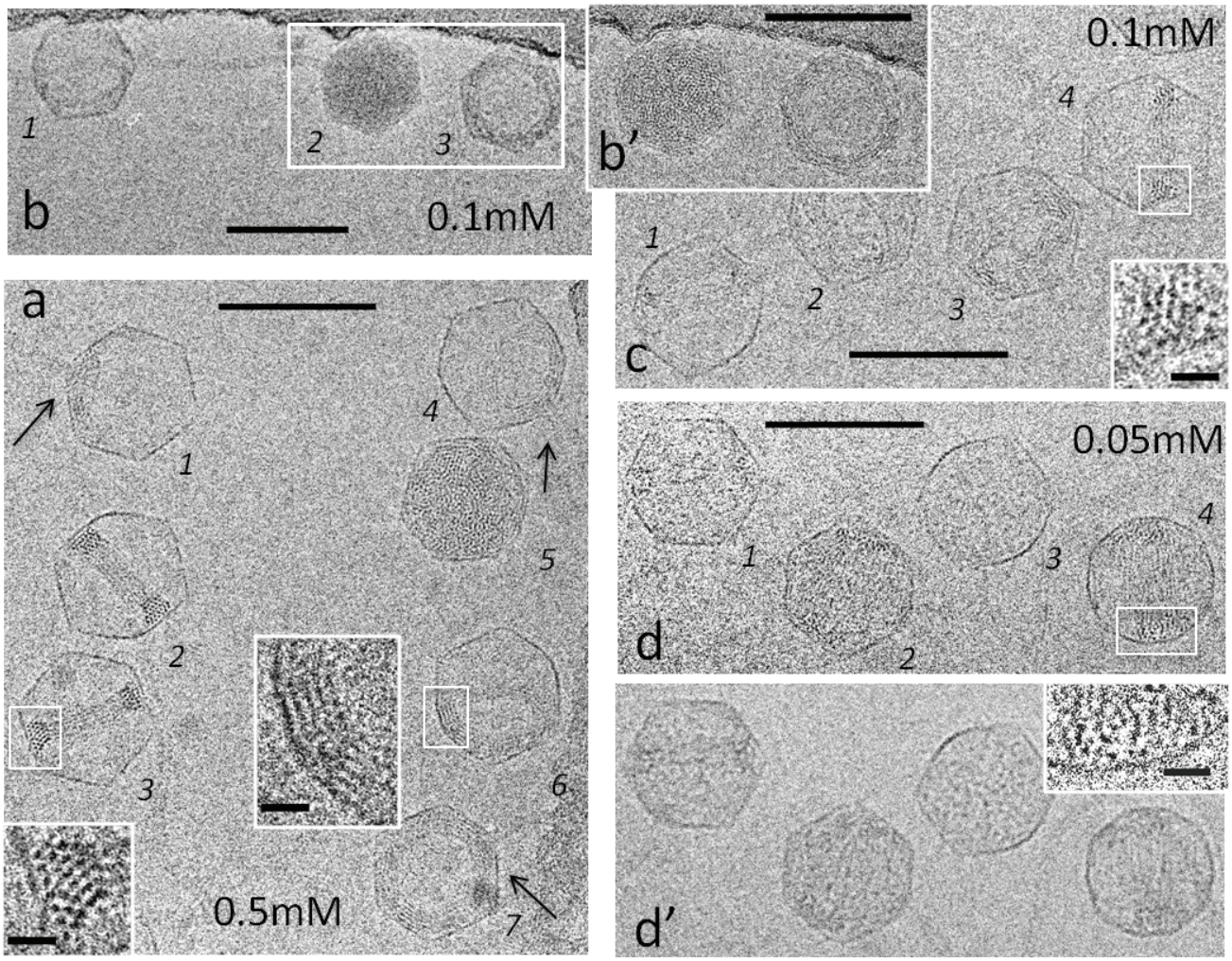

Figure 2: CryoEM of DNA chains condensed inside the T5 bacteriophage capsids with various concentrations of spermine: 0.05 mM (d,d'), 0.1 mM (b,b',c) and 0.5 mM (a). Part of the DNA molecule was ejected from the T5 bacteriophage (upon interaction with the receptor FhuA) and the DNA segment kept in the capsid was secondarily condensed with spermine. The same capsids have been imaged with two conditions: -880 nm (a, b', c, d) and -3000 nm (b, d') underfocus. The densities observed at large underfocus provide us with the distribution of DNA in the 3D volume of the capsid, whereas details are resolved at -800 nm. Details of the DNA packing in the toroids are enlarged (inserts). Scale bar = 100 nm in the figures and 10 nm in the inserts.

Following the protocol described in Figure 1, we are handling a population of capsids, each containing a unique DNA chain whose length ranges from a few thousands of base pairs up to the full genome. Using the fact that the bacteriophage capsid is permeable to water and ions, we analyzed previously the conformation of the chain under "good solvent" conditions, in the absence of any condensing agent (Leforestier and Livolant, 2009) (where the chain occupies the whole capsid) and after its collapse into a toroidal globule by 5 mM spermine (Leforestier et al., 2008). Our goal is now to investigate the conformation of the DNA chain in a lower range of spermine concentration to detect possible intermediate conformations between the confined globule and the dense toroid. Among the 151, 49 and 108 capsids observed at 0.05, 0.1 and 0.5mM spermine respectively, we will concentrate on the 74, 36 and 92 capsids partially filled with DNA.

For $C_{spermine}$ = 0.5 mM, all incompletely filled capsids present toroids visible under multiple orientations: side views (capsids 2 and 3), top views (capsid 6) and oblique views (capsid 4) (Figure 2a). The toroids present the characteristics described earlier: a hexagonal packing of the DNA segments, a faceting of the bundle section, and the alignment of the reticular planes parallel to the faces of the capsid (enlargements of capsids 3 and 6). Periodic striations with $d = a_H\sqrt{3}/2$, underlining the reticular planes, are seen locally under favorable orientations (Figure 2a, capsid 6), as described earlier (Hud and Downing, 2001; Leforestier et al., 2008). The length of each DNA fragment trapped in the capsids can be determined when toroids are seen in side views, by measuring the diameter and the section of the toroid -to determine its volume- and the interhelix distance a_H. As an example, the toroid in capsid 2, is made of a 5 µm long DNA fragment. In most cases, the external diameter of the toroid is fixed by the internal diameter of the capsid (toroids 2, 3, 7). As shown earlier longer chains form distorted toroids, in good agreement with theoretical predictions (Tzlil et al., 2003). Short DNA chains may form toroids with a diameter smaller than the capsid (toroids 1, 4, 6).

For $C_{spermine}$ = 0.1 mM, we also recognize capsids filled with variable amounts of DNA (Figure 2b, c). Toroidal DNA is seen along multiple orientations: top view (capsid 3 in Figure 2b), side view (capsids 1 and 4 in Figure 2c) and oblique view (capsids 2, 3 in Figure 2c), and better recognized at higher defocus (Figure 2b, capsid 1). The local hexagonal ordering of DNA is still recognized but it is often less defined than in toroids formed at 0.5 mM sp. The measured interhelical distance is also larger and the facetting is not so clearly seen although the main reticular planes are still aligned parallel to the capsid surface (enlargement of the hexagonal lattice in capsid 4 in Figure 2c).

For $C_{spermine}$ = 0.05 mM, we notice a larger variation of the DNA chain conformation inside the capsids (Figure 2d,d'). We still recognize the classical toroidal structures (capsid 1 with a short DNA length and capsid 4 with a larger one). The local packing of DNA segments is less defined and does not extend above the next neighbor (enlargement of capsid 4 in Figure 2d). In other side-views of the toroids, we do not recognize the local hexagonal order at all. DNA is not hexagonally packed in the toroid. In other cases (Figure 2d, capsid 3), DNA occupies a large volume of the capsid as also observed in the absence of condensing ions (Leforestier and Livolant, 2010). Nevertheless, the content of the capsid looks more granular than usual and this is better seen in highly underfocused images (-3000 nm) (Figure 2d'). In such cases, we suspect that segments of the chain may stick side by side along short distances to form localized thin bundles connected by single DNA segments. This granular aspect of DNA would correspond to an intermediate conformation between the confined coil and the initial step of the toroid formation. In many other capsids, the DNA chain adopts more complex configurations as in Figure 2d,d' (capsid 2 for example). It happens that there is a continuum of conformations between a complete disordered isotropic organization and a quite well defined toroidal structure. In some capsids, DNA may adopt an intrachain segregated structure with part of

the chain being collapsed and the other one being extended. Due to their loose structure, these DNA chains are much more difficult to image.

We present on Figure 3 a selection of pairs of toroids imaged first at 800 nm underfocus to observe details of the structure (Figure 3a-f) and secondly at -3000 nm to get more contrasted images (Figure 3a'-f') in order to determine the contour of the condensed DNA. For each spermine concentration, we selected a representative toroid seen in top view and another one in side view. There is no ambiguity to identify the limits of the toroids formed at 0.5mM sp, either in top and side views (Figure 3e,e'-f,f'). DNA is highly compacted, forms a regular hexagonal lattice (a_H = 2.85±0.03 nm) that leads to well-defined parallel striations that extend from the inside to the outside of the bundle along identified sectors of the toroid. In contrast, boundaries of the toroids are fuzzy at 0.05mM (Figure 3a,a'-b,b'), the DNA lattice is ill-defined with larger interhelix distances (a_H = 3.24±0.09 nm). The local lateral striations are seen very locally and do not extend over the whole diameter of the bundle. Unexpectedly, DNA densities are also visible in the core of the top view toroids. They are easily seen at large defocus (Figure 3a') and then recognized at lower defocus (Figure 3a). This non-toroidal DNA is also detected in side views above and below the toroid (Figure 3b', arrows). To establish unambiguously the presence of this uncondensed DNA, it appeared necessary to compare the signal coming from the uncondensed DNA around the toroid with the signal recorded in the empty capsid. We present in Figure 4 one capsid containing a toroid seen in top view and one empty capsid surrounded by a homogeneous film of vitrified water. Profile plots of two rectangular domains of identical dimensions have been recorded using ImageJ on the scanned micrograph recorded at -3000 nm defocus. The fluctuations of the grey signal are low in the vitrified film of water (colored in grey) and in the empty capsid (blue) with a very modest difference between the two mean values that corresponds to twice the thickness of the protein capsid wall. By comparison, the signal from the toroidal DNA (yellow) is higher as well as the signal coming from the uncondensed DNA close by (orange). Even more significant are the fluctuations of the intensity coming from the phase contrast imaging mode and visible only when DNA is present. Therefore, we can conclude that part of the DNA is not condensed in the toroid and occupies the remaining free volume. We cannot precise whether this non-toroidal DNA is in a coil configuration or locally collapsed. In many capsids, we also detected non-toroidal DNA at the intermediate 0.1 mM sp concentration (Figure 3c-d', arrows). For this spermine concentration, a_H = 2.99±0.06 nm. We may roughly estimate that this non-toroidal DNA would represent about 0-20% of the DNA chain in 0.1 mM spermine and 40-100% at 0.05 mM spermine. The number of capsids that we analyzed is not large enough to determine whether the amount of non-toroidal DNA depends on the total length of DNA inside the capsid. These "hairy" toroids have been observed 1h and also 3 days after addition of spermine. We did not check their presence for longer equilibration time, and therefore we cannot certify that the equilibrium conditions were reached.

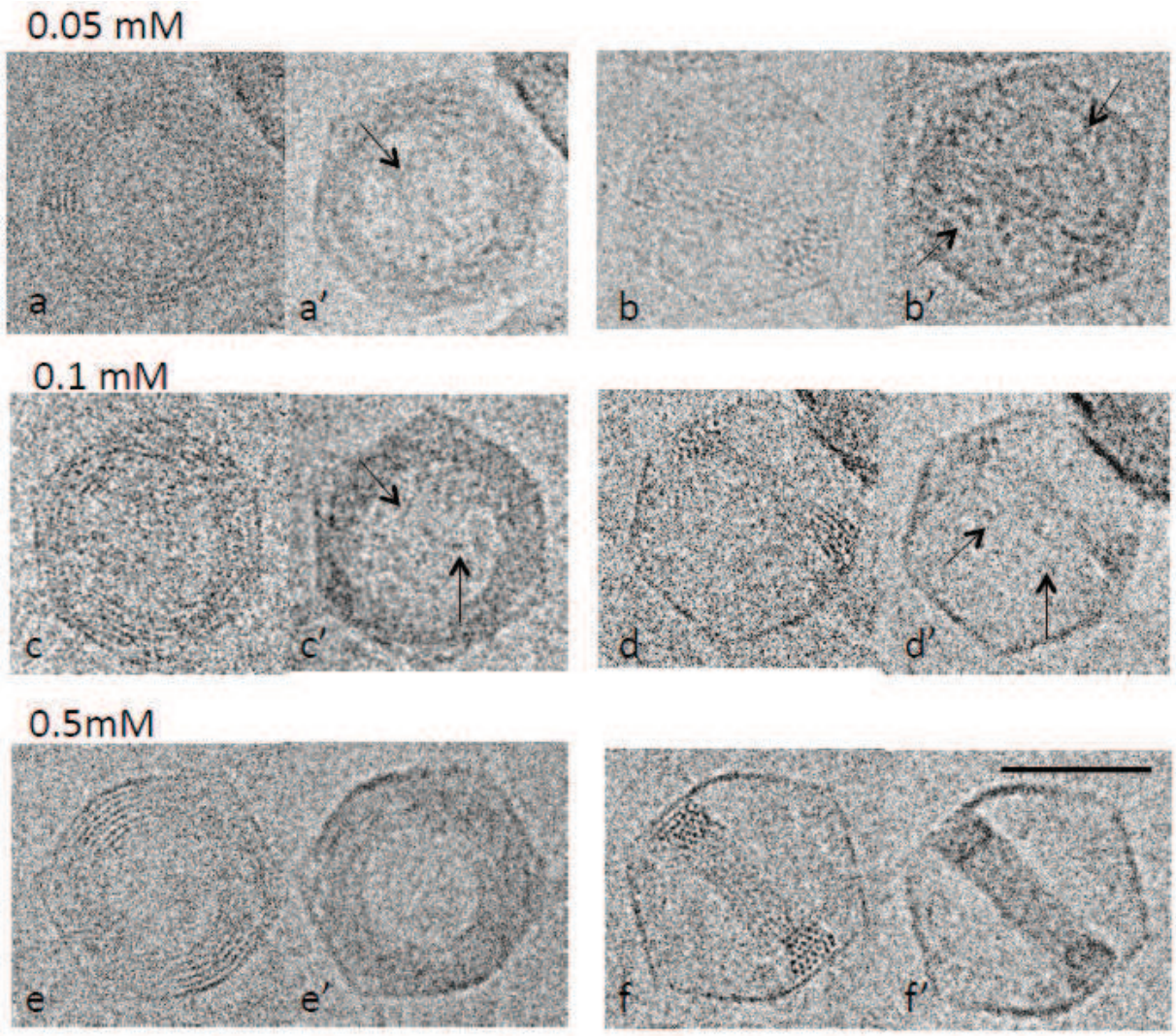

Figure 3: Comparison of DNA conformations in the capsid for multiple spermine concentrations: Csp = 0.05 mM (a, a', b, b'), 0.1 mM (c, c', d, d') and 0.5 mM (e, e', f, f'). Micrographs were taken at two underfocus values in order to estimate the volume occupied by the chain (z = -3000 nm, a'-f') and to visualize its local organization (z = -800 nm, a-f). For each spermine concentration, top views (a, a', c,c', e, e') and side views of the toroids (b, b', d, d', f, f') have been selected. The volume occupied by the DNA chain depends on the spermine concentration. Compared to Csp = 0.5 mM, were all DNA is concentrated in the toroid and shows a local hexagonal lattice (f), a non-condensed part of the DNA molecule is seen outside of the toroid in at Csp = 0.05 mM (a, a', b, b') and at Csp = 0.1 mM (c, c', d, d') (arrows). Scale bar = 50 nm.

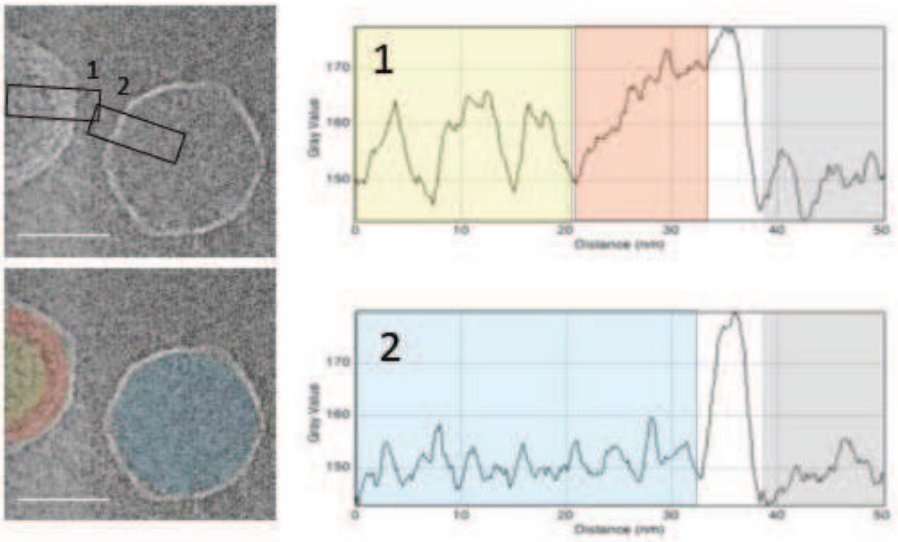

Figure 4: Comparison of the intensity profiles of two half capsids (in 0.05 mM spermine), one containing a DNA chain partly condensed into a toroid (1) and one completely empty (2). The signals coming from DNA (orange for the uncondensed chain and yellow for the condensed toroid) can be distinguished from the background signal (the empty capsid in blue) that is itself only very slightly above the signal from the vitrified film of water (grey). Signals were recorded using ImageJ on a -3000 nm defocus micrograph scanned at 4000 pixels/inch.

DISCUSSION

CryoEM of individual DNA chains trapped in the semi-permeable capsids let us explore the conformation of the DNA chain in the region where coils and globules coexist (0.05 and 0.1 mM sp), between the region of pure coils, in the absence of any condensing agents (Leforestier and Livolant, 2010) (11) and the region where all chains form toroids (0.5 mM sp in this work and 5 mM sp in Leforestier et al., 2008) (Figure 5a).

Domain of coexistence between coils and globules

The coexistence of coils and globules has been reported long ago by Gosule and Schellman (1978) by analyzing flow linear dichroism signals of very dilute T7 DNA solutions to which increasing amounts of the polyamines spermidine and spermine were added under low ionic strength conditions (2 mM monovalent ions). It was also observed by Post and Zimm (1982) by light scattering experiments with magnesium in ethanol-water solvent. More recently, Yoshikawa and coworkers observed directly the coexistence of “giant” T4 molecules coils and globules by fluorescence microscopy in highly dilute solutions with a large variety of condensing agents (Ueda and Yoshikawa, 1996; Minagawa et al., 1991; Melnikov et al., 1995; Yamasaki et al., 2003). When long DNA chains are condensed by the tetravalent polyamine spermine (sp), the transition region between the two extreme states of pure coils and pure globules is rather narrow compared to the divalent and trivalent polyamines (Takahashi et al., 1997). Jary and Sikorav (1999) also studied by sedimentation the conformation of Lambda DNA chains. They defined five regions for increasing spermidine (spd) concentrations. In two of them coils and globules coexist, on both sides of the region of pure coils.

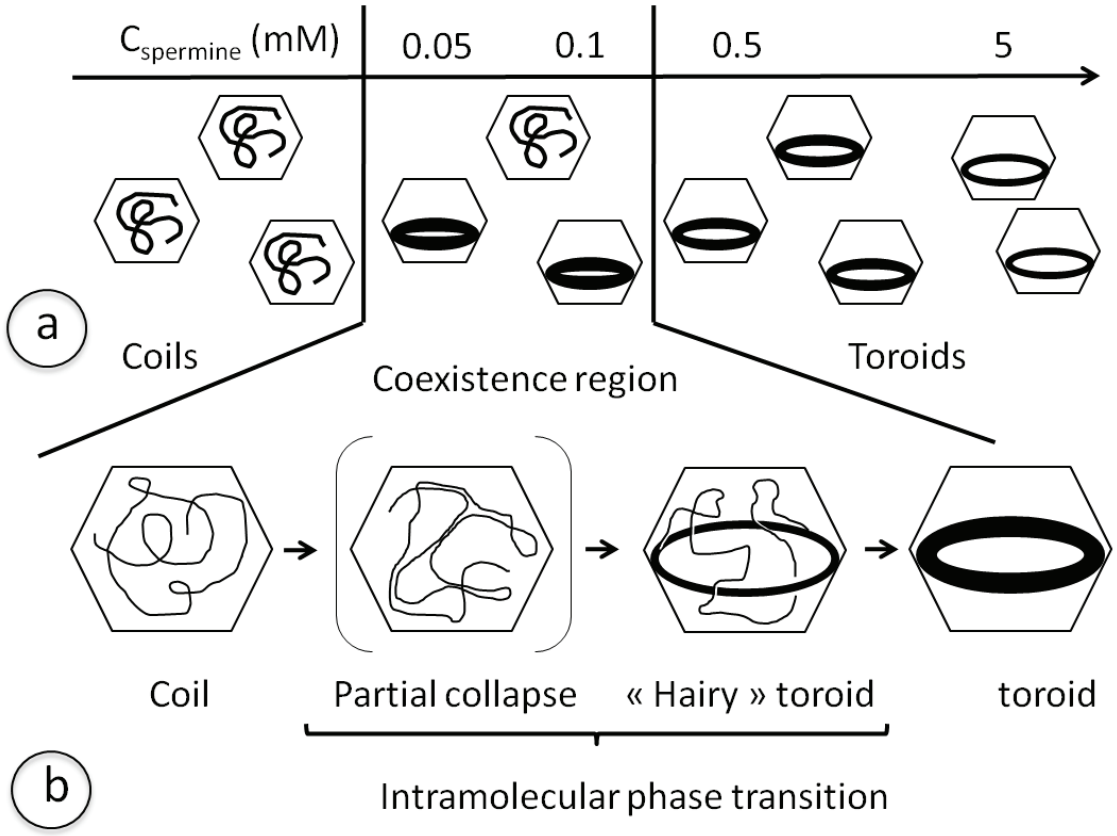

Figure 5: Schematic representation of our observations: coils (below 0.05 mM sp), toroids for $C_{spermine} \geq 0.5$ mM and multiple states in the coexistence region (0.05 and 0.1 mM sp).

Multiple globular states

CryoEM makes possible to analyze the conformation of the chain as a whole and the local DNA packing inside the globule as well.

- *Variation of the interhelix distance.* The interhelix distance a_H measured in the toroids decreases from 3.24±0.09 nm at 0.05mM sp to 2.99±0.06 nm at 0.1 mM sp and to 2.85±0.03 nm at 0.5 mM sp. An analysis of variance to compare the means of the three series of data reveals that there is a significant difference between them ($p < 1.4 \times 10^{-5}$). Pairwise comparisons of the means shows that each mean is significantly different from the others (p value < 0.04 in the three comparisons). For comparison, a_H was equal to 2.84 nm in toroids formed with 5 mM sp in 10 mM Tris, 10 mM $MgCl_2$, 1 mM $CaCl_2$ (pH 7.6), to 2.88 nm with 5 mM sp, 10 mM Tris, 1 mM $MgCl_2$, 1 mM $CaCl_2$, 100 mM NaCl) (Leforestier and Livolant, 2009) and also to 2.8 nm when DNA was condensed with 0.1 mM $Co(NH_3)_6$ in 10 mM Tris, 1 mM EDTA, pH 7.0 (Hud and Downing, 2001). The measured decrease of the interhelix distance with the spermine concentration can be compared to the X-ray data collected earlier with short DNA fragments in the high DNA concentration regime (around 90 mM DNA Ph) (Raspaud et al., 2005; Todd et al., 2008). Starting with Na-DNA, a fraction of DNA is aggregated at spermine concentrations above 15 mM (*i.e.* 60 mM positive charges) close to the charge compensation and was collected for diffraction experiments. The interhelix distances decreases first until all condensed monovalent counterions ions are replaced by spermine, and further increases. In our experiments, DNA was neutralized in the capsid mostly with Na counterions, but divalent ions were also present to maintain the stability of the capsids at the initial stages of our experiments. We also worked with a larger concentration of added salt (10 mM Tris, 7 mM NaCl, 1 mM $MgCl_2$, 1 mM $CaCl_2$) compared to 10 mM Tris in Raspaud et al experiments. Our experiments are also performed at lower DNA concentration, 0.45 mM phosphate (0.15 mg/ml) compared to

90 mM phosphate. This DNA concentration takes into account the total volume of the sample, with the DNA inside the capsids and also the nucleotides outside of the capsids that result from the nuclease activity. Nevertheless, this concentration seems to be high enough to follow the progressive release of the initially condensed monovalent (and divalent) counterions upon addition of spermine. As reported before, the presence of monovalent counterions initially condensed on DNA controls the interhelix distance (Raspaud et al., 2005). The fact that spermine is added directly to the DNA solution in Raspaud et al experiments whereas spermine is added here to the buffer around the capsids that act as dialysis bags does not matter because added spermine cations freely diffuse through the capsid and immediately condense onto DNA. Nevertheless, since we are working with small volumes of buffer around the capsids, we must consider not only the spermine concentration in the buffer but also the charge ratio. Considering the 4 charges carried per spermine molecule, the concentrations used in our experiments (0.5, 0.1 and 0.05 mM sp) correspond respectively to 2, 0.4 and 0.2 mM positive charges. Compared to the 0.45 mM negative phosphate charges, there is enough spermine to neutralize all phosphate groups with 0.5 mM spermine, whereas 0.1 and 0.05 mM sp do not permit to fully neutralize DNA.

In this transition region, we measured a significant variation of the interhelix spacing by changing the ionic conditions. The largest distances are compatible with a cholesteric instead of a hexagonal liquid crystalline organization of DNA in the globule, and agree with the predicted possible coexistence of several globular states of DNA (Grosberg and Khokhlov, 1994).

- *Conformation of the chain. I*n the coexistence region, we observe a continuum of DNA conformations between the pure coil that occupies the entire volume of the capsid and the fully toroidal globule (Figure 5b). In many cases, the single chain forms “hairy toroids”, the chain being partly in a coil and partly in a toroidal conformation. This situation corresponds to an intra-molecular phase transition. The length of the DNA segments in the coil and in the toroid varies. We suspect that the ratio L_{toroid}/L_{total} ranges from 0 to 1 but quantitative measurement have not been undertaken yet. For this, we need to handle a population of capsids containing DNA segments of identical length. Bacteriophages such as Lambda should be used for that purpose since they have been shown to eject a DNA segment of a given length for each applied osmotic pressure (Evilevitch et al., 2005), as opposed to T5 for which the ejection stops at several steps for a given applied pressure (Leforestier et al., 2008).

These two parameters, the ratio between the coil and the toroidal DNA fragments, and the interhelix spacing in the toroid determine the density of the DNA globule. Our observations agree with measurements of sedimentation coefficient (Cs) of λ-DNA globules condensed by spermidine in 10 mM Tris buffer at a concentration of 50 ng DNA/ml (Jary, 1998; Jary and Sikorav, 1999). The authors reported the coexistence of globules with Cs = 180S with coils of a much lower density (40S) in the coexistence region. Their density increases up to 380S in the domain where all chains are condensed into globules. The increase from 180S to 380S likely reflects mostly the decrease of the interhelix spacing with the variation of the spermidine concentration. The visualization of intermediate states of monomolecular condensation reveals that the collapse transition is not a two state reaction, in agreement with measurements of the diffusion coefficient of Lambda chains collapsed by $Co^{3+}(NH_3)_6$ through the transition zone, in solutions equilibrated for 16h (Widom and Baldwin, 1983).

Based on many fluorescence microscopy experiments, it was shown that the DNA collapse transition can proceed by one of two ways, either i) a direct transition from the coil to the globule or ii) via an intermediate intrachain segregated state. Using chitosan polycations as the condensing agent, Philippova et al showed how the intrachain segregation between condensed and extended fragments occurring in the low salt regime can switch to a discrete transition in the high salt regime (Jary and Sikorav, 1999). For polyamines, the situation seems unclear yet. Using T4 DNA chains (166 kbp) Takayashi et al. (1997) reported that the collapse transition was discrete on the level of individual chains (in 30 mM Tris with 10 mM NaCl, pH 6.0). Later on, Iwaki et al. (2008) predicted that a folded chain would appear accompanied by unfolded fragments of non-negligible size

at a high concentration of salt (10 mM monovalent salt and above). Their experimental observations, using T4 chains and no Tris buffer, supported these predictions. High resolution fluorescence microscopy is a very powerful method allowing the simultaneous observation of a large number of individual chains. Nevertheless, the resolution of fluorescence microscopy is limited due to the blurring effect and may explain the difficulties to identify the nature of the transition in some cases, as reported by Iwaki et al. (2008). In addition, this method requires the presence of dyes that may interfere with the DNA electrostatics.

Classical Electron microscopy has also been widely used over the years. It requires multiple steps of preparation (adsorption on a positively charged surface, dehydration and addition of charged contrasting agents such as uranyl acetate). Despite these limitations, we should mention the description of a few globules connected to disperse DNA around, that the authors suspected to be incompletely formed or in the process of being unraveled (Jary, 1998). These may correspond to our “hairy” globules. Interestingly, partially folded chains of T4 DNA chains were also observed by AFM between the elongated coil and the condensed globule for intermediate concentrations of the condensing agent (a dimeric gemini surfactant) (Iwaki et al., 2008).

To our knowledge, this is the first high-resolution observation of DNA chains at the coil globule transition revealing the presence of an intramolecular phase transition upon addition of polyamines. In addition to the increased resolution, the interest of cryoEM is to control the ionic environment of the chain and to avoid the presence of dye and the adsorption of the chains onto surfaces.

Does the confinement modify the conformation of the DNA globule?

In fluorescence experiments, the DNA is confined between slide and coverslip, which leads to the “extended coil” configuration of the chain, which may sometimes be additionally stretched under flow (Miyazawa et al., 2005). Under such conditions, the presence of multiple toroids along the chain was reported sometimes upon addition of condensing agents (Iwaki et al., 2008; Brewer et al., 1999). Other experiments (Zhang et al., 2009) reported how DNA chains confined in nanochannels first elongate and finally condense into a globule (whose detailed structure cannot be analyzed for experimental reasons). In this case, the condensation was induced by macromolecular crowding. In our experiments, the confinement of the chain in the quasi-spherical volume of the capsid is isotropic and should mimic more closely the confinement of the chain that exists in any living systems.

Biological interest of a complex globular conformation of DNA

In the coexistence region were the complex globule configurations are observed, spermine cations are not in sufficient amount to collapse the total DNA. Due to the cooperative effect of the counterions, part of the chain is saturated with spermine (and its charge close to neutrality) while the other part is still highly negatively charged with no (or low amounts of) condensed spermine. The loose globule is therefore made of a neutral domain (the toroid) and of negatively charged hairs (the coil segment). Kundagrami and Muthukumar (2010) reported in other systems how the collection of counterions by the collapsing polymer occurs in tandem with the polymer collapse and how there is a unique mapping between the effective charge and the average coil size. From a biological point of view, DNA chains are always confined in the cell nucleus, and exposed to low amounts of condensing polycations and other condensing agents. These complex conformations of the globule are therefore of the highest interest because the coexistence of neighbouring condensed /uncondensed segments of the chains together with a fine regulation of the interdistance and nature of the DNA/DNA interactions should provide a fine regulation of the control of the activity of the molecule.

ACKNOWLEDGEMENTS. We thank M. de Frutos who gave us T5 bacteriophages and M. Renouard who purified the receptor FhuA.

References

Bloomfield VA: DNA condensation. *Curr. Opin. Struct. Biol*. **6**: 334-341 (1996)

Boulanger P, LeMaire M, Bonhivers M, Dubois S, Desmadril M, Letellier L: Purification and structural and functional characterization of FhuA, a transporter of the Escherichia coli outer membrane. *Biochemistry* **35**: 14216–14224 (1996)

Brewer LR, Corzett M, Balhorn R: Protamine-induced condensation and decondensation of the same DNA molecule. *Science* **286**: 120-123 (1999)

Chattoraj DK, Gosule LC, Schellman JA: DNA condensation with polyamines. II. Electron micorscopy Studies. *J. Mol. Biol.* **121**: 327-337 (1978)

Evilevitch A, Gober JW, Phillips M, Knobler CM, Gelbart WM: Measurements of DNA lengths remaining in a viral capsid after osmotically suppressed partial éjection. *Biophys. J.* **88**: 751-756 (2005)

Gosule LC and Schellman JA: Compact form of DNA induced by spermidine. *Nature* **259**: 333-335 (1976)

Grosberg AU and Khokhlov AR: *Statistical Physics of Macromolecules*. (American Institute of Physics, NY, USA, 1994)

Hud NV and Downing K: Cryoelectron microscopy of lambda phage DNA condensates in vitreous ice: the fine structure of DNA toroids. *Proc. Natl. Acad. Sci. USA* **98**: 14925-14930 (2001)

Iwaki T, Makita N, Yoshikawa K: Folding transition of a single semiflexible polyelectrolyte through toroidal bundling of loop structures. *J. Chem. Phys.* **129**: 065103 (2008)

Jary D : *Etude des propriétés statiques et dynamiques de longues chaines d'ADN sur deux exemples : rhéologie de solutions semi-diluées et cyclisation d'une chaine globulaire*. PhD Thesis, Orsay University, 1998 (France)

Jary D and Sikorav JL: Cyclization of globular DNA. Implications for DNA-DNA interactions *in vivo. Biochemistry* **38**: 3223-3227 (1999)

Kundagrami A and Muthukumar M: Effective charge and coil-globule transition of a polyelectrolyte chain. *Macromolecules* **43**: 2574-2581 (2010)

Leforestier A, Brasilès S, de Frutos M, Raspaud E, Letellier L, Tavares P, Livolant F: Bacteriophage T5 DNA ejection under pressure. *J. Mol. Biol.* **384**: 730-739 (2008)

Leforestier A and Livolant F: Structure of toroidal DNA collapsed inside the phage capsid. *Proc. Natl. Acad. Sci. USA* **106**: 9157-9162 (2009)

Leforestier A and Livolant F: The bacteriophage genome undergoes a succession of intracapsid phase transitions upon DNA ejection. *J. Mol. Biol.* **396**: 384-395 (2010)

Marx KA and Ruben GC: Evidence for hydrated spermidine-calf thymus DNA toruses organized by circumferential DNA wrapping. *Nucl. Acids Res.* **11**: 1839–1854 (1983)

Melnikov SM, Sergeyev VG, Yoshikawa K: Discrete coil-globule transition of large DNA induced by cationic surfactant. *J. Amer. Chem. Soc.* **117**: 2401-2408 (1995)

Minagawa K, Matsuzawa Y, Yoshikawa K, Matsumoto M, Doi M: Direct observation of the biphasic conformational change of DNA induced by cationic polymers. *FEBS Lett.* **295**: 67-69 (1991)

Miyazawa N, Sakaue T, Yoshikawa K, Zana R: Rings-on-a-string chain structure in DNA. *J. Chem. Phys*. **122**: 044902 (2005)

Philippova OE, Akitaya T, Mullagaliev IR, Khokhlov AR, Yoshikawa K: Salt-controlled intrachain/interchain ségrégation in DNA complexes with polycation of natural origoin. *Macromolecules* **38**: 9359-9365 (2005)

Post CB and Zimm BH: Light-scattering study of DNA condensation: Competition between collapse and agrégation. *Biopolymers* **21**: 2139-2160 (1982)

Raspaud E, Durand D, Livolant F: Interhelical spacing in liquid crystalline spermine and spermidine-DNA precipitates. *Biophys. J.* **88**: 392-403 (2005)

Takahashi M, Yoshikawa K, Vasilevskaya VV, Khokhlov AR: Discrete coil-globule transition of single duplex DNAs induced by polyamines. *J. Phys. Chem. B* **101**: 45, 9396-9401 (1997)

Todd BA, Parsegian AV, Shirahata A, Thomas TJ, Rau DC: Attractive forces between cation condensed DNA double helices. *Biophys. J.* **94**: 4775-4782 (2008)

Tzlil S, Kindt JT, Gelbart WM, Ben-Shaul A: Forces and pressures in DNA packaging and release from viral capsids. *Biophys. J.* **84**: 1616-1627 (2003)

Ueda M and Yoshikawa K: Phase transition and phase segregation in a single double-stranded DNA molecule. *Phys. Rev. Lett.* **77(10)**: 2133-2136 (1996)

Widom J and Baldwin RL: Molecular Condensation of λ-DNA induced by cobalt hexamine. *Biopolymers* **22**: 1595-1620 (1983)

Yamasaki Y, Katayose S, Kataoka K, Yoshikawa K: PEG-PLL blok copolymers induce reversible large descrete coil-globule transition in a single DNA molecule through cooperative complex formation. *Macromol.* **36**: 6276-6279 (2003)

Zhang C, Shao PG, van Kan JA, van der Maarel JRC: Macromolecular crowding induced elongation and compaction of single DNA molecules confined in a nanochannel. *Proc. Natl. Acad. Sci. USA* **106**: 16651-16656 (2009)

Zinchenko ZA, Sergeyev VG, Murata S, Yoshikawa K: Controlling the interchain segregation on a single DNA molecule. *J. Am. Chem. Soc.* **125**: 4414-4415 (2003)

GENERAL DISCUSSION AND CONCLUSION

The two parts of this thesis correspond to different experimental conditions. In the first part, I analyzed long DNA chains diluted in the bulk and followed their collapse and aggregation upon addition of varying amounts of spermine. In the second part, I analyzed long DNA chains already confined in the capsid of the phage before addition of the condensing spermine. The initial conformation and environment of the DNA chain was therefore different in the two series of experiments. The chain was in a coil configuration in bulk experiments (in the dilute regime since CDNA = 10 µg/ml < C^* = 33 µg/ml). Under confinement, the DNA molecule cannot be in a classical coil configuration because its end-to-end distance is much larger than the capsid dimension.

In bulk experiments (part I), I have observed that:

(1) The shape and the structure of the DNA condensates (toroids, globules, rods versus bundles) can be controlled by the polycation (spermine) concentration.
By x-ray diffraction, it had been previously known that the structure, which is represented by the interhelical spacing a_H, depends on polyamine, salt (NaCl), and DNA concentrations (Raspaud et al., 2005). I have found that the morphology of the condensate, depends on the spermine concentration as well. We showed that toroids present always a local hexagonal structure. Bundles instead are probably cholesteric.

(2) There exists a fine network of DNA fibers which are composed of 2-4 DNA chains in the redissolution regime.
In previous studies using light scattering and x-ray diffraction, it was assumed that the DNA precipitates re-enter the soluble state. Recently, there have been two studies that report the existence of small (<100 nm) colloidal DNA particles (by TEM, Trubetskoy et al., 2003) or the DNA network (by fluorescence microscopy; Iwataki et al., 2004) in a large excess of spermine or spermidine. Using cryo-EM, I have confirmed the existence of the DNA fiber networks above the redissolution limit and imaged them with high resolution without using any contrasting or staining agents.

(3) *The dimensions of the DNA toroids and bundles can be controlled by the reaction time.*
It was shown by light scattering experiments that the size of the DNA aggregates increases with time (Widom and Baldwin, 1983; Porschke, 1984; He et al., 2000; Lee et al., 2001), and I confirmed their observations with cryo-EM. Furthermore, I observed the increase of the thickness of the toroids and bundles and the increase of the toroid diameter with time. There is a recent time-resolved cryo-EM study of the morphologies of DNA condensed with a cationic dendrimer (Carnerup et al., 2009), but the analysis of the evolution of the condensates dimensions is lacking.

(4) *The variation of the interhelix distance with the concentration of spermine*.
I confirmed by cryoEM measurements the X-ray data collected by Raspaud et al (2005). In addition, I enlarged the explored range of spermine concentration to lower and larger values, showing a low increase of the a_H value at the lowest spermine concentration and a significant increase of a_H for the highest explored spermine concentrations. Ainalem et al. (2009) and Carnerup et al. (2011) have recently investigated the changes in the size and morphology of the DNA condensates with cationic dendrimers of varying charge by using cryo-EM, which are similar approaches to my study but do not focus on the changes in size/shape and structure (a_H) on the dissolution-precipitation-redissolution phase diagram.

(5) *I found conditions (reaction time <10 s) in which monomolecular toroids are formed.* It was known that the monomolecular and the multimolecular condensations cannot be separated during the aggregation process when the condensing agent is spermine or spermidine (Widom and Baldwin, 1983). However, in my observation, isolated toroids were obtained when samples are frozen within less than 10 seconds.

Under confinement of DNA chains inside the capsid, I observed

1) *Original conformations of a unique DNA chain*.
In the coexistence regime between the regimes where all chains are in a coil conformation and the regime where all chains are fully collapsed toroids, there exist "hairy" toroids that have condensed and uncondensed segments coexisting along the same DNA chain.

2) *A decrease of the interhelical distances when increasing the spermine concentration.*

Previously, several confinements have been applied to DNA chains (liposome, viral capsid, nanochannel, and liquid droplet) before condensing DNA. It happens that the confinement contributes to the condensation process: reducing nanochannel width (Zhang et al., 2009) or decreasing liquid droplet diameter on a mica surface even without any condensing agent (Hou et al., 2009) can facilitate the DNA chain collapse. The originality of our work comes from the fact that we performed experiments with high resolution (compared to fluorescence microscopy methods) and that we kept ionic conditions unchanged which are not possible in classical TEM observations that require dehydration and staining of the sample. We showed that the T5 capsid confining the DNA chain is likely to influence the DNA collapse process.

Apart from the confinement effect that we discussed above, how can we compare these two sets of experiments? Let us first summarize similarities and differences in the two series of experiments (se also Table 1):

- We used long DNA chains in both cases (48.5 kbp lambda chains in part I and 12-54 kbp T5 chains in part II). The DNA length is considered by theoreticians as a critical parameter for the coil-globule transition and the size/morphology of the collapsed globule (Post et Zimm, 1982; Stukan et al., 2003). Nevertheless, we do not consider that the difference in DNA length is significant here compared to the other parameters that differ between the two sets of experiments.

- We used spermine as the condensing agents in both series of experiments as well, under ionic conditions that can be considered as low monovalent salt conditions in both cases. The addition of 7 mM NaCl and very low amounts of divalent cations (1 mM $CaCl_2$ and 1 mM $MgCl_2$) to 10 mM Tris was required to maintain the stability of the bacteriophage capsid but has minor affects on the condensation process.

More important are two other parameters, the initial DNA concentration and the +/- charge ratio.

- In order to prevent the aggregation of the chains in bulk experiments, the DNA concentration was fixed at the lowest possible concentration (10 µg/ml, *i.e.* 0.03 mM phosphates). Lower concentrations would have been even better but they were incompatible with cryoelectron microscopy studies since it was necessary to find enough objects in the cryofilm after condensation. For experiments in part II, it was not necessary anymore to work with low DNA concentrations because each chain is trapped inside its capsid and cannot interact with the others. The initial DNA concentration inside the capsid is high, and ranges from 0.4 to $1.6x10^5$ µg/ml (40-160 mg/ml *i.e.* 120-480 mM phosphates) because of the small dimensions of the capsid (diameter 80 nm) that contains the DNA chain (15-24 kbp in the conditions of our experiments). If we consider the DNA concentration in the solution of phages ($1x10^{12}$ phages/ml), it is close to 0.45mM Ph under our conditions of imaging.

  The DNA concentration is an important parameter because the spermine concentration (C_{precip}) that triggers the DNA precipitation varies with the DNA concentration (see the phase diagram in Raspaud et al, 1998). The C_{precip} is constant in the low C_{DNA} regime (<0.1 mM Ph) and increases with C_{DNA} in the intermediate C_{DNA} concentration regime (0.1-10 mM Ph). It also increases with spermine in the high DNA concentration regime but the slope is different.

- We also explored two different ranges of charges ratio. In bulk experiments (part I), the positive charges (4+ for each spermine) were in excess in the solution for all experimental conditions (+/- ratio ranging from 6.7 to $5.3x10^4$), whereas in experiments with capsids (part II) the negative charges (1 for each phosphate) were in large excess in the solution (+/- ratio ranging from $1.7x10^{-3}$ to $4.2x10^{-4}$). This should be true also inside the capsids if we hypothesize that all spermine cations are condensed onto DNA, but we do not have access to this information. This means that experiments in part I are all done above the precipitation line (see the phase diagram) and that experiments in part II are done close to the precipitation line (just below or just above). The charge ratio has been traditionally thought as a key parameter in the theories of polyelectrolyte behaviors regarding DNA condensation, in which undercharging, neutralization and overcharging are related to the ionic distributions and determine the interchain forces (Oosawa, 1968, Manning, 1969).

	PART I	PART II
Long DNA chains	48.5 kbp	12-54 kbp
Condensing agent	Spermine (4+)	Spermine (4+)
Similar ionic conditions	10 mM Tris & 1 mM EDTA	10 mM Tris, 7 mM NaCl, 1 mM MgCl2, 1 mM CaCl2
Different +/- charge ratios	$6.7\text{-}5.3\times10^4$ (Excess of **+** charge)	0.2-2 (Excess of **–** charge)
Different DNA concentrations	Low (10 µg/ml)	High (0.15 mg/ml)
Different physical environments	Bulk experiment	Confinement within phage capsid

Table 1: Comparison of the main characteristics of the two experiments:

We present on Figure 1, a graphical comparison of conditions where experiments have been performed, based on the phase diagram.

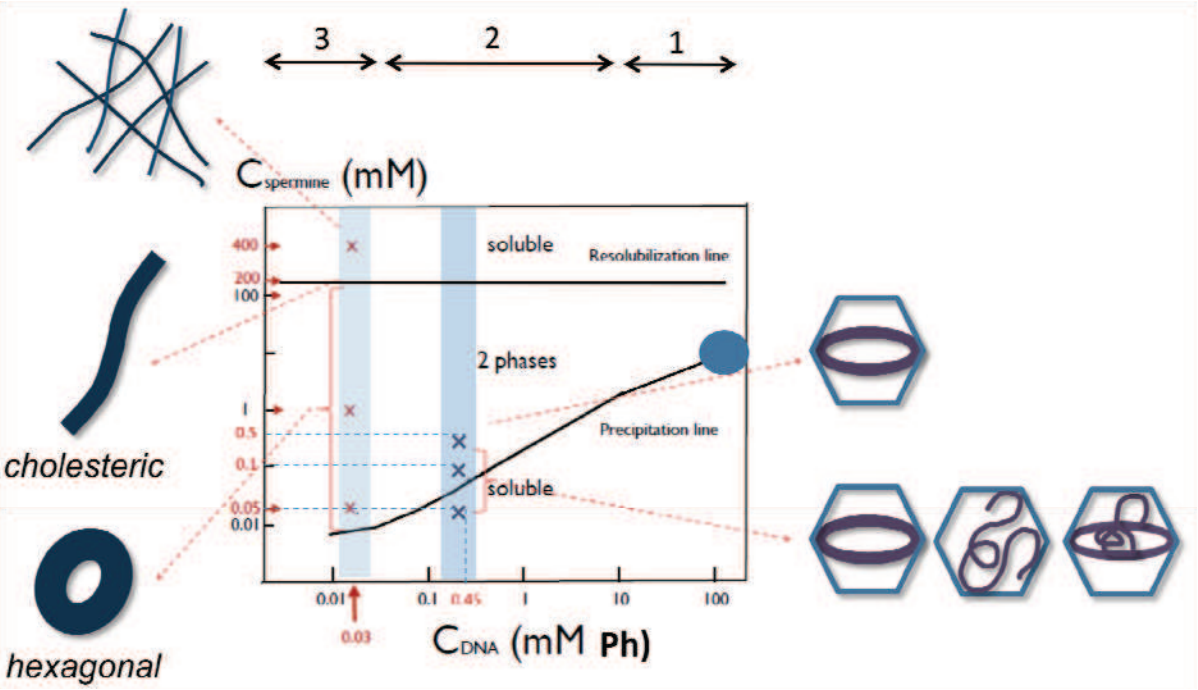

Figure 1: Experimental conditions and results are presented on the phase diagram. Domains indicated by the double arrows 1, 2 and 3 correspond respectively to the high, intermediate and low DNA concentration régimes described in Raspaud et al. (1998).

Experiments in part I of this thesis have been done in the low DNA concentration regime (small red crosses in light blue zone, in regime 3). Experiments in part II have been done at a higher DNA concentration and we may be dealing either with regime 2 or regime 1. Indeed, if we consider the whole sample (the capsids and the buffer around), the concentrations are respectively 0.45 mM Ph DNA and 0.05-0.5 mM spermine, we are in the intermediate regime (large blue crosses in regime 2). Interestingly, we see that we are really close to the precipitation line. Therefore, the confinement of DNA does not modify much (if it does) the critical concentrations at which occurs the DNA condensation. We cannot discuss his point more precisely because of possible errors in our measurements because we handled very small volumes of the capsids suspension in our experiments.

We could also consider the DNA concentration inside each capsid, and in this case we would be dealing with the high DNA concentration regime (1) (blue circle on Figure 1) but we lack precise information about the spermine concentration inside the capsid to consider this situation in detail. Nevertheless there are some arguments suggesting that it would be more realistic to consider these local concentrations. Indeed, when we follow the evolution of the interhelix spacing, we notice how the a_H value decreases while increasing the spermine concentration. This behavior mimics what was described in the high DNA concentration regime only (Raspaud et al., 2005) and interpreted as a progressive release of the large number of condensed monovalent cations Na+ upon addition of more and more spermine. It would be interesting to perform more experiments to explore how varies the DNA packing inside the capsid under a larger range of ionic conditions.

In both systems, it has been shown that the condensed morphology and local structure of DNA chains can be effectively changed by ionic environments. We recall that there are multiple local concentrations of DNA in a living cell with various ionic environments (mono and multivalent cationic species). This study may imply that dynamic DNA conformations can exist *in vivo* with varying concentrations of the multivalent cations (for example spermine and other polyamines).

There are two different fields of applications of this study.

First, this study can be a model system mimicking real biological genetic processes, because, the genetic material is always condensed and confined *in vivo*: chromosomes in eukaryotic cells, DNA in bacterial nucleoids, and DNA chains in viruses. The confinement effects remain to be analyzed in detail and simplified systems such as the bacteriophage may provide an interesting tool for approaching the phenomena.

Second, we may think of applications in the field of gene therapy. The main objective being to design nano-scale condensed objects of genetic materials in order to vectorize them into living cells, the concept of DNA condensation is essential. It has been proven in this study that it is difficult to prevent DNA aggregation, and that it is necessary to keep DNA molecules isolated by confinement or by other protocols. In this context, our study may give a direction for future investigations.

References

Carnerup AM, Ainalem ML, Alfredsson V, Nylander T: Watching DNA condensation induced by Poly'(amido amine) dendrimers with time-resolved cryo-TEM. *Langmuir Lett.* **25**: 12466-12470 (2009)

Gosule LC and Schellman JA: Compact form of DNA induced by spermidine. *Nature* **259**: 333-335 (1976)

He S, Arscott PG, Bloomfield VA: Condensation of DNA by multivalent cations: experimental studies of condensation kinetics. *Biopolymers* **53**: 329-341 (2000)

Hou XM, Li W, Dou SX, Zhang LY, Xie P, Wang WC, Wang PY: Formation of DNA toroids inside confined droplets adsorbed on mica surfaces. *Phys. Rev. E* **79**: 051912 (2009)

Iwaki T, Makita N, Yoshikawa K: Folding transition of a single semiflexible polyelectrolyte through toroidal bundling of loop structures. *J. Chem. Phys.* **129**: 065103 (2008)

Iwataki T, Kidoaki S, Sakaue T, Yoshikawa K, Abramchuk SS: Competition between compaction of single chains and bundling of multiple chains in giant DNA molecules. *J. Chem. Phys.* **120**: 4004-4011 (2004)

Lee LK, Mount CN, Shamlou PA: Characterisation of the physical stability of colloidal polycation-DNA complexes for gene therapy and DNA vaccines. *Chem. Eng. Sci.* **56**: 3163-3172 (2001)

Manning GS: Limiting laws and counterion condensation in polyelectrolyte solutions I. Colligative properties. J. Chem. Phys. 51: 924-933 (1969)

Oosawa F: Interaction between parallel rodlike macroions. *Biopolymers* **6**: 1633-1647 (1968)

Philippova OE, Akitaya T, Mullagaliev IR, Khokhlov AR, Yoshikawa K: Salt-controlled intrachain/interchain segregation in DNA complexes with polycation of natural origoin. *Macromolecules* **38**: 9359-9365 (2005)

Porschke D: Dynamics of DNA condensation. *Biochemistry* **23**: 4821-4828 (1984)

Post CB and Zimm BH: Light-scattering study of DNA condensation: Competition between collapse and aggregation. *Biopolymers* **21**: 2139-2160 (1982)

Raspaud E, Olvera de la Cruz M, Sikorav JL, Livolant F: Precipitation of DNA by polyamines: a polyelectrolyte behavior. *Biophys. J.* **74**: 381-393 (1998)

Raspaud E, Durand D, Livolant F: Interhelical spacing in liquid crystalline spermine and spermidine-DNA precipitates. *Biophys. J.* **88**: 392-403 (2005)

Stukan MR, Ivanov VA, Grosberg AY, Paul W, Binder K: Chain length dependence of the state diagram of a stiff-chain macromolecules: theory and Monte Carlo simulation. *J. Chem. Phys.* **118**: 3392-3400 (2003)

Takahashi M, Yoshikawa K, Vasilevskaya VV, Khokhlov AR: Discrete coil-globule transition of single duplex DNAs induced by polyamines. *J. Phys. Chem. B* **101**: 45, 9396-9401 (1997)

Trubetskoy VS, Wolf JA, Budker VG: The role of a microscopic colloidally stabilized phase in solubilizing oligoamine-condensed DNA complexes. *Biophys. J.* **84**: 1124-1130 (2003)

Widom J and Baldwin RL: Molecular condensation of λ-DNA induced by cobalt hexamine. *Biopolymers* **22**: 1595-1620 (1983)

Yoshikawa K, Yoshikawa Y, Koyama Y, Kanbe T: Highly effective compaction of long duplex DNA induced by polyethylene glycol with pendant amino groups. *J. Am. Chem. Soc.* **119**: 6473-6477 (1997)

Zhang C, Shao PG, van Kan JA, van der Maarel JRC : Macromolecular crowding induced elongation and compaction of single DNA molecules confined in a nanochannel. *Proc. Natl. Acad. Sci. U.S.A.* **106**: 16651-16656 (2009)

La 4ème page de la couverture doit comporter :

◆ Un résumé de la thèse (3-4 lignes)

By using cryo-electron microscopy, we analyzed the morphology and structure of long double-stranded DNA chains condensed upon addition of varying amounts of the tetravalent polycation spermine (polyamine). Experiments have been performed i) with chains diluted in the bulk and ii) with individual chains confined in the bacteriophage capsid.

◆ Une liste des mots clés relatifs au sujet de la thèse

DNA condensation, cryo-electron microscopy, spermine, bacteriophage, toroid, liquid crystal

◆ Le nom du laboratoire de rattachement

Laboratoire de Physique des Solides, UMR CNRS 8502

Université Paris-XI, Centre d'Orsay, France

PÔLE : INGENIERIE DES PROTEINES ET CIBLES THERAPEUTIQUES

UNIVERSITÉ PARIS-SUD 11

UFR «FACULTÉ DE PHARMACIE DE CHATENAY-MALABRY »

5, rue Jean Baptiste Clément

92296 CHÂTENAY-MALABRY Cedex